Interaction of powerful laser radiation with the surfaces of semiconductors and metals: nonlinear optical effects and nonlinear optical diagnostics

S. A. Akhmanov, V. I. Emel'yanov, N. I. Koroteev, and V. N. Seminogov

M. V. Lomonosov Moscow State University

Usp. Fiz. Nauk **147**, 675–745 (December 1985)

This article reviews the present status of research on strongly nonequilibrium physical effects produced near and at the surfaces of metals, semiconductors, and dielectrics by high-power pulsed laser radiation, and their diagnostics by nonlinear-optical methods. The basic stages of the absorption and relaxation of the energy of laser radiation in the electronic and phonon subsystems of semiconductors and heating of the lattice are studied. The questions associated with fast laser-induced phase transformations in surface layers are discussed: melting-solidification and amorphous-solid-to-crystal and vice versa phase transitions, occurring with nano- and picosecond laser pulse durations (laser annealing). Different methods of laser diagnostics of the surfaces and nonequilibrium ultrafast processes on the surfaces of metals and semiconductors are reviewed. Special attention is devoted to nonlinear-optical methods of surface diagnostics (generation of second and third harmonics and difference frequencies in reflection, and Raman scattering of light). The high information content and sensitivity of these methods compared with other methods for studying surfaces is pointed out. The problem of the appearance of spatially periodic surface structures induced by laser radiation is examined. The theories of different laser-induced instabilities of the surface relief, giving rise to the formation of these structures (generation of surface acoustic and capillary waves and evaporation waves), are reviewed. Theoretical and experimental results are compared.

CONTENTS

Introduction ... 1084

1. Absorption and relaxation of the energy of a laser pulse. Heating of the lattice ... 1086
   1.1. Impulsive laser excitation and relaxation of the electronic subsystem. 1.2. Electron-phonon relaxation and heating of the lattice. 1.3. Impulsive laser annealing of semiconductor surfaces. Thermal and plasma mechanisms of annealing.
2. Linear and nonlinear optical methods for recording the state and laser-induced phase transformations of the surfaces of condensed media ... 1091
   2.1. New data from linear optical spectroscopy on fast laser-induced processes on semiconductor and metal surfaces. 2.2. Nonlinear-optical diagnostics of laser-induced phase transitions on a semiconductor surface; generation of optical harmonics and combination frequencies in reflection. 2.3. Study of the states and fast phase transformations of semiconductor surfaces with the help of the generation of optical harmonics and sum frequencies on reflection.
3. Nonlinear-optical processes determined by the modulation of the surface relief and of the surface temperature of condensed media ... 1105
   3.1. Laser-induced instabilities of the surface relief and the problem of the formation of ordered surface structures. 3.2. Diffraction of light waves by spatial-temporal modulations of the surface relief. 3.3. Feedback mechanisms in the premelting state. Generation of coupled surface electromagnetic and acoustic waves. 3.4. Generation of capillary waves and evaporation waves accompanying the interaction of laser radiation with liquid metals, semiconductors, and dielectrics. 3.5. Dependence of the interference instability of laser evaporation on the dielectric permittivity of the medium. 3.6. Experiments on the excitation of surface gratings and the theory of laser-induced instabilities.

Conclusions ... 1120

References ... 1122

INTRODUCTION

1. In this review we shall outline an area of physics which has been growing rapidly in recent years and which encompasses a large group of physical phenomena associated with the excitation of strongly nonequilibrium states, induced in the surface layers of metals, semiconductors and dielectrics by high-power pulsed laser radiation. We shall place special emphasis on the role of the nonlinear response of materials in these processes and their diagnostics.

The absorption of laser radiation which is strongly concentrated in space and time gives rise to the appearance of an

 0038-5670/85/121084-41$01.80 © 1986 American Institute of Physics

entire cascade of energy transformation processes, including the successive excitation and relaxation of the electronic subsystem, electron-phonon relaxation, phonon-phonon relaxation, and finally diverse thermal processes (heating, melting, and evaporation).

The final thermal stage of this chain in metals has now been studied for at least 20 years (see, for example, Refs. 1–4); experiments with laser pulses whose duration falls in the range $\sim 10^{-3}$–10^{-6} s give exhaustive physical information about this stage.

The thermal interaction of laser radiation with metals has opened up an extensive field of applications. We mention here laser cutting, welding, hardening, drilling of metal items, and laser thermochemical treatment of these items.

2. The results of analogous experiments with strongly absorbing semiconductor crystals turned out to be extremely interesting.

The action of powerful laser pulses gives rise to rapid and high-quality recrystallization of the surface layers of semiconductors which have been rendered amorphous by ion implantation or for other reasons—impulsive laser annealing occurs.[5–12] In spite of the fact that laser annealing is now a well-mastered technological tool, experiments on laser annealing have raised a number of still unsolved fundamental physical questions. Studies carried out in the last three to five years have shown that fast laser-induced phase transformations in surface layers of semiconductors (melting-solidification, amorphous-solid–crystal and crystal–amorphous-solid phase transformations) occur on nano-, pico-, and even subpicosecond time scales. A detailed explanation of these diverse and in many ways unexpected phenomena requires answering a number of fundamental questions about the behavior of semiconductors in a strong laser field.

What is the nature of and how high are the rates of electronic, electron-phonon, and phonon-phonon relaxation processes under conditions when intense laser action generates within times of 10^{-9}–10^{-14} s up to 10^{22} free carriers per cm^3, highly excited above the bottom of the conduction band? What is the state of this dense laser-induced electron-hole plasma? How and through what stages does melting of a crystal, containing this dense hot plasma, proceed: through a direct transfer of excess energy of free carriers by lattice vibrations or through the plasma-induced soft phonon modes? And, does the crystal melt after the energy obtained from the electronic subsystem is thermalized among all phonon modes or when it is concentrated only in the short-wavelength part of the phonon spectrum, while the phonon modes from the center of the Brillouin zone remain cold?

Existing theories give different, sometimes contradictory answers to these questions, so that experimental diagnostics plays a fundamental role in obtaining unambiguous results.

At the present time most experimental data support the "thermal" mechanism of laser annealing of elementary group IV semiconductors and $A^{III}B^{V}$ compounds for laser pulse durations of several picoseconds and longer (see Refs. 11 and 12, and Sec. 1). According to this model, impulsive laser annealing is accompanied by very fast (characteristic times $\gtrsim 1$ ps) heating of the crystal lattice owing to electron-phonon relaxation and followed by equally fast melting of the surface layer of the crystal. At the end of the laser pulse, after the surface has cooled, the reverse first-order phase transition into either the crystalline or the polycrystalline or the solid amorphous state occurs.

However, there also exist experimental data which do not fit into the "thermal" scheme. It is therefore of great interest that realistic possibilities for following experimentally the kinetics of all stages of the conversion of the energy of a laser pulse semiconductors and metals up to times of $\sim 10^{-14}$ s and for answering clearly the questions posed above have now appeared.

This is linked to the creation of stable frequency-tunable generators of femtosecond optical pulses (1 fs $= 10^{-15}$ s)[13–15]—pulses whose envelopes encompass only a few cycles of the optical field—adequate for optical diagnostics methods. Of course, the significance of these studies extends far beyond the technological requirements of laser annealing.

3. Probably the most characteristic feature of the present stage of study of laser-induced nonequilibrium states and laser-induced phase transitions is the clear understanding of the important and often decisive role of the *nonlinearity of the response* of the material in the phenomena under discussion.

In laser thermochemistry, for example, an entire class of nonlinear processes giving rise to the formation of spatially and temporally ordered structures has been studied in detail.[17]

A vivid example of the role of the optical nonlinearity in the process of laser excitation of semiconductors and metals are the spontaneously arising instabilities of the surface relief, giving rise to the formation of periodic surface structures.[12,20]

It has turned out that the formation of periodic structures on the surfaces of solids irradiated by laser light is a universal phenomenon, always arising spontaneously when the intensity of the laser radiation is high enough. The physics of their appearance is linked to the spatially nonuniform heating of the surface; the nonuniform field required for this is formed by the interference of the incident laser wave with the field formed by the scattering (diffraction) of laser radiation by fluctuation modulations of the surface relief. The possible appearance of feedback, when the periodic structures formed begin to affect substantially the scattering of the laser radiation in the diffracted wave, is of special physical interest. The resultant instability is analogous to the one appearing in the presence of stimulated scattering. The surface-acoustic wave (SAW) and capillary wave (CW) instabilities in melts and liquid metals and, finally, the interference surface-evaporation instability (IEI) can occur under different conditions.

The nature of the relaxation of nonequilibrium states, created by powerful laser pulses, also depends strongly on the level of excitation (and is therefore nonlinear). This type of nonlinear relaxation, which has been studied in great de-

tail in polyatomic molecules,[21] is ever more often encountered in condensed media.[22–24] Finally, unique information on the development of excitation and relaxation processes on a real time scale (including down to times of $\sim 10^{-14}$ s) is obtained by methods of nonlinear spectroscopy; the generation of optical harmonics and combination frequencies "in reflection" are very effective here[17,19]; the active spectroscopy of light scattering by plasma oscillations and optical and acoustic vibrations of the lattice is promising.[21,214] Thus *nonlinear excitation, nonlinear relaxation, and nonlinear-optical diagnostics* of nonequilibrium processes have actually become key questions in the physics of the interaction of powerful laser radiation with matter.

These questions for semiconductors and metals are emphasized in this review.

The review consists of three parts. The modern ideas regarding the physics of the relaxation of optical excitation energy in semiconductors and metals are presented in Sec. 1. Section 2 is devoted to the optical diagnostics of phase transitions at the surface; the emphasis is on the new possibilities of nonlinear-optical methods. Finally, Sec. 3 is devoted to nonlinear-optical phenomena giving rise to instabilities of the relief of the irradiated surface.

1. ABSORPTION AND RELAXATION OF THE ENERGY OF A LASER PULSE. HEATING OF THE LATTICE

When laser radiation with energy $\hbar\omega$ substantially exceeding the gap width $E_g: \hbar\omega > E_g$ interacts with a semiconductor (Fig. 1), light is absorbed in a thin surface layer with thickness $\alpha^{-1} \sim 10^{-4}$–10^{-6} cm, where α is the coefficient of optical absorption. (The latter value is also characteristic for the penetration depth of the field in a metal.) Under pulsed action of this kind, when the intensity of the radiation is high ($I \sim 10^6$–10^{12} W/cm^2), a strongly nonequilibrium and nonstationary state of both the electronic and phonon subsystems is created.

Because the primary act of energy absorption occurs in the electronic system the electron temperature T_e differs substantially from the lattice temperature T. The process of energy transfer and thermalization in the lattice includes a series of relaxation stages both within the electron-hole subsystem and electron-phonon and phonon-phonon relaxation.

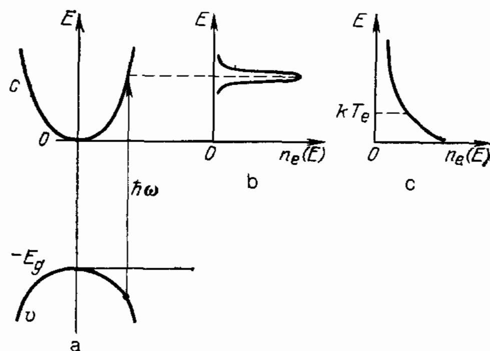

FIG. 1. Laser excitation and intraband energy relaxation of carriers in a semiconductor. a) Interband transition with absorption of a quantum $\hbar\omega$; b) initial form of the electron distribution function; c) final form of the energy distribution function.

In this section we shall study in greater detail each of the mentioned stages of the interaction of laser radiation with the surface of a semiconductor and subsequent processes.

1.1. Impulsive laser excitation and relaxation of the electronic subsystem

When pulsed laser radiation with an energy density W, pulse duration τ_p, and energy $\hbar\omega > E_g$ interacts with the surface of a semiconductor, owing to interband absorption (see Fig. 1) nonequilibrium electron-hole pairs are generated at a rate which can be determined from the following relation:

$$G(t, z, T) = \frac{\alpha(t, z, T)(1-R)}{\hbar\omega\tau_p} W \exp\left(-\int_0^z \alpha(t, z', T)\,dz'\right)$$
$$\approx G_0 \exp(-\alpha z); \qquad (1.1)$$

here $\alpha = \alpha_l + \alpha_{nl}$ is the sum of the linear and nonlinear absorption coefficients, which depend on the coordinate z (the z axis is directed into the medium perpendicular to the surface) and the temperature T; $R = R(t,T)$ is the coefficient of optical reflection. Table I presents the values of the optical parameters entering into (1.1) for crystalline and amorphous silicon (Si, $E_g = 1.12$ eV) and amorphous gallium arsenide (GaAs, $E_g = 1.43$ eV) at certain frequencies corresponding to the wavelengths of pulsed lasers used in laser annealing. It is evident that the rate of laser-induced generation of free carriers can reach enormous values $G_0 = 10^{30}$–10^{35} cm^{-3}/s (for $W = 0.1$ J/cm^2 and $\tau_p = 10^{-8}$–10^{-13} s).

Photoexcited electrons have an energy of $\sim \hbar\omega - E_g$ (the energy is measured from the bottom of the conduction band) and an initially strongly nonequilibrium energy distribution function centered near the energy $E = \hbar\omega - E_g$ (see Fig. 1). The holes (h) have an analogous distribution.

The nature of the subsequent relaxation of nonequilibrium carriers in the energy and coordinate spaces depends substantially on the carrier density in the photoexcited electron-hole plasma n_c ($n_c = 2n_e = 2n_h$). For purposes of estimating the initial density of nonequilibrium carriers n_c, created by the end of the picosecond or femtosecond pulses, we shall neglect the diffusion and recombination of carriers. Then, from Table I we obtain the following estimates of the upper limit:

$$n_c \lesssim \left(\frac{dn_c}{dt}\right)_{gen} \tau_p \approx G_0\tau_p$$
$$\approx \begin{cases} 10^{22}\ \text{cm}^{-3} & \tau_p = 30\ \text{ps}, \\ 10^{21} - 10^{22}\ \text{cm}^{-3} & \tau_p = 90\ \text{fs}. \end{cases}$$

For nanosecond pulses recombination must be taken into account. At high nonequilibrium carrier densities nonradiative Auger recombination, in which process an electron and a hole, by recombining, give up their energy to a third carrier, dominates (see Fig. 2 and Refs. 22 and 23). At the same time the recombination rate is given by the expression $R_c = Cn_c^3$, where $C = \text{const}$ (for example, for silicon $C = 4 \cdot 10^{-31}$ cm^6/s). This is one example of the nonlinear (dependent on the intensity of excitation) relaxation in a

TABLE I. Typical characteristics of laser pulses and semiconductor crystals used in impulsive laser annealing.

Laser	Wave-length normal λ, nm	Pulse duration τ_p, s	Coefficient of interband absorption at $T_0 \approx 300$K α, cm^{-1} *)		Coefficient of reflection at $T_0 = 300$K R *)		Rate of generation of free carriers with $W = 0.1$ J/cm^2 G_0, cm^{-3}/s	
			Si	GaAs	Si	GaAs	Si	GaAs
Second harmonic Nd : YAG	532,1	$1{,}5\cdot10^{-8}$ $2\cdot10^{-11}$	$1{,}25\cdot10^{4}$	$8{,}09\cdot10^{4}$	0,37	0,38	$1{,}4\cdot10^{29}$ $1{,}0\cdot10^{32}$	$0{,}9\cdot10^{30}$ $6{,}4\cdot10^{32}$
Third harmonic Nd : YAG	354,7	$1{,}5\cdot10^{-8}$ $2\cdot10^{-11}$	$1{,}07\cdot10^{6}$	$7{,}14\cdot10^{5}$	0,57	0,42	$0{,}5\cdot10^{32}$ $0{,}37\cdot10^{34}$	$0{,}5\cdot10^{31}$ $0{,}37\cdot10^{34}$
Fourth harmonic Nd : YAG	266,0	$1\cdot10^{-8}$ $1{,}5\cdot10^{-11}$	$2{,}08\cdot10^{6}$	$1{,}61\cdot10^{6}$	0,74	0,55	$0{,}7\cdot10^{31}$ $0{,}46\cdot10^{34}$	$0{,}9\cdot10^{31}$ $0{,}6\cdot10^{34}$
Dye	620,0	$0{,}9\cdot10^{-13}$	$4{,}47\cdot10^{3}$	$4{,}28\cdot10^{4}$	0,35	0,35	$1\cdot10^{34}$	$0{,}9\cdot10^{35}$
Ruby	694,3	$3\cdot10^{-8}$	$2{,}35\cdot10^{3}$	$2{,}7\cdot10^{4}$	0,34	0,34	$1{,}8\cdot10^{28}$	$2\cdot10^{29}$

*) D. E. Aspnes and A. A. Studna, Phys. Rev. B. **278**, 985 (1983).

strongly excited electron-hole subsystem of the crystal, which was mentioned in the introduction. We shall determine the recombination time from the formula

$$R_c = \frac{n_c}{\tau_r}, \quad \tau_r = \frac{1}{Cn_c^2}. \tag{1.2}$$

(We note that screening of Coulomb interactions in a dense plasma limits the decrease in τ_r with increasing n_c. Thus, according to theoretical estimates,[24] τ_r decreases asymptotically to the value $\tau_r = 6$ ps when n_c exceeds the value $n_c = 10^{21}$ cm^{-3}.)

For sufficiently powerful pulses with $\tau_p > \tau_r$ a stationary state of the carrier density is established. From the equation for the nonequilibrium carrier density

$$\frac{\partial n_c}{\partial t} = D\frac{\partial^2 n_c}{\partial z^2} + G - R$$

(D is the diffusion coefficient) with $\partial n_c = \partial t = 0$ and neglecting diffusion, we obtain $R = G$, whence, using (1.2) and Table I, we have with $\tau_p = 15$ ns in Si and $\lambda = 532$ nm:

$$n_c \leqslant G_0\tau_r \approx 10^{20}\ \text{cm}^{-3}$$
$$\tau_r \approx 0.5\cdot10^{-9}\ \text{s}.$$

This estimate is valid if the distance over which the carrier diffuses before recombining is $l_r = (D\tau_r)^{1/2} \lesssim \alpha^{-1}$, where α^{-1} is the absorption length. In our example $D \sim 10$ cm^2/s, and $l_r \approx 0.7\times10^{-4}$ cm $\sim \alpha^{-1}$.

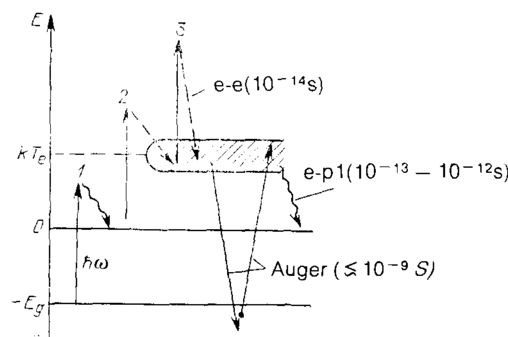

FIG. 2. Schematic energy diagram of electronic transitions in a semiconductor under the conditions of intense laser irradiation (Ref. 8, p. 6). 1) Interband absorption; 2, 3) absorption of light by free carriers. The letters e-e and e-p denote the electron-electron and electron-phonon collisions; Auger indicates Auger processes.

The estimates made above show that for $G_0 \gtrsim 10^{30}$ cm^{-3}/s the nonequilibrium carrier density n_c under typical conditions for laser annealing can easily exceed the value $n_c = 10^{19}$ cm^{-3}. We shall call such a state a highly excited state.

With such high carrier densities the frequency of collisions between carriers $\tau_{e-e}^{-1} \approx \tau_{e-h}^{-1} \sim n_c$ ($\tau_{e-e}^{-1} \approx 10^{14}$ s^{-11} with $n_c \approx 10^{19}$ cm^{-3}) exceeds the inverse emission time of longitudinal (LO) and transverse (TO) optical phonons $\tau_{e-TO}^{-1} \sim \tau_{e-LO}^{-1} \sim 10^{14} \div 10^{13}$ s^{-1}, which is independent of (or weakly dependent on) n_c.[26] Intraband relaxation over energies in the highly excited state therefore occurs over a time of the order of τ_{e-e} owing to interparticle collisions, conserving the total energy of the system of carriers. In addition, as already pointed out, in this state Auger recombination processes also conserve the total energy of the system of carriers. Because of these two circumstances virtually all of the absorbed energy of the laser pulse at times of the order of τ_{e-e} remains within the plasma subsystem of the semiconductor and "is thermalized"—the energy distribution of the electrons and holes are thermal distributions, characterized by the same values of the temperatures: $T_e = T_h \equiv T_c$ (see Fig. 1). The latter quantity depends on the absorbed energy and can substantially exceed the temperature of the lattice T (which at these times remains practically equal to the starting temperature T_0). The value of T_c, of course, depends on the density n_c, and for $n_c \approx 10^{21}$ cm^{-3} the temperature of the hot carriers can reach values of $T_c \sim 10^4$ K.[24,27]

Thus in the highly excited state at times $t \sim \tau_{e-e} \sim 10^{-14}$ s the semiconductor is characterized by the existence of an extremely hot ($T_e \sim 10^4$ K) and dense ($n_c \sim 10^{21}$ cm^{-3}) plasma and a hot lattice ($T \sim T_0 \approx 300$ K).

An analogous anamolous heating of the electronic subsystem (with the phonon system remaining cold) was discussed for metals theoretically in Ref. 68; in recent years reports of experiments in which this electron-phonon nonequilibrium state was recorded with the use of femtosecond laser pulses (though indirectly) have appeared.[69]

At low excitation levels ($n_c < 10^{19}$ cm^{-3}) the emission time of optical phonons in the semiconductor $\tau_{e-LO} < \tau_{e-e}$, and the relaxation of excited carriers over energies occurs over a time $\tau_{e-LO} \sim 10^{-13}$ s^{-1} owing to the emission of optical phonons.[189]

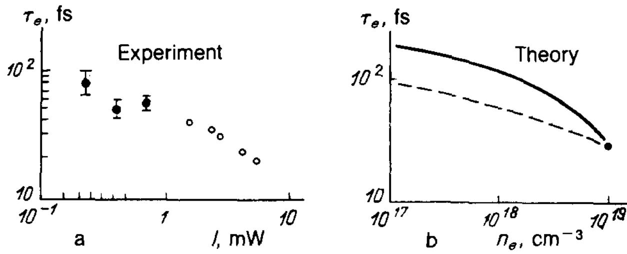

FIG. 3. a) Experimental dependence of the intraband energy relaxation time for electrons (τ_e) in $Al_{0.34}Ga_{0.66}As$ on the average intensity of the laser pump I[28] (for $I \sim 1$ mV, the density of photoexcited electrons $n_e \sim 7 \cdot 10^{18}$ cm^{-3}); b) the solid line, computed in Ref. 29, is the theoretical dependence of the time τ_e in GaAs ($T \approx 300$ K) on the free-carrier density neglecting intervalley scattering; the broken curve is the same, but taking into account intervalley scattering using the data from the experiment of Ref. 29.

As pointed out in the introduction, the direct observation of relaxation over energies from the photoexcited nonequilibrium carrier distribution became possible with the advent of lasers generating femtosecond pulses.[13–15] The times τ_{e-LO} and τ_{e-e} in the semiconductor $Al_xGa_{1-x}As$ ($x = 0.34$) were measured in Ref. 28. The results of this experiment are shown in Fig. 3 (an excitation intensity of the order of 1 mW corresponds, according to the estimates in Ref. 28, to a carrier density of the order of 10^{19} cm^{-3}). It is evident that when $n_c \lesssim 10^{19}$ cm^{-3} electron-phonon collisions make the main contribution to the effective relaxation constant $\tau_e^{-1} = \tau_{e-e}^{-1} + \tau_{e-LO}^{-1}$, i.e., the intraband relaxation time $\tau_e \approx \tau_{e-LO}$ and is independent of n_c, while for $n_c \gtrsim 10^{19}$ cm^{-3} the interparticle collisions make the main contribution and $\tau_e \approx \tau_{e-e} \sim 1/n_e$. The experimental results of Ref. 28, obtained for $Al_xGa_{1-x}As$, are to a certain extent applicable also to GaAs, which follows from their good agreement with the theoretical calculations of τ_e, presented for GaAs in Ref. 29.

The simple picture of the single-electron intraband relaxation, studied above, as we saw, is confirmed by experiment. Nevertheless in the general case the possibility of the manifestation of collective and nonlinear effects in the dense plasma must be taken into account. Thus screening of the electron-phonon interaction[30] can cause the time τ_{e-LO} to increase with n_c. The critical densities at which the effect of screening on τ_{e-LO} becomes important are, according to theoretical estimates,[24] of the order of $10^{19} - 10^{21}$ cm^{-3} depending on the type of electron-phonon scattering. Experimental data supporting the existence of this effect are presented in Ref. 30, which is devoted to the study of hot carriers in semiconductors with the help of picosecond lasers. In addition, the value of τ_{e-LO} can be affected by the change in the populations of the phonon modes owing to emission of phonons accompanying cascade relaxation of carriers to the bottom of the band.

It is well known[25,31] that at very low plasma temperatures ($T \sim 4$ K) and densities much lower than those studied here ($n_c \sim 10^{17}$ cm^{-3}) exchange and correlation effects radically change the nature of the plasma, causing it to condense into an electron-hole liquid. The possibility that such effects also appear at high temperatures and high levels of excitation has not been excluded. The hypothesis that the formation and condensation of excitons occur under the conditions of laser annealing was stated by van Vechten (see the review of Ref. 32). This idea formed the foundation for the so-called plasma model of laser annealing (see Sec. 1.3).

1.2. Electron-phonon relaxation and heating of the lattice

Because the initial difference between the carrier temperature T_c and the lattice temperature T is large, the probability of phonon emission by carriers is much higher than the probability of phonon absorption, so that the rate of energy transfer from the hot plasma to the lattice is independent of T. The expression for this rate can therefore be written in the form

$$S = \frac{\hbar\omega_0 n_e}{\tau_{e-LO}}, \tag{1.3}$$

where $\omega_0 \approx 10^{12} - 10^{13}$ s^{-1} is the frequency of the optical phonon. Energy transfer from the electron subsystem to the nonequilibrium optical phonons occurs over times longer than τ_{e-LO} (see below). At these times the diffusion of hot carriers changes the value of n_e from the estimates of Sec. 1.

To estimate the value of n_e for $t > \tau_{e-LO}$ we shall write the balance equation for the total energy density of the system of hot carriers E_e[33]:

$$\frac{\partial E_e}{\partial t} = G_0(\hbar\omega - E_g)\, e^{-\alpha z} + \langle\varepsilon_e\rangle D \frac{\partial^2 n_e}{\partial z^2} - \hbar\omega_0 n_e \tau_{e-LO}^{-1}. \tag{1.4}$$

The first term on the right side describes the increment to the energy owing to photoexcitation of electron-hole pairs; the second term describes the diffusion outflow of energy into the bulk of the medium ($\langle\varepsilon_e\rangle = E_e/n_e$ is the energy per carrier); and, the last term determines the rate of energy transfer to the lattice.

The density n_e decays with distance into the medium over the characteristic distance $l_e = \min(\alpha^{-1}, l_*)$, where l_* the effective diffusion length; see below. It is evident from (1.4) that the effective time constant for establishing the stationary state is $\tau_{E_e}^{-1} = Dl_e^{-2} + \tau_{e-LO}^{*-1}$, where $\tau^*_{e-LO} = (\langle\varepsilon_e\rangle/\hbar\omega_0)\tau_{e-LO}$ is the time over which a hot carrier gives up its energy $\langle\varepsilon_e\rangle$ to the lattice in the process of $\langle\varepsilon_e\rangle/\hbar\omega_0 \sim 10 - 10^2$ acts of phonon emission ($\tau^*_{e-LO} \sim 10^{-12} - 10^{-10}$ s, $(D\alpha^2)^{-1} \sim 10^{-11}$ s, $D \sim 10$ cm^2/s, $\alpha \sim 10^5$ cm^{-1}). At times $t > \tau_E$ we have $\partial E_e/\partial t = 0$, and from (1.4) we obtain an inhomogeneous equation for the stationary density n_e. Its solution has the form ($\partial n_e/\partial z|_{z=0} = 0$):

$$n_e = G_0 \tau_{e-LO} \frac{(\hbar\omega - E_g)\, l_*^{-1}\alpha^{-1}}{\hbar\omega_0 (1 - l_*^{-2}\alpha^{-2})} \left(e^{-z/l_*} - \frac{1}{l_*\alpha} e^{-\alpha z}\right). \tag{1.5}$$

Here the effective diffusion length is $l_* = (D\tau^*_{e-LO})^{1/2}$.

In the presence of weak optical absorption ($\alpha < l_*^{-1}$), for the rate of energy transfer to the lattice we have from (1.3) and (1.4)

$$S = G_0(\hbar\omega - E_g)e^{-\alpha z}. \tag{1.6}$$

In this case the laser energy stored in the electronic subsystem is transferred to the lattice at the same rate and in the same amount with which it is absorbed.

In the presence of strong absorption ($\alpha \gg l_*^{-1}$) we have

$$S=\frac{G_0(\hbar\omega-E_g)\,e^{-z/l_*}}{\alpha l^*}. \tag{1.7}$$

Now the absorbed laser energy is transferred to the lattice in a layer of thickness l_*, determined by diffusion, and the rate at which energy is transferred at the surface $z=0$ is a factor of αl_* lower than with (1.7). The coefficient of diffusion

$$D=\frac{2kT\tau_{e-LO}\tau_{h-LO}}{m_e^*\tau_{h-LO}+m_h^*\tau_{e-LO}}$$

at high temperatures ($T_c\sim10^4$ K) can reach values of $D\sim10^2$ cm^2/s^{-1} and $l^*\approx10^{-5}-10^{-4}$ cm. Thus the diffusion of hot carriers can substantially decrease the rate at which the lattice is heated.

Energy transfer at times $\tau^*_{e-LO,TO}$ goes into definite optical vibrational modes of the lattice, and the probability of the emission of acoustical phonons by electrons is substantially lower. Acoustical (transverse TA or longitudinal LA) phonons with a nonthermal spectrum form as a result of the decay of each optical phonon into a pair of acoustical phonons (Ref. 42; Fig. 4).

These processes occur over times τ_{LO-TA}, τ_{LO-LA}. Finally, owing to the scattering of phonons by one another the energy is gradually thermalized over times τ_{LA-T}, τ_{TA-T}. It should be noted that because of the differences in the thermalization times ($\tau^{-1}\sim\omega^3_{phon}$) at very short times there is not enough time for the low-frequency and especially the long-wavelength phonons (in particular, optical phonons) to become thermalized, while the short-wavelength phonons are already completely thermalized. This circumstance should be kept in mind when interpreting the controversial results of experiments on the measurement of the lattice temperature by the methods of Raman scattering (see Sec. 2.3.3).

The entire process of energy transfer from the initial electron-hole excitation to thermal vibrations of the lattice can be characterized by an effective energy-thermalization time τ_{e-T}.

A theoretical estimate of the phonon-phonon relaxation time[34] gives $\tau_{LO,LA-TA}\sim10^{-12}$ s. Experiments on the study of fast phonon-phonon relaxation in semiconductors, carried out at low temperatures ($T\sim4$ K) and low intensities of the exciting radiation ($n_c<10^{19}$ cm^{-3}),[35-38] confirmed this estimate.

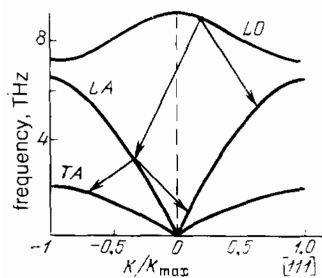

FIG. 4. Schematic diagram of the decay of high-energy long-wavelength longitudinal optical (LO) phonons, produced during the relaxation of hot carriers, into longitudinal (LA) and transverse (TA) acoustic phonons with conservation of energy and momentum in each event and an example of the subsequent chain of decays.[36]

In addition, in a series of experiments performed at $T_0=300$ K and high W (under conditions of laser annealing) it was demonstrated that the effective energy thermalization time is very short and is equal to $\tau_{e-T}\lesssim1$ ps (see Ref. 39 and Sec. 2.2).

Assuming now that the energy is thermalized practically instantaneously, the rate at which the lattice is heated by the laser pulse can be estimated. Using (1.8), we have at the surface ($z=0$), neglecting diffusion of heat and hot carriers.

$$c_V\frac{\partial T}{\partial t}=S=G_0(\hbar\omega-E_g);$$

here c_v is the heat capacity per unit volume, and T is the temperature of the lattice. For $\omega\sim4\times10^{15}$ s^{-1}, $\tau_p\sim30$ ns, $W\sim1$ J/cm^2, $c_v\sim1$ J/cm^3 K and $G_0=10^{30}$ cm^{-3}s^{-1} we have $\partial T/\partial t\sim10^{12}$ deg/s. Even higher values of $\partial T/\partial t$ are reached when picosecond pulses are used ($G_0\sim10^{33}$ cm^{-3}s^{-1}). Such enormous rates of pulsed laser heating, which cannot be achieved by ordinary thermal heating of the surface of a semiconductor, open up unique possibilities for stimulating nonequilibrium phase transitions at the surface; their kinetics are best studied by the methods of ultrafast linear and nonlinear laser spectroscopy (see Secs. 1.3, 2.2, and 2.3).

A more accurate quantitative description of lattice heating by a laser pulse when $\tau_p>\tau_{e-T}$ is obtained thermodynamically with the help of the solution of the heat-conduction equation. The heat source in this equation, S, is defined in terms of the rate at which energy is transferred to the lattice under the condition that the energy is instantaneously thermalized.

The equation of heat conduction is the starting equation for studying the laser annealing process from the viewpoint of the thermal mode[39-41] (see Secs. 1.3, 2.3.1). Equations of this type are also used in the analysis of a number of nonlinear-optical processes occurring on the surfaces of semiconductors, metals, dielectrics, and their alloys, which are determined by the spatially and temporally periodic heating of the surface by laser radiation (see Sec. 3).

1.3. Impulsive laser annealing of semiconductor surfaces. Thermal and plasma mechanisms of annealing

The phenomenon of impulsive laser annealing (ILA) in the narrow, intrinsic meaning of this concept, consists of extremely fast (usually within several tens of nanoseconds) restoration of the crystalline structure of the previously disordered or even completely amorphous surface layer of the semiconductor material by the action of a powerful laser pulse the energy of whose quanta exceeds the gap width.

This interesting and practically important effect, discovered in our country in the mid-1970's,[5,6] has now been comprehensively studied and is extensively used in the technology of semiconducting materials (see the reviews and monographs of Refs. 6–12). Impulsive laser annealing is most widely used to eliminate structural imperfections and radiation defects introduced into the surface layer of a crystal during ion implantation, i.e., when the required impurities are injected into this layer by bombardment of the sur-

face with accelerated ions of these impurities.[43]

For example, ILA provides a technologically important possibility of obtaining perfect crystalline structures in the surface layers with dopant concentrations which are not attainable with ordinary thermal annealing (up to 10^{21} cm^{-3} and higher[44]).

Such high impurity concentrations cannot be obtained in the usual method of annealing of the structural defects introduced by ion bombardment by slow heating in a furnace (up to 900–1000° C) and equally slow cooling[43] because of the diffusion of impurity particles into the bulk of the material, which is unavoidable with this method.[45] With fast impulsive laser annealing diffusion of impurities is substantially suppressed.

Aside from applications in microelectronics, the perfect crystalline layers, obtained with the help of ILA, with ultrahigh concentrations of minority carriers are of physical interest. Under these conditions it is possible to observe processes occurring because of the presence of a dense plasma (softening of the phonon modes with increasing carrier density[46] and change in the gap width as a function of n_c[47]), which are difficult to realize, as well as to record the n_c-dependent optical and electrical phenomena in semiconductors.[48]

The spatial coherence of laser radiation used for ILA enables the creation of periodic spatial structures on the surface of the annealed crystal, for example, gratings formed by alternating crystalline and amorphous regions (so-called interference laser annealing[49,50]).

It has been proposed that the ultrafast regeneration of the perfect crystalline structure during ILA be used for narrowing the gamma emission lines of short-lived nuclear isomers, excited by pulsed neutron pumping.[51] Intense neutron pumping, which is required in order to amplify gamma emission, unavoidably destroys the crystalline structure and eliminates the possibility of utilizing the Mössbauer and Bormann effects to optimize the parameters of a gamma laser. The use of ILA for regeneration of the crystalline structure within several tens of nanoseconds after excitation of the nuclei can help solve this problem.[51]

Since the discovery of the phenomenon of impulsive laser annealing, theoreticians and experimenters have expended great effort on the clarification of the physical mechanism of ILA. Thus far two alternative mechanisms for ILA have been studied: "thermal" and "plasma."

The traditional "thermal" model of laser annealing[39–41] is based on the idea of fast energy transfer from the system of hot carriers to the lattice (see Sec. 1.2). According to this model, in those cases when the energy density of the laser pulse W is high enough, an amorphous surface layer 50–500 nm thick melts, and a first-order phase transition occurs. The melt front moves rapidly from the surface into the bulk of the material and reaches the crystalline substrate. With the opposite motion of the melt front toward the surface, as the sample cools after termination of the pulse, epitaxial growth of the crystal occurs. Analytical estimates, based on the assumption that all the energy in the laser pulse is rapidly transferred to the lattice (see Sec. 3.6) and the numerical solution of the heat-conduction equation (see below, Fig. 8), show that the melting temperature is easily reached for values of W typically used in ILA (see also Refs. 44 and 45).

In accordance with Lindemann's criterion,[52] melting of the crystal ($T = T_{\text{melt}}$) begins when the mean-square displacement of an atom from its equilbrium position ($\langle u^2\rangle$) is a definite fraction x of the squared unit-cell size a^2 (for most materials $0.2 < x < 0.25$). At high temperatures we have

$$\langle u^2\rangle = \frac{9\hbar^2 T}{MkT_{\text{D}}^2} = \frac{1}{MN}\sum_j \langle |q_j|^2\rangle, \tag{1.8}$$

where M is the mass of the atom, T_{D} is the Debye temperature ($T > T_{\text{D}}$), N is the number of atoms in the crystal, and q_j is the amplitude of the jth normal mode of the acoustic vibrations of the crystal. Then the melting temperature is equal to

$$T_{\text{melt}} = \frac{x}{9\hbar^2} MkT_{\text{D}}^2 a^2.$$

(For Si, for example, $T_{\text{D}} = 625$ K, $a = 1.18$ Å, and $x = 0.2$, and from the given formula we have $T_{\text{melt}} = 1685$ K, in agreement with the experimental value.)

The question of whether or not the solid-liquid phase transition occurs after the energy is thermalized over all phonon modes j ($1 < j < N$) entering into (1.8) or when only several of the strongest "built up" phonon modes have such large amplitudes q_j that Lindemann's criterion holds remains open.

The thermal model of laser annealing is confirmed by comprehensive investigations of semiconductor surfaces during and after termination of the laser pulse. This includes a large number of experiments on ultrafast laser spectroscopy of the surface of strongly excited semiconductors (see Sec. 2). Measurements of the velocities of atoms evaporated from the surface during laser annealing show that the temperature of the surface reaches approximately 2000 K, i.e., it exceeds the melting temperature of Si.[53] The thermal model is also confirmed by measurements of the temporal evolution of the temperature with the help of synchrotron x-ray radiation,[54,55] the photoemission and electrical conductivity,[56,57] and the impurity distribution after laser annealing.[58,44,45]

At the same time many investigators continue to defend another point of view regarding the mechanism of pulsed laser annealing, developing the so-called plasma or collective model of ILA.[32,59]

In the thermal model a crystal melts owing to intense thermal motion of the lattice atoms, whereas in the plasma model the solid-liquid phase transition is caused by "softening" of the transverse acoustic phonons in covalent semiconductors accompanying growth of the electron-hole plasma density:

$$\omega_{\text{TA}} = \omega_{\text{TA}}^0 \left(1 - \frac{f\varepsilon_\infty n_c}{4n}\right),$$

where $f \sim 1$ (for Si, $f = 0.85$), ε_∞ is the dielectric permittivity of the crystal, and n is the number density of the atoms.

This effect is determined by the fact that in the transition out of the valence band into the conduction band an electron is transferred out of a bonding state into an antibonding state, so that the covalent bond is weakened. The softening of acoustic phonons can also lower the temperature of "ordinary" melting.[60]

The experimental foundation for the plasma model are the measurements of the lattice temperature by the method of Raman scattering (RS) of light (see Sec. 2). The temperature estimated from the ratio of the intensities of the Stokes and anti-Stokes components of RS in Si during impulsive laser annealing at first turned out to be equal to only 600 K.[61,62] The results of the first RS studies were criticized by a number of authors,[63,64] but in subsequent publications on this subject Compaan *et al.*[65,66] continued to defend the validity of their first results; the latest study by von der Linde's group[212] possibly closed this discussion.

Another difference between the predictions of the two models, which can be checked experimentally, is the difference in the symmetry of the phase forming under the action of the laser pulse. In the thermal model the melt which is formed is an isotropic medium, while in the plasma model, in accordance with Ref. 67, the dipole-dipole interaction between excitons must give rise to the formation of a noncentrosymmetrical exciton state with T_d symmetry (similar to the symmetry of GaP and GaAs crystals). The generation of the second harmonic in reflection is sensitive to the symmetry of the surface layer. The first experiments on the generation of the second harmonic of the probing radiation in reflection in GaAs[18] support the thermal model (see Sec. 2.3). The same result was later obtained in Ref. 16, where the second harmonic of the probing radiation from Si under the action of a powerful femtosecond laser pulse was observed.

Thus although a large part of the experimental results on the study of the mechanism of impulsive laser annealing supports the thermal model, some experiments contradict it but are in agreement with the plasma model.[32]

Another nonthermal model of laser annealing was proposed in Ref. 70. According to this model, during annealing a Peierls dielectric-to-metal and metal-to-dielectric phase transition occurs. The possibility of annealing defects owing to the appearance of relative vibrations of sublattices in a crystal was also studied on the basis of this model.[71] A model of "cold" melting of the lattice owing to the generation of static stresses accompanying the absorption of the laser pulse was recently developed.[190]

It may therefore be concluded that the lack of a complete physical picture of the interaction of laser radiation with the surface of a semiconductor is largely determined by the lack of experimental diagnostic procedures which are adequate for the physical problem under study. It is precisely for this reason that in recent years fundamentally new methods of diagnostics of laser-induced phase transitions on the surfaces of solids, which we shall discuss in the next section (see also the conclusion), were developed in a number of laboratories.

2. LINEAR AND NONLINEAR OPTICAL METHODS FOR RECORDING THE STATE AND LASER-INDUCED PHASE TRANSFORMATIONS OF THE SURFACES OF CONDENSED MEDIA

We already pointed out in the Introduction that the most dramatic result of the progress in laser technology over the last two to three years was the development and use in physical experiments of lasers emitting ultrashort pulses of femtosecond duration.[13–15,72–75] Of course, we cannot give an exhaustive review of the application of ultrashort laser pulses to the study of all types of fast photoprocesses in solids (there already exist a good review of previous work on this subject,[30] collective monographs,[74,76] and proceedings of international conferences on ultrafast phenomena[14,75,77–80]). Nevertheless, in this section, we shall briefly review the studies published in the last three to four years on the use of pulsed laser techniques for diagnostics of fast processes on the surfaces of solids (Sec. 2.1); we shall study in greater detail the nonlinear-optical aspect of these studies separately in Secs. 2.2 and 2.3.

2.1. New data from linear optical spectroscopy on fast laser-induced processes on semiconductor and metal surfaces

2.1.1. Investigation of reflection from a surface in real time under the conditions of ILA

The works of D. Auston *et al.*[81,82] on the measurement as a function of time of the linear optical reflection from the surface of a semiconductor subjected to ILA provided the impetus for extensive application of nonperturbing local highly informative methods of optical spectroscopy for diagnostics of fast laser-induced phase transitions on the surfaces of solids. The well-known controversy, which was later resolved, regarding the physical mechanism of pulsed laser annealing arose during these studies, and important data on processes occurring on the surfaces of semiconductors and metals were obtained.

The femtosecond dynamics of optical reflection from a Si surface subjected to ILA under the action of a 90-fs pulse was studied for the first time in a recent work by Shank *et al.*[16] The main laser was a dye laser with self-locked longitudinal modes, in which the technique of "colliding pulses" was used. A single 90-fs pulse picked out by an electrooptical shutter was amplified in a cascade of pulsed amplifiers and divided into two channels. The pulse in one channel served as the annealing pulse; the weaker pulse in the other channel was the probe pulse. To perform measurements in a wide spectral range, the frequency of the probe pulse was converted into a broad continuum (covering practically the entire visible and including the near-*IR* ranges) with the help of stimulated Raman scattering and the accompanying nonlinear processes in a cell with heavy water. The entire process of carrying out the measurements and collecting the experimental data was controlled by a microcomputer. The reflection of the probe pulse from the (111) surface of crystalline Si in different spectral regions as a function of the delay of the probe pulse relative to the annealing pulse was studied.

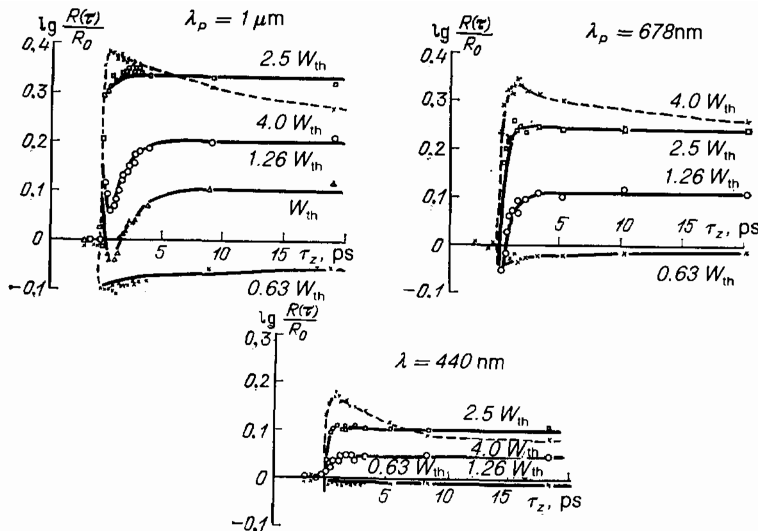

FIG. 5. The reflection of the (111) surface of crystalline silicon as a function of the delay time between the annealing ($\lambda = 620$ nm, $\tau_p = 90$ fs) and probing pulses for three values of the probing wavelength.[16] The solid lines with $W = 0.63$ W_{th} were calculated taking into account carrier diffusion inside the crystal; the solid lines for $W > W_{th}$ were calculated on the basis of the model of a thin layer of melt of variable thickness; the broken curves with $W = 4$ W_{th} were drawn "freehand".

Figure 5 shows the experimental data[16] for three values of the probing wavelengths: l_p = 1000, 678, and 440 nm. The energy density of the annealing pulse W is given in units of the threshold energy, $W_{th} = 0.1$ J/cm^2; the latter was determined by the appearance of an amorphous film on the silicon surface.

Shank *et al.*[16] proposed a quite simple physical model, which explains all their data.

According to this model, at the earliest stage, several hundreds of femtoseconds after the annealing pulse is absorbed in the surface layer with a thickness of $d \approx \alpha^{-1} \approx 3$ μm (α is the coefficient of absorption of the annealing radiation with $\lambda = 620$ nm), the changes in the reflection of the probe pulse with $\lambda_p = 1000$ and 670 nm are caused by the dense photostimulated electron-hole plasma. (This stage was previously observed by von der Linde *et al.*[83] and by Bloembergen *et al.*[84])

The optical properties of the plasma are described by the dielectric permittivity

$$\varepsilon(\omega) = \varepsilon_0 \left(1 - \frac{\omega_p^2}{\omega^2}\right), \qquad (2.1)$$

where $\omega_p = (4\pi n_e e^2/m^* \varepsilon_0)^{1/2}$ is the plasma frequency, n_e is the carrier density, m^* is the reduced mass, and ε_0 characterizes the contribution of the lattice and the interband transitions.

According to estimates, for $W \approx 0.6$ W_{th} $n_e \approx 5 \cdot 10^{21}$ cm^{-3} (for $m^* \approx m$—the mass of a free electron; see, however, the objections in Ref. 85). As W increases, both n_e and ω_p increase, so that the drop in the coefficient of reflection at $\lambda = 1$ μm when $\omega_p > \omega$ is replaced by a rise when $\omega_p < \omega$. From a comparison of Figs. 5a–c it may be concluded that the maximum value of ω_p corresponded to the wavelength λ_p, 678 nm $< \lambda_p <$ 1000 nm.

The change in the coefficient of reflection at long delay times is explained by heating and fast melting of the surface layer owing to the energy transferred to the lattice from the plasma, and the motion of the melt front into the crystal.

The solid lines in Fig. 5 were calculated taking these two stages into account.

Thus, for the first time, the optical characteristics of strongly excited silicon (about 10% of whose valence electrons are excited into the conduction band) immediately prior to and during subpicosecond melting of its crystal lattice were recorded in this experiment. The melting process proceeded on time scales (hundreds of femtoseconds) comparable to the period of the vibrations in the LO phonon (70 fs). This circumstance forces Shank *et al.*[16] to pose the serious conceptual question about what should be understood by melting over such short time intervals. Of course, the question formulated in Sec. 1 regarding the existence (or absence) of thermodynamic equilibrium in the phonon subsystem in such short time intervals also remains open.

It should be pointed out, however, that, as in the case of the earlier results obtained by Auston[81,82] and other data from linear optical spectroscopy, the data in Ref. 16 can also be interpreted from the viewpoint of the "plasma" model of ILA[32] (see Sec. 1.1). To give a more unequivocal answer to this question, data from nonlinear-optical spectroscopy, which carries structural information (see Sec. 2.3), must be invoked.

A large volume of experimental data on the picosecond stage of ILA of Si and Ge surfaces was collected in the works of Bloembergen *et al.*,[39,84,86–90] who also used the technique of measuring the changes in the optical reflection by the annealed surface.

Together with optical reflection, diagnostics of the ILA process is also performed by measuring the temporal behavior of the optical transmission of thin semiconducting films under conditions of impulsive laser action. The interpretation of the transmission data evidently requires a knowledge of the distribution of the absorption coefficient both along the direction of propagation of the probing beam and along the radius. It is clear that these data are by no means always accessible, so that errors can arise in the interpretation of the transmission data. Thus the assertion made in Ref. 91 based

on transmission data for thin Si films that melting does not occur in ILA turned out to be incorrect (see Refs. 92–94).

2.1.2. Raman and Mandel'shtam-Brillouin scattering of light by laser-excited surfaces of semiconductors

The measurements of the temperature of the Si surface subjected to ILA with the help of spontaneous Raman scattering (RS) of light, carried out by Compaan *et al.*,[95,96] gave rise to substantial disagreements and a long-standing controversy. In these experiments the ratio of the intensities of the Stokes I_s and the anti-Stokes I_{as} components of RS by the 522-cm^{-1} mode of the crystalline silicon, which serves as a measure of the degree of heating of the substance under study, was measured. The lattice temperature can be determined from the following formula[61,63]:

$$\frac{I_s}{I_{as}} = C\frac{n+1}{n} = Ce^{\hbar\Omega/kT}, \tag{2.2}$$

where n is the occupation number of the phonon modes, Ω is the frequency of the phonon studied, T is the lattice temperature,

$$C = \left(\frac{\omega_s}{\omega_{as}}\right)^3 \frac{\sigma_s}{\sigma_{as}} \frac{\alpha+\alpha_{as}}{\alpha+\alpha_s}, \quad \omega_s = \omega - \Omega, \ \omega_{as} = \omega + \Omega \tag{2.3}$$

are the frequencies of the Stokes and anti-Stokes components of the RS, respectively; σ_s (σ_{as}) are the cross sections for the Stokes (anti-Stokes) RS; and, α, $\alpha_{s,as}$ are the coefficients of absorption at the frequencies ω, ω_s, and ω_{as}, respectively.

The first measurements of the lattice temperature using this technique[95,96] gave the value $T \lesssim 700$ K, i.e., much lower than the melting temperature of Si ($T_{melt} \simeq 1680$ K), for $W \approx 0.3$–0.4 J/cm^2, which obviously exceeds the threshold of the ILA effect. These results were later questioned by a number of authors,[63,64,87,97] and a repeat experiment by von der Linde and Wartmann[62,63] initially gave a much higher value of T, equal to or exceeding the value of T_{melt} for silicon. Later more accurate measurements by Compaan's group[61,65] and then a combined experiment by Compaan and von der Linde[66] gave results which were close to the initial data obtained by Compaan's group, i.e., they gave a value of the surface temperature of a Si sample subjected to ILA which was two times lower than the melting temperature under normal conditions. Later, however, it was acknowledged that if all sources of error are correctly taken into account, then a surface temperature during ILA close to the melting temperature is obtained.[212]

The main difficulties in the experiments on the determination of T from the RS spectra are linked to the required high spatial and temporal resolution of the experiment, the determination of the factor C in the formula (2.2), and the temperature dependence of the position of the RS lines.

We already pointed out in Sec. 1 that most experimental data, including direct measurements of the surface temperature from measurements of the velocities of the evaporated atoms[53] and scattering of x-rays,[54,55] unequivocally indicate that the Si surface melts during ILA. It should be noted, however, that phonons from the center of the Brillouin zone, with practically zero wave vectors, are manifested in the RS, while melting proceeds primarily with the participation of mainly short-wavelength phonons from the periphery of the first Brillouin zone; the latter phonons can be "hot" enough for Lindemann's criterion (1.8) for melting of the lattice to hold, while the former phonons, owing to the supposed nonequilibrium state of the phonon subsystem (see Sec. 1.1), remain relatively cold.

To clarify this situation, data from active Raman-scattering spectroscopy with high temporal and spectral resolution could be very useful (see Refs. 21, 214).

Mandel'shtam-Brillouin scattering spectra, under conditions of significant excitation of the surface layers of a semiconducting crystal owing to direct interband absorption of laser radiation, also exhibit anomalies in a number of cases. A marked increase in the ratio of the anti-Stokes and Stokes components of Mandel'shtam-Brillouin scattering by surface acoustic waves in GaAs accompanying an increase in the intensity of argon laser radiation used to excite the spectra was observed by Schmidt and Dansfeld.[98] The observed growth was too strong to be attributed solely to an increase in the lattice temperature accompanying an increase in the absorbed optical radiation energy. The effect could be linked to the stimulated generation of acoustic phonons accompanying indirect transitions into the region of optical absorption decreasing with frequency.[99]

2.1.3. Optical recording of the periodic change in the surface structure and relief

Interference impulsive laser annealing (ILA),[49,100] realizable with two crossed coherent light beams, produces a periodic sequence of crystalline (annealed) and amorphous (unannealed) sections in the surface layer of the semiconductor. This artificial periodic surface structure, easily observed by the diffraction of the probing optical beam incident on it, is a convenient tool for investigating the conditions of epitaxial growth of crystalline surface layers forming with ILA; it enables very accurate determination of the threshold values of the energy density and depth of the crystallization layer. The formation of such a structure and its basic characteristics can be easily described on the basis of the usual thermal model of ILA.[101]

At the same time, the conditions of ILA can be easily controlled by changing the spacing of the interference pattern formed by the annealing beams and by changing the parameters of the laser radiation, in particular, it is possible to create significant temperature gradients along the surface.[102,103]

This technique enabled Alferov *et al.*[103] to observe, aside from the main amorphous ring, an additional amorphous ring around the section of GaAs irradiated with a picosecond laser pulse and to attribute it to the manifestation of a new, previously unknown, phase of the GaAs crystal.

The observation of a diffraction pattern from the probing beam in the far field on the periodically disturbed relief of the surface has become in recent years the standard method for recording such perturbations, forming spontaneously on

the surfaces of solids under the action of powerful laser radiation (this method was first used for these purposes in Refs. 104 and 180; see Sec. 3).

2.2. Nonlinear-optical diagnostics of laser-induced phase transitions on a semiconductor surface; generation of optical harmonics and combination frequencies in reflection

2.2.1. Nonlinear optical diagnostics of the surface

Substantially new information on the state of the surface layers can be obtained from an analysis of their nonlinear response, manifested in nonlinear reflection, i.e., in the appearance of optical harmonics and combination frequencies in the reflected light beam. The physics of the phenomenon is quite simple (see below, Fig. 6).

Optical harmonics and combination frequencies, which are absent in the spectrum of the laser beam incident on the interface, appear in the reflected light because of the uncompensated "backwards" radiation of optically induced oscillators from the boundary layers of the nonlinear medium. Because of the nonlinearity of the oscillators in the reflecting medium the "backwards" reradiated field, which in classical optics gives rise to the usual "Fresnel" reflection, contains, in addition to the frequency components initially present in the spectrum of the incident field, also new spectral components with multiple and combination frequencies.

We should mention that the general regularities of nonlinear reflection described above were established more than 20 years ago.[105]

In Ref. 18 we called attention to the fact that the *anisotropy and nonlocal nature of the nonlinear response* of the surface layer (in many cases they are important under conditions when the linear response is isotropic and local) are sources of unique information on the fine details of the crystalline structure. Subsequent work showed that nonlinear optical methods are extremely informative and fast and have high spatial resolution.

The application of modern means for filtering and accumulating weak optical signals as well as the use of high-intensity pico- and femtosecond pulses, following with high frequency one after another, now enable recording easily and reliably the nonlinear optical response of a surface and using it to obtain structural information about the surface under study (which is often, inaccessible to linear optical methods).

These effects are now used for the observation of molecular layers adsorbed on the surfaces of solids, surface excitations, and their interaction with one another and with volume electromagnetic waves.[106–112]

In a series of studies,[18,113,114] carried out in our laboratory, the phenomenon of second-harmonic generation (SHG) in reflection from the surface of a noncentrosymmetrical gallium arsenide crystal (class $\bar{4}3$ m) was first used to study the dynamics of ILA. In its simplest variant the essence of the proposed method consists of the following: the surface layer of the crystal becomes centrosymmetrical as a result of melting (or being rendered amorphous by ion implantation) and therefore does not make a dipole contribution to the reflected second harmonic. Restoration of the crystalline lattice during the ILA process causes the appearance of the reflected wave of the second harmonic of the probing radiation. Measurement of the intensity of this second harmonic as a function of time enables studying the dynamics of recrystallization of the surface of the sample during ILA. Analysis of the polarization characteristics of the second harmonic enables extraction of information on the quality of the amorphous and restored crystalline lattice, while measurement of the time dependence of SHG gives information on the dynamics of phase transformations of the crystal surface accompanying ILA.

Soon after the publication of our first results on SHG in GaAs[18] (see also the note in Ref. 128) studies in which SHG was observed in reflection from the centrosymmetrical Si crystal under conditions of strong excitation close to ILA appeared.[129,130] The effect was interpreted in Ref. 130 (apparently incorrectly) in terms of a change in the symmetry of the crystal and the generation of Fresnel excitons. Shank *et al.*,[126] who correctly interpreted the SHG in Si as the manifestation of the nonlocal nonlinearity of a quadrupole type (see Sec. 2.3.4), used this effect for the diagnostics of structural changes of the surface during the first phase of ILA—melting of the surface layer—on a subpicosecond time scale. Very recently the anisotropy of the nonlinear response of the "reconstructed" silicon surface was used to study phase transitions on the surface.[154]

2.2.2. Theory of generation of optical harmonics in reflection. Nonlinear surface source

The starting point for the theoretical analysis of nonlinear reflection are Maxwell's equations with the corresponding nonlinear sources and boundary conditions, taking into account the continuity of the tangential components of the field at the interface.[115–118]

Neglecting the magnetic dipole contribution, we can, by using the definition in Ref. 118, write down for the components of the volume nonlinear polarization vector P^{NL} the following expression:

$$P_i^{NL} = N\left(\langle d_i\rangle_{av} - \nabla_j \langle Q_{ij}\rangle_{av}\right), \tag{2.4}$$

where

$$d_i = -ex_i, \quad Q_{ij} = -\frac{1}{2} ex_i x_j$$

are, respectively, the components of the dipole vector and the quadrupole-moment tensor, arising in each unit cell in the volume of the crystal under the action of the optical field; the angular brackets $\langle ...\rangle_{av}$ indicate averaging over all electrons in the cell; N is the total number of unit cells per unit volume; the gradient operator, ∇_j, operates along the coordinate X_j, which gives the position of the selected cell; $x_{i,j}$ characterizes the part of the relative displacement of the electrons which is nonlinear in the field within one cell. Here and below repeated indices are summed over from 1 to 3.

The expansion of the source in powers of the field of the incident wave has the form

$$P_i^{NL} = P_i^{(2)} + P_i^{(3)} + \dots, \tag{2.5}$$

$$P_i^{(2)} = \chi_{ijk}^{(2)D} E_j E_k + \frac{1}{2}\chi_{ijkl}^{(2)Q} \nabla_j E_k E_l, \tag{2.6}$$

$$P_i^{(3)} = \chi_{ijkl}^{(3)D} E_j E_k E_l + \frac{1}{3} \chi_{ijklm}^{(3)Q} \nabla_j E_k E_l E_m; \quad (2.7)$$

here E_j and E_k are the components of the electric field vector of the incident light wave; $\chi_{ijk}^{(2)D}$, $\chi_{ijkl}^{(3)D}$ are the tensors of the dipole and $\chi_{ijkl}^{(2)Q}$, $\chi_{ijklm}^{(3)Q}$ are the tensors of the quadrupole quadratic and cubic susceptibilities, respectively:

$$N \langle d_i \rangle_{av} = \chi_{ijk}^{(2)D} E_j E_k + \chi_{ijkl}^{(3)D} E_j E_k E_l + \ldots,$$

$$N \langle Q_{ij} \rangle = -\frac{1}{2} \left(\chi_{ijkl}^{(2)Q} E_k E_l + \chi_{ijklm}^{(3)Q} E_k E_l E_m + \ldots \right). \quad (2.8)$$

The tensors $\chi_{ijk}^{(2)D}$, $\chi_{ijkl}^{(2)Q}$, $\chi_{ijkl}^{(3)D}$,... describe the properties of the medium giveing rise to the corresponding "volume" nonlinear optical response. According to Neumann's crystallographic principle, the symmetry of these tensors and, therefore, the number and mutual coupling of their nonzero components, are determined by the point symmetry group of the crystal. The general symmetry rules are the same for tensors with the same rank, so that, for example, the crystallographic "selection rules" for the components of the tensors $\chi_{ijkl}^{(2)Q}$ and $\chi_{ijkl}^{(3)D}$ are the same. And, vice versa, the information about the crystalline structure which can be obtained by determining the symmetry of the last two tensors is, generally speaking, the same.

In what follows we shall require data on the structure of the nonlinear susceptibility tensors of a number of cubic crystals, belonging to the centrosymmetric class $m3m$ (to which crystalline silicon and germanium belong) and the noncentrosymmetric class $\bar{4}3m$ (to which gallium arsenide and gallium phosphide as well as other crystals belong). According to Refs. 119 and 120 we have:

a) *the class m3m*: 1) all $\chi_{ijk}^{(2)D} = 0$. 2) Twenty-one of the 81 components of the tensors of rank 4 $\chi_{ijkl}^{(3)Q}$ and $\chi_{ijkl}^{(3)D}$ differ from zero, and of these only four are independent. In terms of the principal crystallographic axes these components have the form

$$\chi_{1111} = \chi_{2222} = \chi_{3333}, \quad \chi_{1122} = \chi_{iijj}, \quad (2.9)$$
$$\chi_{1212} = \chi_{ijij}, \quad \chi_{1221} = \chi_{ijji},$$

where $i = j$ and $i, j = 1,2,3$. The quantity $\zeta_{Q,D}$

$$\zeta_{Q,D} = \chi_{1111}^{Q,D} - (\chi_{1122}^{Q,D} + \chi_{1212}^{Q,D} + \chi_{1221}^{Q,D}) \quad (2.10)$$

is the parameter of the nonlinear optical anisotropy (in linear optics these crystals are isotropic), since in an isotropic medium this quantity vanishes for both dipole and quadrupole nonlinearities.

b) *The class* $\bar{4}3m$: 1) The dipole quadratic susceptibility has one independent component

$$\chi_{123}^{(2)D} \neq 0 \quad (2.11)$$

and five more components, obtained by permuting the indices, equal to it. 2) The tensors of rank four have the same structure as in the class $m3m$.

In the expansion (2.6) and (2.7) the quadrupole terms, as a rule, are much smaller than the dipole terms. An important exception are crystals with a center of inversion and isotropic media, where all $\chi_{ijk}^{(2)D} = 0$ and for this reason the effects which are quadratic in the field, for example SHG, are described by the quadrupole (as well as dipole surface (see below)) terms.

It is clear that the symmetry of the surface of a crystal differs from that of the "volume" part of the crystal (even without taking into account the unavoidable "restructurings" and the appearance of adsorbed layers), so that "surface"terms with an analogous structure must, generally speaking, be added to the expansion (2.6). We shall assume that these terms correspond to the contribution of a thin (several atomic layers thick) nonrestructured surface section of the crystal to the nonlinear polarization. The symmetry group of this layer is evidently a subgroup of the point symmetry group of the entire crystal.

Taking into account this circumstance the expression for the polarization which is quadratic in the field assumes the following form:

$$P_i^{(2)} = \chi_{ijk}^{(2)D} E_j E_k + \chi_{ijk}^{(2)Ds} E_j E_k + \frac{1}{2} \chi_{ijkl}^{(2)Q} \nabla_j E_k E_l + \frac{1}{2} \chi_{ijkl}^{(2)Qs} \nabla_j E_k E_l + \ldots \quad (2.6')$$

Here the susceptibilities marked with the index s describe the surface contribution, and their symmetry is fixed by the surface structure. In most cases this contribution can be neglected compared to the volume contribution, but in the particular case of a centrosymmetric medium this cannot be done, because the dipole surface and quadrupole volume contributions to the quadratic polarization may turn out to be comparable (for example, in silicon—see below and Ref. 19), while the dipole volume contribution, as already pointed out, vanishes.[1)]

In centrosymmetrical crystals of class $m3m$ all crystallographic faces also have a center of symmetry,[121] so that all components of $\chi_{\xi\eta\delta}^{(2)Ds}$, where the indices ξ, η, δ enumerate the axes lying in the reflection plane, vanish. Only some of the components, for which one or three of the indices ξ, η, and δ refer to the axis perpendicular to the face under study differ from zero. We introduce for these nonzero components the following notation:

$$\chi_{\perp\perp\perp}^{(2)Ds}, \quad \chi_{\perp\parallel\parallel}^{(2)Ds}, \quad \chi_{\parallel\perp\parallel}^{(2)Ds}, \quad \chi_{\parallel\parallel\perp}^{(2)Ds}, \quad (2.12)$$

where the symbols $\perp$, $\parallel$ correspond to the direction of polarization perpendicular or parallel to the face under study—the reflection plane, respectively.

The nonlinear surface source described by the susceptibilities (2.12) is evidently insensitive to the orientation of the crystallographic axes relative to the plane of incidence.

In concluding this section, we shall present expressions which are more compact than (2.6) and (2.7) and which will be used below for the quadratic polarization $P^{(2)}(2\omega)$ at the frequency of the second harmonic (SH) of the incident monochromatic field $\mathbf{E} = (1/2)\mathbf{E}_0 e^{-i\omega t} + \text{c.c.}$ and for the cubic volume dipole polarization $P_i^{(3)D}(3\omega)$ at the frequency of the third harmonic (TH) of the same field in cubic crystals and isotropic media. From the definitions (2.6) and (2.7) and using (2.8) and (2.10), we obtain the following expression in the principal crystallographic system of coordinates of centrosymmetrical cubic crystals $m3m$ for the quadrupole volume polarization:

$$P_i^{(2)Q}(2\omega) = \frac{1}{2} \chi_{ijkl}^{(2)Q} \nabla_j E_k E_l = \chi_{ijkl}^{(2)Q} E_j \nabla_k E_l$$

$$=\zeta_Q E_i \nabla_i E_i + \chi^{(2)Q}_{1122} E_i (\nabla E) + \frac{1}{2}\chi^{(2)Q}_{1212} \nabla_i (EE) + \chi^{(2)Q}_{1221} (E\nabla) E_i. \quad (2.13)$$

In (2.13) the second and fourth index in $\chi^{(2)D}_{ijkl}$ correspond to the frequency ω of the optical field, while the third index corresponds to the differentiation operation. For dipolar cubic polarization at the frequency of the TH in cubic classes $m3m$ and $\bar{4}3m$ we have:

$$P^{(3)D}_i (3\omega) = \zeta_D E_i^3 + (\chi^{(3)D}_{1122} + \chi^{(3)D}_{1212} + \chi^{(3)D}_{1221}) E_i (EE). \quad (2.14)$$

In (2.13) and (2.14) summation over the repeated index i is not performed. The expressions (2.13) and (2.14) are also valid for isotropic media, if we set $\zeta_{Q,D} = 0$.

Instead of the quadrupole susceptibilities $\chi^{(2)Q}_{ijkl}$ in isotropic media and cubic crystals a set of different parameters β, γ, and δ is sometimes introduced[19,116]

$$\beta = \chi^{(2)Q}_{1122}, \quad \gamma = \frac{1}{2}\chi^{(2)Q}_{1212}, \quad \delta - \beta - 2\gamma = \chi^{(2)Q}_{1221}. \quad (2.15)$$

Evidently, in an isotropic medium $\delta = \chi^{(2)Q}_{1111}$. In addition, in an isotropic nonconducting medium, as Bloembergen *et al.* showed,[116] in the low-frequency limit (i.e., for $\omega \ll E_g/\hbar$, where E_g is the gap width) the following relations hold:

$$\beta = -2\gamma = \frac{3}{4Ne} (\chi^{(1)D}(\omega))^2, \quad \delta = 0, \quad (2.16)$$

where $\chi^{(1)D}(\omega)$ is the linear (dipole) susceptibility of the medium and N is the density of the valence electrons.

2.2.3. Field of the reflected second and third harmonics, generated by a nonlinear source

Let a plane wave with frequency ω be incident at an angle θ from the vacuum on the flat boundary of a solid. We choose the coordinate system so that the boundary coincides with the plane $z = 0$ and the plane of incidence coincides with the plane $y = 0$; the substance occupies the half-space $z \leqslant 0$. Then the incident light wave is described by the vector

$$E_{in} = \frac{1}{2} e_{in} E \exp\left(-\frac{i\omega}{c} z\cos\theta - \frac{i\omega}{c} x \sin\theta\right) \times \exp(-i\omega t) + \text{c.c} = \frac{1}{2} e_{in} E \exp(ik_z z + ik_x x - i\omega t) + \text{c.c} \quad (2.17)$$

and

$$e_{in} = (\cos\theta\cos\varphi,\ \sin\varphi,\ -\sin\theta\cos\varphi), \quad (2.18)$$

where φ is the angle between the plane of incidence and the polarization vector of the incident wave. The "linear" transmitted and reflected waves are described by the usual Fresnel formulas.

The wave passing into the crystal generates in it a nonlinear polarization in accordance with the expansion (2.5)–(2.7). The polarization dependence of the signal of the reflected SH (TH) is determined from the fact that the amplitude of the harmonic wave is proportional to the projection of the vector of the nonlinear source on the direction of polarization of the recorded harmonic. The final form for the field of the reflected harmonic E_H (with frequency ω_H) is as follows[19]:

$$E_{H,s} = (E_H)_y = i\frac{4\pi\omega_H^2}{c^2(k_{1z}+k_{2z})} P^{NL}_y(\omega_H); \quad E_{H,p} = i\frac{4\pi\omega_H^2 k_1}{c^2(k_2^2 k_{1z}+k_1^2 k_{2z})} (k_{2x}P^{NL}_z + k_{2z}P^{NL}_x); \quad (2.19)$$

where the symbols s and p on the amplitudes of the harmonic fields refer to s ($\varphi = \pi/2$) and p ($\varphi = 0$) polarization of these fields; the indices 1 and 2 on the wave vectors of the harmonics correspond to the vacuum (2.4) and the nonlinear medium (2.5):

$$k_1 = \frac{\omega_H}{c}, \quad k_2^2 = \left(\frac{\omega_H}{c}\right)^2 \varepsilon(\omega_H).$$

In the simplest case of the generation of the second harmonic in reflection from a noncentrosymmetric crystal the volume dipole source quadratic in the field—the first term in the expansion (2.6) makes the determining contribution to the nonlinear polarization $P^{NL}(2\omega)$ on the right side of Eq. (2.19) (see Refs. 105, 118, 122). Information on the structure of the crystalline surface in this case is contained in the dependence of the intensity of the SH on the direction of polarization of the incident radiation relative to the plane of incidence, $I_{SH}(\varphi)$, and on the orientation of the crystal axes relative to the same plane, $I_{SH}(\psi)$.

For example, SHG in reflection from the (100) plane of crystals belonging to the class $\bar{4}3m$ (GaAs, GaP), in which only the quadratic dipole susceptibility is nonvanishing (see (2.11)), is characterized by the following dependence on φ and ψ—the angles between the plane of incidence and the [010] axis:

$$I_{SH}(\varphi,\psi) \sim (\mathbf{P}^{(2)D}, \mathbf{e}_s)^2 \sim |\chi^{(2)D}_{123}|^2 \,|\cos\theta\cos 2\psi(1+\cos 2\varphi) - \sin 2\varphi \sin 2\psi|^2, \quad (2.20)$$

$$I_{SH}(\varphi,\psi) \sim (\mathbf{P}^{(2)D}, \mathbf{e}_p) \sim |\chi^{(2)D}_{123}|^2 \,|\cos\theta \sin 2\psi + \cos 2\varphi(\cos\theta\sin 2\psi - \cos 2\psi)|^2; \quad (2.21)$$

where $\mathbf{e}_p$, $\mathbf{e}_s$ are unit p (in the plane of incidence) and s (perpendicular to the plane of incidence) polarization vectors and θ is the angle of refraction.

For a strictly s or p polarized wave at the fundamental frequency the dependence $I_{SH,s,p}$ reflects the symmetry of the (100) plane.

Second-harmonic generation in reflection from a centrosymmetric crystal or an isotropic medium is a much less efficient process, since it is determined either by the relatively weak volume quadrupole susceptibilities or by the dipole susceptibilities of several surface atomic layers.

We note first that as follows from (2.10) and (2.16) the SH signal in reflection from an isotropic medium is polarized in the plane of incidence both for s and p polarized waves at the fundamental frequency.

An analogous result also follows from the explicit form of the dependence $E_{SH,s}(\varphi)$, which we do not present here because of its cumbersomeness (see, for example, Eq. (34) in Bloembergen *et al.*[116]).

TABLE II. Dependence of the intensity of the reflected second (SH) and third (TH) harmonics on the angle ψ of rotation of the crystal around the normal to the surface (cubic crystal of class $m3m$).

Surface of the crystal from which the reflection occurs	Polarization of the incident wave	Polarization of the harmonic	The dependence $I_{SH} = I_{SH}(\psi)$	The dependence $I_{TH} = I_{TH}(\psi)$
(100)	p	s	$\lvert\zeta_Q\rvert^2 \sin^2 4\psi$	$\lvert\zeta_D\rvert^2 \sin^2 4\psi$
	s	s	$\lvert\zeta_Q\rvert^2 \sin^2 4\psi$	$\lvert\zeta_D \cos 4\psi + 4\chi_{1111}^{(3)D} - \zeta_D\rvert^2$
	s	p	$\lvert\zeta_Q \cos 4\psi + 8\chi - \zeta_Q + a\chi^s\rvert^2$	$\lvert\zeta_D\rvert^2 \sin^2 4\psi$
	p	p	$\lvert\zeta_Q \cos 4\psi + b\chi + c\zeta_Q + d\chi^s\rvert^2$	$\lvert\zeta_D \cos 4\psi + q\zeta_D + e\chi_{1111}^{(3)D}\rvert^2$
(111)	p	s	$\lvert\zeta_Q\rvert^2 \sin^2 3\psi$	$\lvert\zeta_D\rvert^2 \sin^2 3\psi$
	s	s	$\lvert\zeta_Q\rvert^2 \sin^2 3\psi$	$\left\lvert \chi_{1111}^{(3)D} - \frac{1}{2}\zeta_D \right\rvert^2$
	s	p	$\lvert\zeta_Q \cos 3\psi + f\zeta_Q + g\chi + h\chi^s\rvert^2$	$\lvert\zeta_D\rvert^2 \sin^2 3\psi$
	p	p	$\lvert\zeta_Q \cos 3\psi + k\zeta_Q + l\chi + m\chi^s\rvert^2$	$\lvert\zeta_D \cos 3\psi + n\zeta_D + r\chi_{1111}^{(3)D}\rvert^2$

1) The coefficients $a, b, c, \ldots$ are functions of the angle of refraction θ. 2) The general factors depending solely on the angle θ are not written out in the formulas. 3) χ^s denotes the linear combination of the susceptibilities $\chi_{\perp\|\|}^{Ds}, \chi_{\perp\perp\perp}^{Ds}, \chi_{\|\perp\|}^{Ds}, \chi \equiv \chi_{1212}^{(2)Q}$.

Thus the appearance of an s polarized component in the wave of the second harmonic reflected from a centrosymmetric crystal at $\varphi = 0$ or $\varphi = \pi/2$ must be attributed entirely to the anisotropy of its quadrupole susceptibility: $E_{SH,s} \sim \zeta_Q$.

The anisotropy of the quadrupole quadratic (and also the dipole cubic) susceptibility has another manifestation. The nonvanishing of the parameters ζ_Q (ζ_D) gives rise to the appearance of a dependence of the SH (TH) intensity on the orientation of the crystal relative to the plane of incidence, i.e., a dependence of the form $I_{SH,TH} = I_{SH,TH}(\psi)$. It is clear that there is no such dependence in reflection from an isotropic medium.

The results of the calculation of the dependences $I_{SH}(\psi)$, $I_{TH}(\psi)$ for cubic centrosymmetrical crystals of class $m3m$ in reflection from the (100) and (111) planes in different polarization configurations are summarized in Table II.

It is evident that the dependences $I_{SH}(\psi)$, $I_{TH}(\psi)$ reflect the symmetry of the surface from which the nonlinear reflection occurs.

In discussing the probing of the state of the surface of a crystal with the help of nonlinear optical reflection we have thus far ignored the question of the depth of the surface layer contributing to the reflected harmonic, i.e., the depth of penetration of the probe into the material under study.

To give a quantitative answer to this question it is necessary to solve the problem of generation of a harmonic in reflection from a thin layer of a crystal taking into account the transmission of the incident wave into the layer and reflection of the wave from the back face, and then let d—the thickness of this layer—approach infinity and determine the values of $d > d_0$ for which the result is independent of the thickness. The answer lies in the fact that in reflection from a transparent or weakly absorbing medium, in which volume nonlinear (dipole or quadrupole) polarization predominates, $d_0 \approx \lambda / 4\pi\eta$, where λ is the probing wavelength.[122] If the reflection occurs from a strongly absorbing medium, then

$$d_0 \approx \alpha_\omega^{-1} + \alpha_H^{-1} \qquad (2.22)$$

where α_ω, α_Γ ($\gg \lambda^{-1}$) are the coefficients of absorption of the waves at the fundamental frequency and at the harmonic frequency, respectively. This result can be easily interpreted, since the reflected harmonic is generated by the radiation from nonlinear oscillators of the second medium backwards into the linear medium. In the presence of absorption at fundamental and (or) harmonic frequencies, however, the oscillators lying at depths below the surface exceeding (2.22) cannot contribute to the reflected signal.

The foregoing discussion refers to the volume contribution to the reflected harmonic, since, as already pointed out, the depth of the layer giving rise to the "surface" nonlinear dipole response is equal only to several lattice constants.

Although everywhere here we have thus far, for definiteness, talked about the generation of harmonics in reflection, all the basic results of the analysis can be easily transferred to the case of generation of the sum (SFG), difference (DFG), and combination optical frequencies in those situations, when the incident light field contains two or more frequency components. The main difference in the last case from SHG and THG lies in the possibility of fixing different polarization states by different spectral components of the pump field, as well as in the possibility of selecting a more desirable frequency range in which the surface is probed and the signal is recorded.

A particular case of generation of the sum (or combination) frequency is the observation of the volume dipole second harmonic in reflection from centrosymmetric metals and semiconductors in the presence of a static electric field.[124,125] Actually, in these experiments the process of mixing of three frequencies of the following form occurs: $2\omega = \omega + \omega + 0$, where 0 corresponds to the "frequency" of the static field. On the surface of centrosymmetric media this process is described by the dipole cubic susceptibilities $\chi_{ijkl}^{(3)D}(2\omega; \omega, \omega, 0)$ (compare (2.7)).

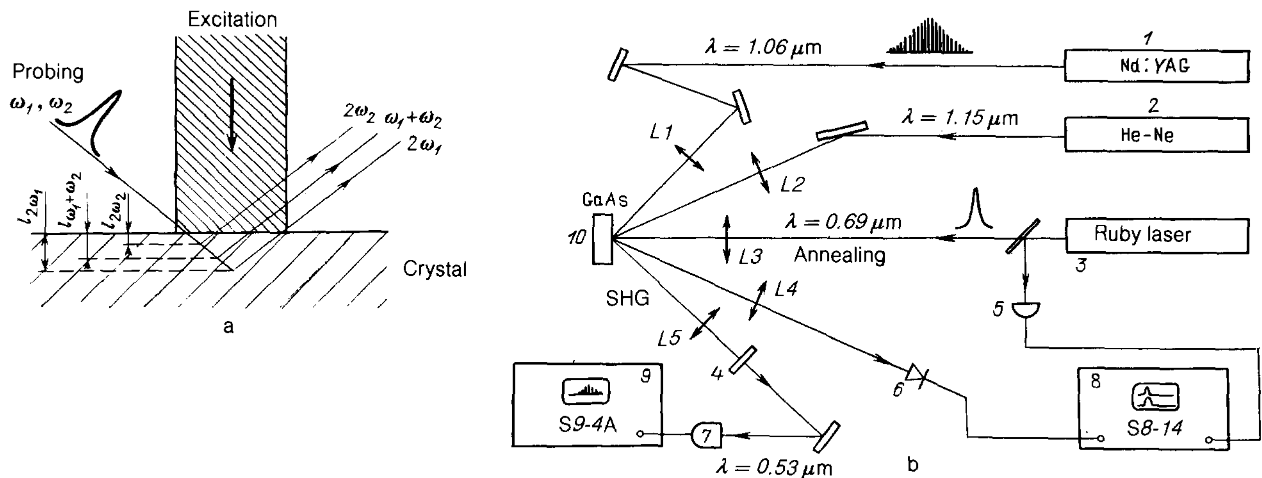

FIG. 6. a) General scheme for recording the nonlinear optical response of a semiconductor surface subjected to pulsed laser action. The probing was performed by weak optical pulses (which do not affect the excitation process) with frequencies ω_1 and ω_2 (it is assumed that $\omega_1 > \omega_2$; in the simplest degenerate case $\omega_1 = \omega_2$); the signals of the second optical harmonic ($2\omega_1, 2\omega_2$) and the sum frequency ($\omega_1 + \omega_2$) carry information on surface layers of different thickness: $l_{2\omega_1} = \alpha^{-1}(2\omega_1) \leqslant l_{\omega_1+\omega_2} = \alpha^{-1}(\omega_1 + \omega_2) \leqslant l_{2\omega_2} = \alpha^{-1}(2\omega_2)$. b) Block diagram of the experiment studying the dynamics of pulsed laser annealing of a gallium arsenide surface by recording in real-time the reflected second harmonic.[18] 1) Nd:YAG laser with active mode-locking and acoustooptical Q-switching; 2) He-Ne laser; 3) ruby laser with electrooptical Q-switching; 4) set of SZS-21 filters; 5) coaxial FK-20 photocell; 6) LFD-2A avalanche photodiode; 7) 18 ÉLU-FM fast photomultiplier; 8) S8-14 oscillograph (200 MHz bandwidth); 9) S9-4A oscillograph (350 MHz bandwidth); 10) GaAs sample.

2.3. Study of the states and fast phase transformations of semiconductor surfaces with the help of the generation of optical harmonics and sum frequencies in reflection

2.3.1. Experiments on SHG in reflection for the study of the dynamics of ILA of GaAs

The block diagram of the experimental arrangement[18] intended for studying the dynamics of ILA of a GaAs surface is shown in Fig. 6.

The annealing was carried out with ruby pulses ($\tau_p \approx 30$ ns); a uniform distribution of the intensity over the transverse cross section of the beam was obtained with the help of a special forming system, consisting of a frosted plate and systems of lenses and diaphragms.

The probing laser was a Nd:YAG laser with simultaneous acoustooptical Q-switching and mode-locking of the longitudinal modes. The laser generated a train of 40 pulses with a duration of 0.3 ns each and a repetition period of 9.5 ns. The beam was amplified (approximately tenfold) in a single-pass amplifier. The total energy of one "packet" of subnanosecond pulses (a typical oscillogram of which is shown in Fig. 7d) did not exceed 1 mJ.

The annealing pulse and the train of probing pulses were synchronized in time by means of electrical synchronization of the corresponding Q switches.

The radiation from a continuous helium-neon laser with a wavelength of $\lambda = 1.15\,\mu$m was used to record at the same time the phase of high reflection (PHR).

The SH signal, arising in reflection of the probe beam from the surface of the sample, was recorded with the help of a fast photomultiplier (18 ÉLU-FM) and an S9-4A oscillograph with a transmission band of 350 MHz. An S8-14 two-beam storage oscillograph was used to obtain a time scan of the PHR as well as to determine the relative position of the reflected and probing pulses in time.

Gallium arsenide ($1\bar{1}0$)-cut samples were used. The annealing beam was incident along the normal to the surface, and the probing beam formed an angle of 45° with the normal.

The results of the experiments are illustrated in Fig. 7, which shows the oscillograms of the annealing (a) and probing (d) pulses, as well as the phases of high reflection (b, c)

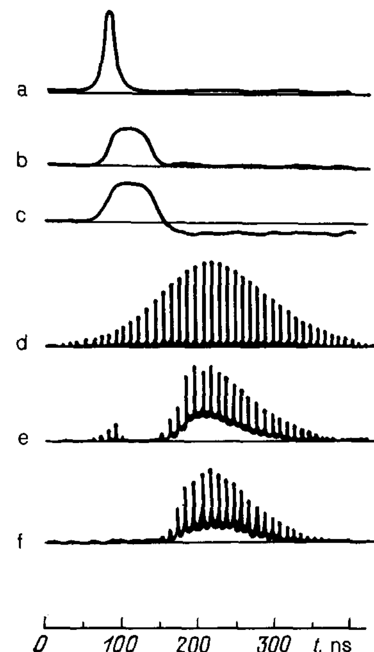

FIG. 7. Oscillograms of the annealing ruby-laser pulse (a), of the reflected probe pulses (b, c), of the probing pulse (d), and of the SH pulses (e, f) from the unimplanted (b, e) and implanted (c, f) sections of the (110) surface of the GaAs crystal.[18] The sweeps in all oscillograms are synchronized.

and the SH signal for the case of annealing of a single-crystalline and amorphous surface (e, f, respectively).

It is evident that the SH from a single-crystalline surface vanishes within a time equal to the duration of the leading edge of PHR, and is absent throughout the entire time interval of the PHR. This behavior of the SH is easily explained on the basis of the thermal model of ILA, if it is assumed that the reflection plateau corresponds to the liquid melted state of the semiconductor. Calculations show that in the competing plasma model of ILA the intensity of the SH should not drop off this much.

Indeed, let the PHR correspond to a dense electron-hole plasma (no melting). Then the following two factors will affect the change in the SH signal: 1) drop in the density of bound electrons n_0 making the main contribution to $\chi^{(2)}$ and 2) additional absorption of the probing radiation and of the SH signal (screening) by the carriers. We shall evaluate each of these factors.

The density n_0 for gallium arsenide is equal to

$$n_0 \approx 5\cdot 10^{23}\ \text{cm}^{-3}.$$

When an annealing pulse with the typical energy density $W = 0.4\ \text{J/cm}^2$ is absorbed in a layer with a thickness of $l_{abs} = 0.3\cdot 10^{-4}$ cm $n_e = W/l\varepsilon = 4\cdot 10^{22}$ electrons per cubic centimeter can be transferred into the conduction band (neglecting recombination); here $\varepsilon = 3\cdot 10^{-19}$ J is the energy of the photon with $\lambda = 0.69\ \mu$m. The density of bound electrons will be equal to $n_1 = n_0 - n_e$. Thus the relative decrease of the intensity of the SH will be equal to

$$\frac{I_1 - I_0}{I_0} = \left|\left(\frac{n_0 - n_e}{n_0}\right)^2 - 1\right| = \left|\left(1 - \frac{4\cdot 10^{22}}{5\cdot 10^{23}}\right)^2 - 1\right| \approx 0.16.$$

Screening has a stronger effect. To take screening into account we measured the coefficient of transmission of the probe radiation during the action of the annealing pulse. The transmission at $\lambda = 1.06\ \mu$m in the presence of the annealing ruby-laser pulse decreased by not more than 40%. We shall assume that this entire change is attributable to absorption by free carriers, created by the annealing ruby laser pulse in the surface region whose depth is determined by the coefficient of absorption of this radiation; $l_{pl} = (3\cdot 10^4\ \text{cm}^{-1})^{-1} \approx 300$ nm (Table III). From here it is possible to give the upper limit of the coefficient of additional "plasma" absorption of the probing radiation: $\alpha^{pl}_{1.06} \simeq 1.8\cdot 10^4\ \text{cm}^{-1}$. The change in the coefficient of absorption of radiation with $\lambda = 0.53\ \mu$m owing to the appearance of the plasma cannot be greater than this quantity for $\lambda = 1.06\ \mu$m, since $\alpha^{pl}_{\omega} \sim [(\omega/\gamma)^2 + 1]^{-1/2}$ where $\omega = 2\pi i/\lambda$ and γ is the electron collision frequency. Therefore

$$\alpha^{pl}_{0.53} \leqslant 1.8\cdot 10^4\ \text{cm}^{-1}.$$

Against the background formed by the main absorption by the bound electrons $\alpha^{b}_{0.53} = 5\cdot 10^4\ \text{cm}^{-1}$ (see Table III) this increase in absorption can decrease the intensity of the SH by not more than 50%, since

$$\frac{I_1}{I_0} \approx \left(\frac{\alpha^{b}_{0.53} + \alpha^{pl}_{0.53}}{\alpha^{b}_{0.53}}\right)^{-2} \approx 0.55.$$

Thus even the maximum drop in the intensity of the SH owing to screening by free carriers is equal to only 50%, while in the experiment the intensity drops by more than two orders of magnitude. This indicates that the main reason for the vanishing of the SH is the destruction of the symmetry of the crystal lattice, i.e., melting of the lattice.

To give a quantitative interpretation of the experimental results on SHG during ILA on the basis of the melting model, in Ref. 132 an analytical calculation of the intensity of the SH was undertaken taking into account multiple reflections (in analogy with the linear case[133]) in a layer of the melt with a thickness of $d(t)$ and using the boundary conditions[105]

$$I_{SH} = \text{const}\ |R_{SH}(t)|^2; \tag{2.23}$$

where

$$R_{SH} = \frac{\exp(i\Delta(2\omega, t) + 2i\Delta(\omega, t))}{[1 - r_{21}(2\omega)\, r_{23}(2\omega)\, e^{2i\Delta(2\omega, t)}]\,[1 - (r_{23}(\omega)\, r_{21}(\omega)\, e^{2i\Delta(\omega)})^2]}, \tag{2.24}$$

$$\Delta(x, t) = \frac{2\pi d(t)}{\lambda}(\varepsilon_2(x))^{1/2}, \quad \varepsilon_2(\omega) = \varepsilon_2' + i\varepsilon_2''$$

is the dielectric permittivity of the melt, $\lambda = 2\pi i/\omega$,

$$r_{\alpha\beta}(\omega) = \frac{(\varepsilon_\alpha(\omega))^{1/2} - (\varepsilon_\beta(\omega))^{1/2}}{(\varepsilon_\alpha(\omega))^{1/2} + (\varepsilon_\beta(\omega))^{1/2}},$$

and the indices α and β refer to the vacuum (1), the melt (2), and the crystal (3).

To calculate $I_{SH}(t)$ using the formula (2.23) it is necessary to know the dynamics of melting, i.e., the dependence $d(t)$. This dependence for GaAs is calculated in Ref. 132 on the basis of the numerical solution of the nonlinear heat-conduction equation with coefficients explicitly depending on the temperature (analogously to Refs. 40 and 41). The change in the coefficient of linear reflection by the surface at the pumping frequency during the ILA process was also taken into account (see the caption to Fig. 8c).

The results of the calculations are presented in Fig. 8. As is evident, under the action of a laser pulse with an energy of $W = 0.4\ \text{J/cm}^2$, the front of the melt moves rapidly into the bulk of the medium, reaches a maximum depth of the order of $6\cdot 10^{-5}$ cm, and returns again to the surface during the recrystallization process. Over the time that the front of the melt traverses a distance of the order of the thickness of the skin layer δ_{sk} (the time τ_{grow}) the coefficient of linear reflection increases approximately twofold, and then

TABLE III. Coefficients of optical absorption of crystalline and amorphous gallium arsenide (according to the data in Refs. 131 and 132).

λ, nm	α_{cryst}, cm^{-1}	α_{amorph}, cm^{-1}
1064,2	0,02	$5\cdot 10^3$
694,2	$2,7\cdot 10^4$	$1,5\cdot 10^5$
532,1	$8,09\cdot 10^4$	$3\cdot 10^5$
354,7	$7,14\cdot 10^5$	$7\cdot 10^5$

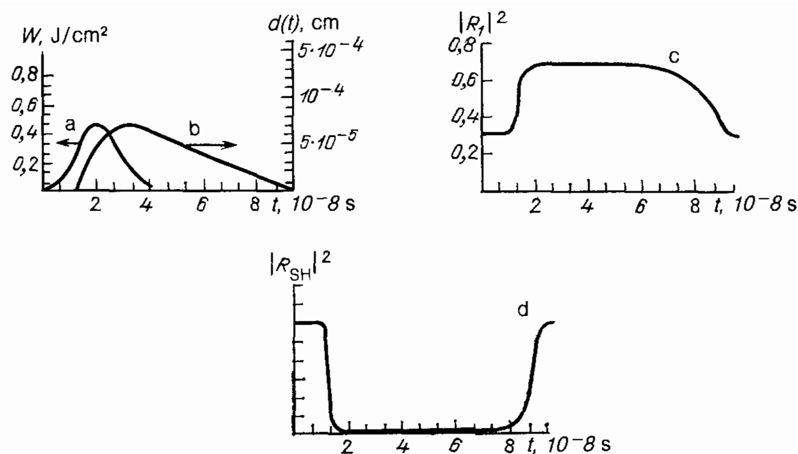

FIG. 8. Dynamics of impulsive laser annealing of GaAs (numerical calculation[132]). a) Laser pulse with $W = 0.14$ J/cm^2, $\tau_p = 20$ ns, $\alpha = 10^{-4}$ cm^{-1}. b) The thickness of the melt d as a function of time; c) coefficient of linear reflection as a function of time ($R_1(t) = [r_{12}(\omega) + r_{23}(\omega)e^{2i\Delta(\omega,t)}][1 + r_{12}(\omega)r_{23}(\omega)e^{2i\Delta(\omega,t)}]^{-1}$); d) SHG as a function of time (according to the formula (2.24)).

emerges onto a plateau (the phase of high reflection—PHR). The duration of the PHR is determined by the round-trip transit time of the melt front into the bulk of the crystal and back. The duration of the decay of the PHR $\tau_{\rm dec}$ is determined by the time required for the melt front to transverse a distance of the order of $\delta_{\rm sk}$. Setting $\delta_{\rm sk} = 20$ nm and estimating according to Fig. 8c $\tau_{\rm grow} \sim 5 \cdot 10^{-9}$ s, we obtain for the velocity of the melt front $v_{\rm dec} \sim 4 \cdot 10^2$ cm/s. Estimating also from Fig. 8c $\tau_{\rm dec} \sim 10^{-8}$ s, we obtain $v_{\blacklozenge} \sim 100$ cm/s for the estimate of the recrystallization velocity.

The efficiency of SH generation drops at the same time that the reflection coefficient increases during the motion of the melt front into the bulk of the crystal. During the subsequent recrystallization the initial efficiency of SHG is restored. The characteristic decay and growth times of the SH approximately coincide with $\tau_{\rm grow}$ and $\tau_{\rm dec}$. This is determined by the fact that in the formula (2.24) $2\Delta(\omega) \gg \Delta(2\omega)$, so that the dynamics of the SH as well as of the coefficient of the linear reflection is determined by the attenuation factor of the wave with the frequency $\omega (e^{-2i\Delta(\omega,t)})$. It is evident that all the typical linear and nonlinear optical characteristics of the dynamics of ILA in GaAs, given by theory and experiment, are in good agreement with one another within the limits of accuracy of the corresponding data (see also Table IV).

N. Bloembergen *et al.*[127] recently used the method described above to measure SHG in reflection from a GaAs crystal in order to estimate the rate at which the melt appears on the surface of the crystal for picosecond durations.

In the experiments of Ref. 127 a single pulse of radiation at the second harmonic of the Nd:YAG laser with a duration of $\tau_p = 12.5$ ps ($\lambda = 532$ nm) was used as the probing pulse. Nonlinear reflection of this pulse, incident at an angle of $\theta = 4$–$5°$ and polarized along the $[1\bar{1}1]$ direction, occurred from the $(1\bar{1}0)$ face of GaAs. The dependence of the energy of the SH pulse ($\lambda_{\rm SH} = 266$ nm) on the energy density W_1 of the pulse at the fundamental frequency ($\lambda_1 = 532$ nm) was studied. The usual quadratic dependence was observed right up to the values $W_1 = W_{\rm th} = 30$ mJ/cm^2 (at which, according to Ref. 41, melting of the GaAs surface occurs): $W_{\rm SH} = \eta W_1^2$, this is a consequence of the analogous dependence for the SH intensity accompanying reflection from a crystal

$$I_{\rm SH} = \eta_{\rm SH} I_1^2, \tag{2.25}$$

following, for example, from the formula (2.19). The measurements gave $\eta_{\rm SH} = 2.5 \times 10^{-18}$ cm^2/W. Above $W_{\rm th}$, however, an appreciable deviation from the quadratic dependence and a transition into the "saturation" state (when W is increased right up to $W = 30\, W_{\rm th}$) are observed; this is apparently linked with the melting of the surface by the leading edge of the pulse. The experimental dependences are in satisfactory agreement with the theory, if

$$\eta_{\rm SH} = \eta_{\rm SH}(r, t) = \begin{cases} \eta_0 & \text{for} \quad t \leqslant t_{\rm m}(r), \\ \eta_0 \exp\left(-\dfrac{t - t_{\rm m}(r)}{\tau_c}\right) & \text{for} \quad t > t_{\rm m}(r), \end{cases}$$

where for each point r within the irradiated spot $t_{\rm m}$ is determined from the condition

TABLE IV. Comparison of the theoretical results of Ref. 132 with experiments[18,113] on the study of the dynamics of impulsive laser annealing in GaAs with the help of SHG in reflection.

Characteristics of ILA	Experiment	Theory
Time of growth of the phase of high reflection $\tau_{\rm PHR}^{\rm grow}$, ns	< 10	5
Decay time of PHR $\tau_{\rm PHR}^{\rm dec}$, ns	~ 15	14
Duration of PHR $\tau_{\rm PHR}$, ns	40	45
Duration of the decay of the intensity of the SH $\tau_{\rm SHG}^{\rm dec}$, ns	10	5
Duration of the growth in the intensity of the SH $\tau_{\rm SHG}^{\rm grow}$, ns	15	14

$$\int_{-\infty}^{t_m} I_1(r, t)\,dt = W_{th}$$

and a time $\tau_s \lesssim 2$ ps is chosen. The upper limit for the duration of the transition of the GaAs surface into the centrosymmetrical phase is thereby determined.

2.3.2. Diagnostics of the quality of laser annealing on the basis of SHG in reflection

The quality of ILA and, in particular, the degree of crystallinity of the annealed section of the GaAs surface previously rendered amorphous can be easily evaluated with the help of a measurement of the efficiency of SHG and the polarization dependence of this effect.

Indeed, the intensity of the SH signal accompanying reflection from a single-crystalline surface with a definite orientation is a function of the angles φ, θ, and ψ, determining the orientation of the crystallographic axes of the sample, the position of the plane of incidence, and the plane of reflection of the probing radiation. For example, the typical dependences of I_{SH} on the angle φ, formed by the polarization vector of the probing radiation relative to the plane of incidence on a $(1\bar{1}0)$-cut GaAs single crystal (the angles θ and ψ are fixed), in Fig. 1 of Ref. 114 have distinct extrema. These extrema I_{SH}^{max}, I_{SH}^{min} will be smeared to a large extent, if the SH signal is generated from a polycrystalline surface, for example, a set of small single-crystalline sections characterized by different angles ψ of the orientation relative to the plane of incidence of the probing radiation.

In addition, the SH intensity at the maximum of the polarization dependence for the annealed section, scaled to the corresponding intensity of the SH from the unimplanted (and, correspondingly, unannealed) crystalline section,

$$\eta_{SH}^{PLA} = \frac{I_{SH}^{PLA}}{I_{SH}^{cryst}} \qquad (2.26)$$

can also characterize the degree of restoration of crystallinity of the surface layer as the result of ILA.

Experiments on the determination of the quality of ILA on the basis of the SHG were conducted on the experimental arrangement shown in Fig. 9. The probe consisted of radiation from a quasicontinuous garnet laser with neodymium, operating with a repetition frequency of 1 kHz. The recording system consisted of an FÉU-106 SH radiation detector, a V9-5 stroboscopic voltage transducer, and an automated complex for collecting and processing data based on the Élektronika-NTs-80 microcomputer. It enabled the detection of weak signals with a high signal-to-noise ratio.

Gallium arsenide $(1\bar{1}0)$-cut samples, into which phosphorus P^+ ions with a dose of $D = 6 \cdot 10^{15}$ cm^{-2} and energy $E = 40$ keV (mechanical polishing) were implanted and which were annealed by a series of ruby laser pulses ($\tau_p = 30$ ns) with different energy densities $W_1 = 0.27$, $W_2 = 0.21$, $W_3 = 0.16$, $W_4 = 0.08$, $W_5 = 0.05$, J/cm^2 were studied.

We note that the SH signal from the amorphous layer was approximately 80 times less intense than the signal from the unimplanted section of the single crystal. The incomplete vanishing of the SH can be linked to the incomplete disordering of the surface layer of the implanted section. Deep disordered layers of the crystal could also make a definite contribution to the residual SHG signal, since the penetration depth of the "probe" was of the same order of magnitude as the depth of the amorphous layer: the latter depth, according to Ref. 31, is equal to ~ 50 nm, while the probing depth, limited by the absorption of the SH radiation in the amorphous GaAs layer, according to Table III is equal to $l_{probe} \approx \alpha_{2\omega}^{-1} \approx 30$ nm. The thickness of the layer in which the annealing radiation is absorbed is equal to ≈ 60 nm.

The experimental results (the dependence $I_{SH}(\varphi)$ are presented in Fig. 10, whence it is evident that the SH does not indicate polycrystallinity for all energy densities of the annealing radiation. At the same time a strong dependence of the amplitude of the signal on the energy of the annealing pulses is observed.

2.3.3. Determination of the degree of disordering of a crystal surface from SHG and SFG in reflection

We already called attention above to the low sensitivity of SHG and SFG to the presence or absence of an amorphous surface layer in a noncentrosymmetrical GaAs crystal. It is clear that these effects, as well as THG (see below), can be used also for quantitative determination of the degree of partial disordering of this layer. At the same time, as will be shown below, nonlinear optical methods are much more sensitive and accurate, more highly localized, and are simpler than other methods for analyzing the degree of amorphousness of the surface used thus far—Rutherford backscatter-

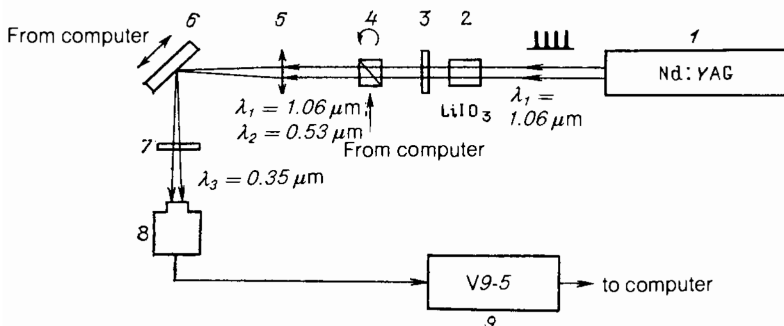

FIG. 9. Block diagram of the experiment for studying with the help of SHG and SFG the degree of amorphousness of a GaAs surface produced by ion implantation and the quality of its laser annealing. 1) Probing Nd:YAG laser with active mode-locking and acoustooptical q-switching; 2) $LiIO_3$ crystal for frequency doubling (used only in experiments on SFG); 3) ZhS-4 filter (cuts off the parasitic radiation with $\lambda_{SF} = 351.7$ nm); 4) polarization rotator; 5) lens; 6) sample; 7) set of SZS-21 light filters (for SHG) or UFS-2 light filters (for SFG); 8) photomultiplier FEU-106; 9) selective amplifier.

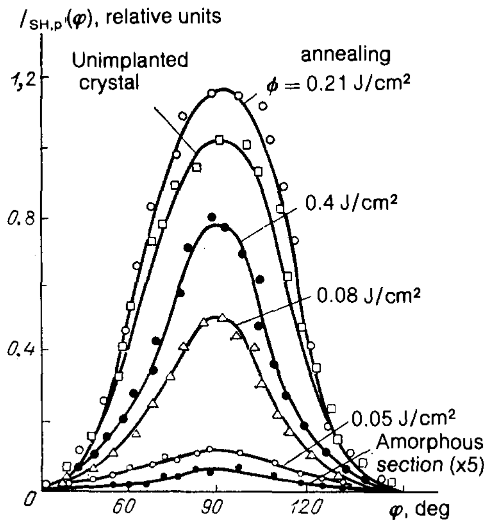

FIG. 10. Polarization dependence of SH on the sections of the $(1\bar{1}0)$ surface of GaAs subjected to ILA with a different dosage of the annealing radiation.

ing of light ions, diffraction of slow electrons, x-ray diffraction analysis, etc.

It is not difficult to see, however, that the characteristics of nonlinearly reflected signals, which it is desirable to use for quantitative description of the degree of perfection of the surface, must be different for noncentrosymmetrical (GaAs, GaP, InSb, etc.) and centrosymmetrical (Si, Ge, etc.) crystals. In analogy to (2.26), the intensity of the second harmonic of the optical radiation probing the disordered section of the crystal surface I^{a}_{SH}, scaled to the intensity of the SH from an undamaged section of the same crystal, I^{cryst}_{SH}, can serve as a characteristic of the degree of disordering of *noncentrosymmetric* crystals:

$$\eta_{SH} = \frac{I^{a}_{SH}}{I^{cryst}_{SH}}. \tag{2.27}$$

In our experiments on SHG, we studied (100)-cut GaAs samples, whose surface was rendered amorphous to one extent or another by the implantation of 80-keV Te^{+} and S^{+} ions with an irradiation dose in the range $1 \cdot 10^{12} - 6 \cdot 10^{15}$ cm^{-2}.[113] The GaAs surface prior to ion bombardment was mechanically polished and chemically etched.

The polarization dependences of the SH signal from the partially disordered surface repeated exactly the same dependences for the undamaged section (and in the latter case they coincided with the dependences computed from the formulas in Ref. 105; see also Sec. 2.2). The intensity of SH from the implanted part of the crystal surface, however, was 1 to 2 orders of magnitude lower than from the crystalline surface—depending on the implantation dosage.

Figure 11 shows the dependence of η_{SH} on the dosage D, which, as can be seen, is quite distinct. It reflects the loss of long-range order of the initially noncentrosymmetrical crystal as the implantation dosage is increased.

The relative efficiency of the sum frequency generation exhibits an even stronger dependence on the dosage D:

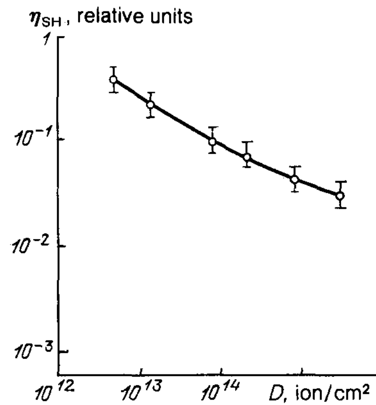

FIG. 11. The degree of amorphousness of the (100) surface according to SHG η_{SH} ($\lambda_{SH} = 532$ nm) as a function of the dosage of surface implantation by Te^{+} ions with an energy of $E = 80$ keV.

$$\eta_{SR} = \frac{I^{a}_{SR}}{I^{cryst}_{SR}}; \tag{2.28}$$

where I^{a}_{SF} is the intensity of the sum frequency signal (SF) with wavelength $\lambda_{SF} = 351.7$ nm, obtained from a section of GaAs, rendered partially amorphous by ion bombardment, by mixing the fundamental radiation of the nd:YAG laser ($\lambda_1 = 1064.2$ nm) and its second harmonic ($\lambda_2 = 532.1$ nm), generated beforehand in an $LiIO_3$ crystal (the waves mixed on the GaAs surface were linearly polarized in orthogonal directions); I^{cryst}_{SF} is the intensity of the SF signal from the undamaged section of the crystalline surface. The dependences $\eta_{SF}(D)$ are illustrated for a number of GaAs samples in Fig. 12.

The difference between $\eta_{SH}(D)$ and $\eta_{SF}(D)$ is linked primarily to the difference of the probing depths: in the case of SH $l_{SH} \approx \alpha^{-1}_{SH} \approx 50$ nm. The latter circumstance is especially important, since it enables obtaining data on the degree of disordering of very thin surface layers.

The quantities η_{SH} and η_{SF} can be easily and accurately measured; they are quantitative characteristics of the degree

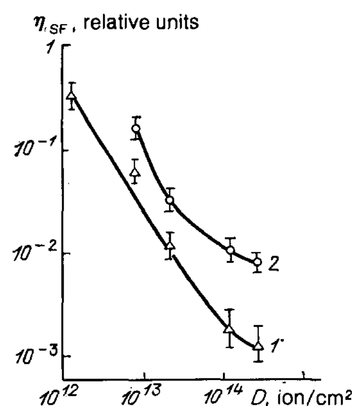

FIG. 12. The degree of amorphousness of the (100) surface of GaAs according to SFG, ($\lambda_{SF} = 351.7$ nm) as a function of the dosage of surface implantation by Te^{+} (1) and S^{+} (2) ions with an energy of $E = 80$ keV.

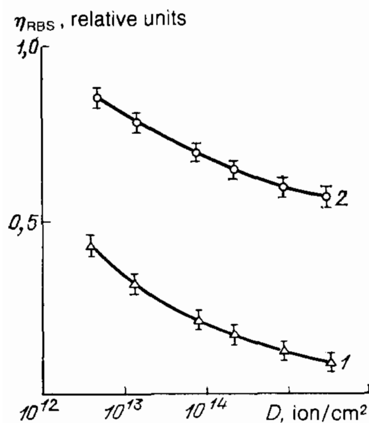

FIG. 13. The degree of amorphousness of the (100) surface of GaAs according to Rutherford backscattering η_{RBS} as a function of the dosage at implantation by Te^+ (1) and S^+ (2) ions with energy $E = 80$ keV.

of amorphousness of the surface layer of a noncentrosymmetric crystal.

With the help of SFG it is easy to record the amorphousness of a GaAs surface produced by such low implantation dosages ($< 10^{12}$ cm^{-2}) that it cannot be recorded by other methods used thus far.

In particular, Fig. 13 shows the implantation dosage dependence of the quantity η_{RBS}—a parameter determined from a comparison of the spectra of Rutherford backscattering (RBS) of helium nuclei from the surfaces of implanted and unimplanted sections of the crystal.[31] The measurements were performed on the same samples as the SHG and SFG measurements (Figs. 11–12). A comparison of Figs. 11–13 shows that the dependence $\eta_{RBS}(D)$ is much less distinct than $\eta_{SF}(D)$ and even $\eta_{SH}(D)$.

With the help of SFG in reflection from a surface rendered amorphous by laser irradiation it is possible to observe amorphous rings obtained by irradiation of the single-crystalline (100) surface of GaAs by short laser pulses with $\lambda = 532$ and 265 nm, pulse duration $\tau_p = 30$ ps, and energy density $W = 0.05$–0.1 J/cm^2 (see Fig. 14).[113] The presence

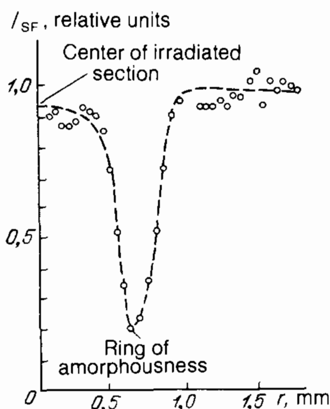

FIG. 14. The amorphous ring along the circumference of a section irradiated with picosecond laser pulse with $\lambda = 266$ nm of the (100) surface of GaAs, observed with the help of SFG in reflection.

of an amorphous ring is easily recorded by the sharp decrease in the intensity of the SF signal in the reflection from the corresponding section. The polarization dependence of the weak SF signal from the section of the laser-induced amorphous ring, as it turned out, coincides precisely with that of the undamaged section, indicating that the long-range order characteristic for the starting crystal is partially preserved in the laser-induced amorphous layer.

In studying crystals with a *centrosymmetric* lattice (for definiteness, we shall refer below to crystalline silicon), the relative intensity of the reflected SH can no longer serve as a reliable quantitative criterion for the perfection of the surface, since both ordered and amorphous media exhibit second-order quadrupole susceptibilities $\chi^{(2)Q}_{ijkl}$, describing the SHG in such media. The magnitude of the anisotropic (i.e., depending on the orientation of the crystal relative to the plane of incidence) contribution to the SH intensity, as well as to the SF and TH intensities could, however, serve as a criterion of perfection.

The layout of the experiment is analogous to that shown in Fig. 9 with the GaAs crystal replaced by an Si sample with the (111) plane serving as the nonlinear mirror. The sample was rotated by a step mover about the [111] axis. The surface was subjected to implantation with 80-keV phosphorus ions.

The dependence of SH on the angle of rotation of the crystal around the normal to the surface ψ, in accordance with Table II, is the result of the interference of the anisotropic ζ_Q and isotropic B contributions:

$$I^{p\to p}_{SH}(\psi) \propto |\zeta_Q \cos 3\psi + B|^2. \qquad (2.29)$$

Because in an isotropic medium $\zeta_Q = 0$, it is natural to expect that as the degree of disordering of the crystalline lattice increases with the implantation dosage D the relative fraction of the anisotropic contribution will decrease.

Figure 15 shows the measured dependences $I_{SH}(\psi)$ for different values of the dosage D. The nature of this dependence for pure Si (Fig. 15a)—six peaks in the interval $\psi = 0 - 360°$—indicates that the anisotropic contribution dominates ($|\zeta_Q| > |B|$). For values $D \lesssim 2 \cdot 10^{13}$ cm^{-2} no appreciable changes occur in the dependence $I_{SH}(\psi)$. As the dosage is further increased (Figs. 15c and d) the magnitudes of the peaks are redistributed, indicating that the isotropic contribution to the SH signal increases. Finally, for $D = 2.4 \cdot 10^{14}$ cm^{-2} the dependence $I_{SH}(\psi)$ no longer has six peaks, but rather three peaks, i.e., $|\zeta_Q/B| < 1$.

Thus the quantity

$$\eta^{Q}_{SH} = \left|\frac{\zeta_Q}{B}\right|, \qquad (2.30)$$

measured for some fixed parameters of the experiment (in particular, with a fixed angle θ) can serve as a quantitative characteristic of the degree of perfection of the crystalline structure of centrosymmetrical crystals.

We note that the anisotropy of the SH signal accompanying reflection from the (100) and (111) faces of crystalline silicon was first observed by Driscoll *et al.*,[129,130] who used in their experiments single pulses from a Nd:YAG mode-locked laser (the pulse duration was $\tau_p = 30$ ps).

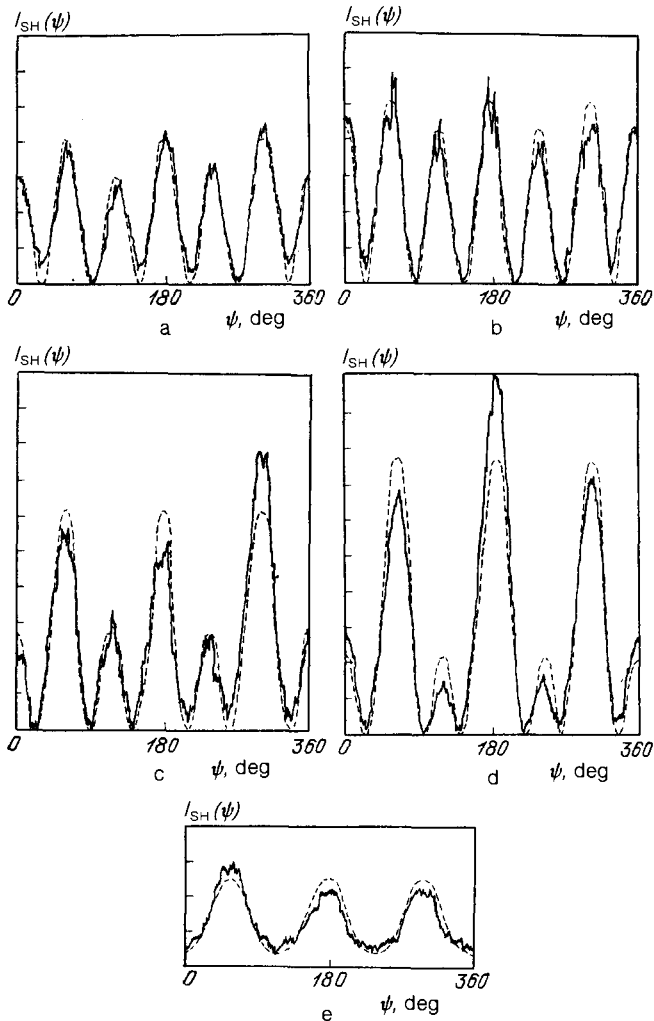

FIG. 15. The intensity of the quadrupole second harmonic ($\lambda_{SH} = 0.53$ μm), reflected from the (111) face of silicon in the $p \to p$ scheme as a function of the angle ψ of rotation of the crystal around the [111] axis with different dosages of surface implantation by phosphorus ions ($E = 80$ keV). The solid lines show the experiment and the broken lines show the curves calculated using the formula (2.26) for five values of the ratio $|\zeta_Q/B|$; the implantation dosage (10^{13} ions/cm^2) = 0 (pure Si); $|\zeta_Q/B = 115$ (*a*); 1.8, 17 (b), 3.6; 4.6 (c), 12; 2.3 (d), and 24; 0.49 (e).

They reported a high efficiency of the SHG process accompanying reflection from the (111) plane in Si (only an order of magnitude lower than for reflection from a noncentrosymmetric GaP crystal) and they recorded the dependence of the s-polarized SH with an s-polarized pump of the form $I_{SH}^{s\to s}(\psi) \sim \sin^2 3\psi$ and a p-polarized SH with a p-polarized pump of the form $I_{SH}^{p\to p}(\psi) \sim (1 - \cos 3\psi)^2$, where ψ is the angle of rotation of the crystal relative to the plane of incidence of the probing beams. We note that in their first experiments Bloembergen *et al.*[116] did not observe the dependence of the SH signal from Ge and Si on the orientation of the medium relative to the plane of incidence.

Somewhat later Shen *et al.*[19] confirmed the experimental data obtained by Driscoll *et al.*[130] showing the existence of a strong anisotropic dependence of SH on the orientation of the Si crystal with reflection from the (100) and (111) planes. They correctly interpreted these results as being a consequence of the anisotropic second-order volume quadrupole nonlinear polarization. The conclusion[19] that the anisotropic surface contribution supposedly present in the dependence $I_{SH}^{s\to s}(\psi)$ accompanying reflection from the "nonreconstructed" (111) face is, however, incorrect, because, as shown in Sec. 2.2.2, owing to the centrosymmetry of all faces in the Si crystal the surface contribution to the quadratic polarization is sensitive to the orientation of the crystal relative to the plane of incidence. Litwin *et al.*[134] later arrived at analogous conclusions.

The situation, however, changes markedly, if the experiments are conducted with very clean surfaces, obtained in an ultrahigh vacuum by means of cleavage of oriented crystals: the presence of "broken" valence bonds in surface atoms gives rise to reconstruction of the surface structure and, therefore, causes its local symmetry to differ from the symmetry of the internal crystalline planes with the same indices. In particular, a clean (111) surface of silicon, as shown in Ref. 154, gives a very strong anisotropic dipole contribution to the reflected SH. When the temperature of the crystal is raised, the anisotropy of this contribution changes, reflecting the surface phase transition from a 2×1 to a 7×7 reconstruction.

The cubic dipole nonlinear susceptibility $\chi_{ijkl}^{(3)D}$, as emphasized above, in the general case also exhibits an anisotropy, just as does the second-order quadrupole susceptibility $\chi_{ijkl}^{(2)Q}$. In particular, as our measurements show, the anisotropy of the tensor $\chi_{ijkl}^{(3)D}(\omega_a; \omega_1, \omega_1, -\omega_2)$ is large in silicon: $|\zeta_D/\chi_{1111}^{(3)D}| \approx 1$ (when two photons ω_1 with the wavelength $\lambda_1 = 1.06\,\mu$m and one photon ω_2 with wavelength $\lambda_2 = 1.17$ μm are mixed). The anisotropy of the tensor $\chi_{ijkl}^{(3)D}(3\omega_1; \omega_1, \omega_1, \omega_1)$, describing the generation of the dipole third harmonic of the fundamental radiation of a Nd:YAG laser, however, is somewhat smaller. Information of this kind can be used to refine the details of the band structure of the crystal.

2.3.4. Subpicosecond dynamics of structural changes of the Si surface accompanying impulsive laser annealing

Shank *et al.*[126] used the technique of SHG in reflection for diagnostics of the fast (subpicosecond) first phase of ILA of the surface of crystalline silicon.

In the experiments the reflection from the (111) face was studied; the pump and the SH signal were polarized in the plane of incidence. In the absence of the annealing pulse, as well as when the surface was probed by SHG prior to the arrival of the annealing pulse (negative delays) the recorded dependence $I_{SH,p}(\psi)$ was well approximated by a theoretical curve of the form $I_{SH,p}(\psi) \sim (1 - \cos 3\psi)^2$ (see the angular dependence in Fig. 16a). Annealing was carried out with a single pulse with an energy density $W > W_{th} = 0.2$ J/cm^2, wavelength $\lambda \approx 620$ nm, and duration $\tau_p = 90$ fs, incident normally on the (111) surface of crystalline Si. The probing was carried out with much weaker pulses with the same wavelength and duration, oriented at an angle of 45° to the irradiated section of the surface with a precisely controllable delay after the annealing pulse. Figures 16b and c show

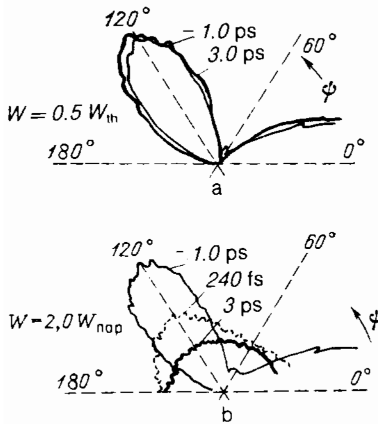

FIG. 16. Polar diagrams of the dependence of the intensity of the reflected second harmonic on the angle of rotation ψ of the crystal Si relative to the plane of incidence of the probing radiation for different values of the delay time between PLA and the SHG probing.[126] a) For $W = 0.5\ W_{th}$ (no melt); b) for $W \approx 2W_{th}$ (with $\tau_3 = 3$ ps the vanishing of the anisotropy of the diagram is seen clearly, indicating the appearance of a melt).

the recorded dependences $I_{SH,p}(\psi)$ 0.3 and 1 ps after the annealing pulse. The striking change in the nature of the dependence $I_{SH,p}(\psi)$ clearly indicates the ultrafast change in the symmetry of the surface, which is in complete agreement with the idea of a laser-induced first order transition—melting of the surface. The isotropic dependence $I_{SH,p}(\psi)$ 1 ps after the annealing action corresponds to isotropic melting of the surface layer.

3. NONLINEAR-OPTICAL PROCESSES DETERMINED BY THE MODULATION OF THE SURFACE RELIEF AND OF THE SURFACE TEMPERATURE OF CONDENSED MEDIA

3.1. Laser-induced instabilities of the surface relief and the problem of the formation of ordered surface structures

3.1.1. Optical excitation of periodic surface structures

The problem of the appearance of ordered surface structures—optically induced gratings—has in recent years occupied an important place in the studies of impulsive laser action on condensed media. The typical layout of an experiment on inducing a grating is very simple. The unfocused beam of a pulsed laser is incident on the surface of an absorbing solid; an almost plane light wave interacts with the surface. Periodic modulation of the relief nevertheless appears on the illuminated surface. It is formed in the process of interaction (its duration varies from 10^{-3} to 10^{-11} s!) and usually remains after the interaction ceases. Figure 17 shows examples of laser-induced periodic structures. These structures were obtained on different materials and with the help of different lasers.

It should be noted that a number of experiments which were not limited solely to recording the "frozen" structures (the most efficient method is based on the study of the diffraction of the probe beam from a continuous laser[180] (see below, Fig. 28)) have been performed; making use of the technique of nonstationary diffraction of the probe beam, these experiments also followed the dynamics of the evolution of the structure during the action of the laser pulse *in situ* (see, for example, Refs. 150–153, 202, 204).

The results of these experiments show that the evolution of periodic structures in time has the character of an instability; the dynamics of the development of the latter has much in common with the nonlinearities accompanying stimulated scattering which are well known in nonlinear optics.

Such periodic structures were first observed about 20 years ago by means of irradiation of Ge and Si semiconductors by ruby laser pulses.[135] But intensive experimental and theoretical investigations of the formation of surface gratings began only approximately in 1980. Amongst the first studies along these lines we mention Refs. 144, 104, 136, 137, 141.

The formation of surface gratings is observed not only in the semiconductors Si, Ge, GaAs, and InSb,[135–143] but also in the metals Ni, Cu, Pb, Al, steel, brass,[144–146] and in the dielectrics NaCl and fused and crystalline quartz.[147–149]

In addition to irreversible gratings (remaining after the action of the laser pulse), reversible gratings existing only for the duration of the pulse are also observed.[150,151] Such

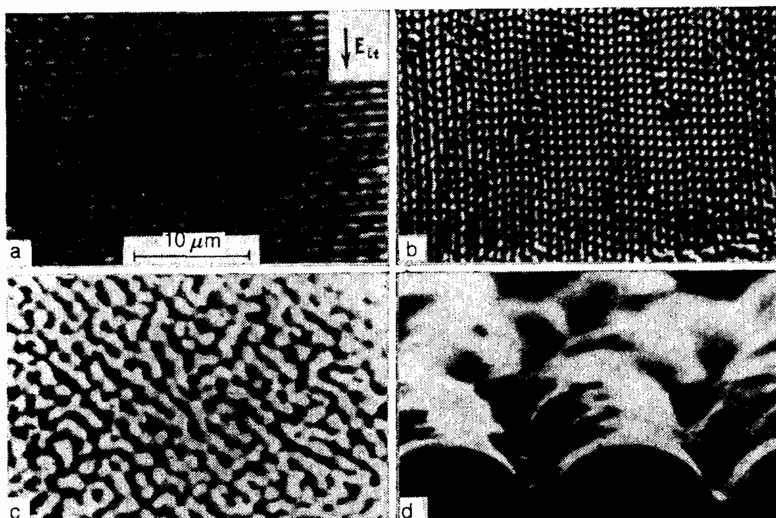

FIG. 17. Characteristic periodic structures induced by laser radiation on the surface of solids. a) One-dimensional grating, formed on the surface of a Ge semiconductor irradiated with a laser pulse with a wavelength $\lambda = 1.06\,\mu$m ($I_i = 10$ MW/cm^2; $\tau_p = 100$ ns, the angle of incidence $\theta \approx 10°$; the arrow marks the orientation of the vector E_{it} [180]; b) two-dimensional grating, formed on the surface of Ge under the action of high-intensity pulses of radiation with $\lambda = 1.06\,\mu$m; the complicated structure could be linked with the interaction of gratings[141]; c) structure formed on the surface of germanium by a circularly polarized wave under oblique incidence (for the interpretation see Fig. 28)[180]; d) "frozen" capillary waves on the surface of quartz initially melted by a CO_2 laser (obtained with the help of a scanning electron microscope).[152]

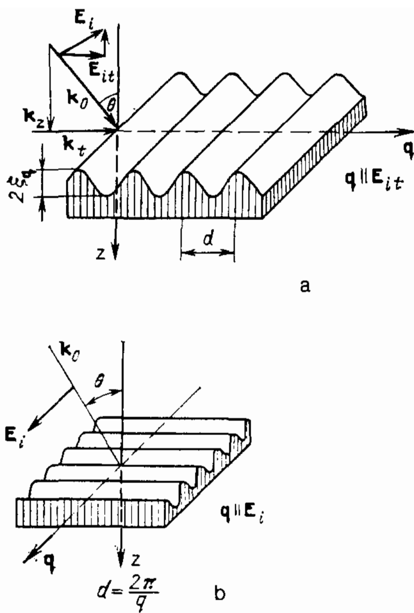

FIG. 18. Geometry of the formation of the most often encountered ("normal") gratings. a) p polarized pump wave (the vector $\mathbf{E}_i$ lies in the plane of incidence); b) s-polarized pump wave (the vector $\mathbf{E}_i$ is perpendicular to the plane of incidence); $\mathbf{q}$ is the wave vector of the wave of modulation of the relief, parallel to the projection of $\mathbf{E}_i$ on the plane of the surface; in both cases θ is the angle of incidence.

reversible gratings also appear under the action of laser pulses on liquid metals[152] and melts of semiconductors.[153] Both one- and two-dimensional structures[138] as well as complicated ordered formations[141] (see Fig. 17) are observed. The periods and orientation of the gratings depend substantially on the characteristics of the laser radiation—the angle of incidence θ, polarization, frequency, and energy (Figs. 18 and 19). The gratings are formed for a wide range of parameters of the laser radiation ($\lambda = 0.308 - 10.6\,\mu$m, pulse durations $\tau_p = 10$ ps–1 ms, and intensities $I_1 = 5 \cdot 10^6 - 5 \cdot 10^8$ W/cm^2) (see Sec. 3.6).

Experiments on optically induced surface periodic structures stimulated numerous theoretical investigations.[136,137,139,199,165,168–172] The physical picture of the generation of periodic structures has now been largely formulated.

For a strongly absorbing surface the process of formation of the periodic structure can be represented schematically as follows.

1. Everything begins with the appearance of a periodically spatially modulated (interference) light field on the surface. This light field is formed by the interference of the incident wave with the wave scattered by the real nonuniform surface. Here both static and dynamic nonuniformities (fluctuation surface waves) are important.

2. Nonuniform heating of the surface occurs in the light field periodically modulated in intensity.

3. Finally, if the intensity of the laser radiation is high enough, then nonuniform heating can give rise to nonuniform melting and evaporation.

It is natural that after the laser pulse is switched off the vestige of nonuniform heating (and especially melting and evaporation) creates a "frozen" periodic structure.

It is completely obvious that the heating, melting, and evaporation processes are linked with the complicated self-consistent interaction of the surface undergoing the phase transition with the laser radiation. Indeed, the light-induced change in the surface structure evidently affects the magnitude of the absorbed and scattered power—feedback occurs. What is the sign of this feedback? Is positive feedback, i.e., nonuniformities growing exponentially in the laser field, possible? What are the physical mechanisms of the feedback? These are undoubtedly the most interesting problems in the physics of the formation of surface structures.

There now exists a basis for believing that positive feedback in many cases determines the basic mechanisms of the formation of periodic structures, while the starting nonuniformities serve only as the "seed" for the exponentially growing process.

Relying primarily on the work carried out in our laboratory[165,168,171,172] we shall present below the theoretical picture of the development of periodic structures; the physics of laser-induced instabilities on the surface is emphasized.

Before considering specific theoretical models, however, we shall discuss in greater detail the qualitative picture of the phenomenon which has been formulated based on the analysis of experimental data.

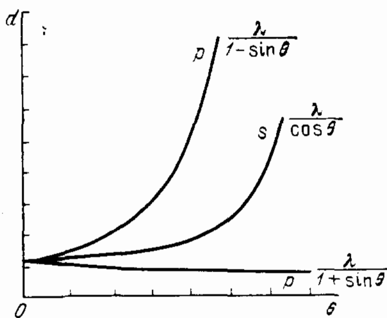

FIG. 19. Experimental dependence of the period of "normal" dominant surface gratings with s and p polarizations of the pumping wave as a function of the angle of incidence θ.[137]

3.1.2. Physics of the interaction of a rough surface with a laser field

The first stage of the process is linked with the appearance of the interference light field on the surface. Since at this stage the problem can be regarded as linear, it is sufficient to study the diffraction of the incident laser radiation with frequency ω by the Fourier-component of the surface relief with wave vector $\mathbf{q}$, frequency $\Omega_{\mathbf{q}}$, and amplitude $\xi_{\mathbf{q}}$. As a result, two diffracted surface waves appear—the Stokes wave with frequency ω_s and wave vector $\mathbf{k}_s$ and the anti-Stokes wave (ω_{as}, $\mathbf{k}_{as}$), in addition, the following conditions are satisfied:

$$\omega_s = \omega - \Omega_{\mathbf{q}}, \quad \omega_{as} = \omega + \Omega_{\mathbf{q}}, \quad \mathbf{k}_s = \mathbf{k}_t - \mathbf{q}, \quad \mathbf{k}_{as} = \mathbf{k}_t + \mathbf{q}, \tag{3.1a}$$

where $\mathbf{k}_t$ is the projection of the wave vector of the incident wave on the plane $z = 0$ (Fig. 20). The interference of the

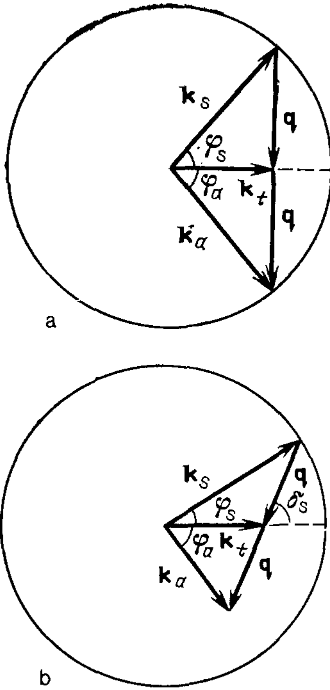

FIG. 20. Vector diagram of the law of conservation of momentum. a) Degenerate case of the relative orientation of the vectors $\mathbf{q}$ and $\mathbf{k}_t$ (in this case $k_s = k_a \approx k_0$); b) nondegenerate case of the relative orientation of the vectors $\mathbf{q}$ and $\mathbf{k}_t$ (in this case $k_s \approx k_0$; $k_a \neq k_0$).

pumping wave $\mathbf{E}_t$ transmitted into the medium and the two diffracted waves $\mathbf{E}_\alpha$ (α = s, as) creates a spatially and temporally periodic distribution of the light intensity in the surface layer.

The most general reason for the appearance of nonuniformities is the roughness of the real surface ($\Omega_\mathbf{q} = 0$); in many cases surface acoustic waves (SAW) could also be important,[155–157] and the interaction with the melted surface is substantially determined by the excitation of capillary waves (CW).[158]

The conditions (3.1a) with $\Omega_\mathbf{q} = 0$ enable constructing a graphic picture of the rough structure of the optically induced gratings on the surface of a metal with the dielectric permittivity $\varepsilon = \varepsilon' + i\varepsilon''$ (usually $|\varepsilon'| \gg 1$) (see Fig. 18a). It is well known that under these conditions a surface wave exponentially decaying for $z > 0$ and $z < 0$, with the wave vector

$$k_{\text{sur}} = \frac{\omega}{c}\left(\frac{|\varepsilon'|}{|\varepsilon'|-1}\right)^{1/2} \approx \frac{\omega}{c} = k_0$$

can propagate.

It is natural that the incident p-polarized laser wave will excite a surface wave especially effectively when $k_s \approx k_{\text{surf}}$, or $k_{\text{as}} \approx k_{\text{sur}}$,

$$|\mathbf{k}_t \pm \mathbf{q}| \approx k_0 \tag{3.1b}$$

and $\mathbf{k}_s$ and $\mathbf{k}_{\text{as}}$ lie in the plane of the surface.

The period of the "resonant" Fourier component for the p wave incident at an angle θ (see Fig. 18a) can be found from (3.1b):

$$\frac{\omega}{c}\sin\theta \pm q = \pm\frac{\omega}{c}\left(\frac{|\varepsilon'|}{|\varepsilon'|-1}\right)^{1/2} \approx \frac{\omega}{c},$$

whence

$$q = \frac{2\pi}{d} = \frac{\omega}{c}(1 \pm \sin\theta), \quad d = \frac{\lambda}{1 \pm \sin\theta}.$$

It is clear that the quantity d found determines the spatial period of the interference field and therefore also the period of the optically induced grating. Gratings of this type ("normal" gratings) are indeed observed experimentally. It is interesting to note that a condition analogous to (3.1b) was discussed already by Rayleigh in connection with the so-called Wood anomaly.[200,201] The same resonances in the case $\varepsilon' < -1$ are partially responsible for the giant Raman scattering of light by molecules adsorbed on a fluted[159] or rough[160] metal surface (see also the review of Ref. 161).

3.1.3. Evolution of structures; feedback mechanisms

The considerations presented above are, of course, only guidelines.

The mechanisms of the formation of surface structures can be different for different materials, different wavelengths, and different laser radiation intensities.

As an example of a situation when the incident wave is diffracted not by the static fluctuation relief, but rather by the propagating wave, we call attention to experiments in which (owing to the high intensity of the laser) the appearance of periodic structures is preceded by uniform melting of the surface. In this case, the periodic structures arise owing to the excitation of capillary waves (CW) (see Ref. 152 and the recent experiment in Ref. 202, where this was revealed especially clearly, as well as Ref. 215).

The dispersion law for CW (these waves are formed owing to the surface tension in the liquid) has the form $\Omega_\mathbf{q} = (\sigma q^3/\rho)^{1/2}$, where σ is the coefficient of surface tension, ρ is the density, and the damping constant of the CW is $\gamma_\mathbf{q} = 2\nu q^2$, where ν is the kinematic viscosity. Using for the Ge melt the value $\sigma \approx 6\cdot 10^2$ g/s^2, $\rho \approx 5$ g/cm^3, $\nu \approx 10^{-3}$ cm^2/s, as well as the fact that under laser excitation of CW $q \sim k_0 \sim 6\cdot 10^4$ cm^{-1} ($\lambda = 1.06\,\mu$m) (see Sec. 3.4), we find that CW with $\Omega_\mathbf{q} \sim 10^8$ s^{-1} and $\gamma_\mathbf{q} = 10^7$ s^{-1}, whose propagation velocity is $v_\mathbf{q} = \Omega_\mathbf{q}/q \sim 10^3$ cm/s, are excited.

As already mentioned the results of many experiments (see, for example, Refs. 202 and 203) indicate that the amplitudes of the starting nonuniformities do not play a significant role in the formation of laser-induced periodic structures; this is a serious argument in support of the idea that positive feedback plays a decisive role.

We present below the theory describing the basic stages of excitation of periodic surface structures. First, the problem of the diffraction of the incident laser wave $\mathbf{E}_i$ by the space-time Fourier component of the modulation of the surface relief is solved. The general solution is presented in Sec. 3.2; expressions are obtained in the approximation linear in $\xi_\mathbf{q}$ for the diffraced fields $\mathbf{E}_s$ and $\mathbf{E}_{\text{as}}$ inside the medium (analogous expressions for the fields outside the medium describe the spontaneous Mandel'shtam-Brillouin scattering by SAW or CW[157]).

Then the fields $\mathbf{E}_s$ and $\mathbf{E}_{\text{as}}$ determined in this manner are used to calculate the temperature field. The last stage—closing of the feedback chain—requires an analysis of the

equation for the specific surface excitation with the corresponding boundary conditions.

For SAW, this is the equation for the elastic displacement vector of the medium; for CW, these are the equations of hydrodynamics (3.20); and, for the interference evaporation instability (IEI), this is the equation for the velocity of the evaporation front (3.17) (the last two equations must be studied simultaneously; see Sec. 3.4).

It is important to emphasize that the solution of the problem of diffraction (and therefore the subsequent stages of the analysis also) are valid for media with an arbitrary dielectric permittivity $\varepsilon(\omega)$. The results for the excitation of SAW, CW, or IEI are therefore applicable for arbitrary condensed media—semiconductors, metals, and dielectrics, as well as their melts.

In the particular case $\varepsilon' < -1$ (metals and melts of semiconductors and polariton-active dielectrics) the diffracted waves correspond to the induced surface electromagnetic waves (SEW).

From the viewpoint of nonlinear optics, SAW or CW are excited as a result of stimulated scattering of light by the surface, analogous to the stimulated scattering of light owing to absorption (ASS) in the volume.[162] However, unlike scattering in the volume, where absorption is small, so that the decay constant of the scattered wave $\gamma_{s,as} \ll \gamma_q$—the decay constants of the material excitation, the opposite case $\gamma_{s,as} \gg \gamma_q$ is realized on the surface. For this reason, here the scattered light wave (SEW) adjusts adiabatically to the acoustic wave (SAW or CW), which is amplified. This analogy is manifested, for example, in the fact that, as with volume ASS, the critical intensity of excitation of SAW is independent of the magnitude of the linear absorption of the medium[165] (in spite of the fact that the heating of the medium plays a primary role in these effects!). We note that induced scattering by the surface of absorbing media, owing to the much weaker ponderomotive forces, was studied previously in Ref. 163, and in the case of transparent media in Ref. 164.

In this section we shall present systematically the theory of the formation of periodic surface structures (the theory of SAW, CW, and IEI instabilities), and in the conclusion we shall discuss in detail the experimental data.

3.2. Diffraction of light waves by spatial-temporal modulations of the surface relief

An arbitrary surface can be characterized by its space-time Fourier spectrum. In the linear case it is therefore sufficient to study the diffraction of a light wave by any one Fourier component of the relief.

Let the flat surface of the medium coincide with the surface $z = 0$, and let the z axis be directed into the medium. In the presence of modulation of the surface the medium fills the half-space $z \geqslant \xi(\mathbf{r},t)$,

$$\xi(\mathbf{r}, t) = \xi_{\mathbf{q}}(t) \exp(-i\mathbf{qr} + i\Omega_{\mathbf{q}}t) + \text{c.c.}, \tag{3.2}$$

where $\mathbf{r} = \{x, y\}$ is a vector lying in the plane $z = 0$ and $\xi_q(t)$ is the slow amplitude. Let a plane light wave

$$\mathbf{E}(\mathbf{r}, z, t) = \mathbf{E}_i \exp(ik_t y + ik_z z - i\omega t) + \text{c.c.}, \tag{3.3}$$

where k_z and k_t are the normal and tangential projections of the wave vector $\mathbf{k}_0$ (see Fig. 18), be incident from the vacuum onto the surface.

If only the first-order diffraction is taken into account, then the field outside the medium ($z < \xi(\mathbf{r},t)$) is a superposition of the incident (i) and reflected (r) waves at frequency ω and two diffracted waves with frequencies ω_α

$$\mathbf{E} = (\mathbf{E}_i e^{ik_z z} + \mathbf{E}_r e^{-ik_z z}) \exp(ik_t y - i\omega t) + \sum_{\alpha = s, as} \mathbf{E}'_\alpha \exp(i\mathbf{k}_\alpha \mathbf{r} + \Gamma_\alpha z - i\omega_\alpha t) + \text{c.c.}, \tag{3.4}$$

where ω_α, $\mathbf{k}_s$ and $\mathbf{k}_{as}$ are given by the formulas (3.1a). The field inside the medium ($z \geqslant \xi(\mathbf{r},t)$) is the sum of the transmitted wave and two diffracted waves,

$$\mathbf{E} = \mathbf{E}_t \exp(ik_t y - \gamma z - i\omega t) + \sum_{\alpha = s, as} \mathbf{E}_\alpha \exp(i\mathbf{k}_\alpha \mathbf{r} - \gamma_\alpha z - i\omega_\alpha t) + \text{c.c.} \tag{3.5}$$

The problem of finding the fields $\mathbf{E}_r$, $\mathbf{E}_t$ and $\mathbf{E}_\alpha$, $\mathbf{E}'_\alpha$ in the approximation linear in ξ_q has been studied in many works (see, for example, Refs. 159 and 137). In the x-ray range of wavelengths the analogous problem was studied in Ref. 206. We shall use here the formulas for diffraction by a dynamic grating, obtained in Ref. 165 but written in the simpler form under the condition that $\Omega_q \ll \omega$. The amplitudes of all fields in (3.4) and (3.5) are found from the condition that the tangential components of the vectors of the electric and magnetic fields be continuous at the interface $z = \xi(\mathbf{r},t)$.

We introduce the constants

$$\gamma^2 = k_t^2 - k_0^2\varepsilon, \quad \gamma_\alpha^2 = k_\alpha^2 - k_0^2\varepsilon, \quad \Gamma_\alpha^2 = k_\alpha^2 - k_0^2. \tag{3.6}$$

$$(\operatorname{Re}\gamma, \gamma_\alpha > 0, \ \operatorname{Re}\Gamma_\alpha > 0 \ \text{for} \ k_\alpha > k_0, \quad \operatorname{Im}\Gamma_\alpha < 0 \ \text{for} \ k_\alpha < k_0).$$

Then the expressions for the amplitudes of the fields inside the medium can be written in the form

$$E_{tx} = \frac{2k_z}{k_z + i\gamma} E_{ix}, \quad E_{ty} = \frac{-2i\gamma k_z}{k_t(k_z\varepsilon + i\gamma)} E_{iz}, \quad E_{tz} = \frac{2k_z}{k_z\varepsilon + i\gamma} E_{iz}, \tag{3.7}$$

$$E_{\alpha x} = \frac{2k_z(1-\varepsilon)}{\varepsilon\Gamma_\alpha + \gamma_\alpha} \xi_\alpha \left[\frac{k_{\alpha y}^2 - \gamma_\alpha\Gamma_\alpha}{k_z + i\gamma} E_{ix} - ik_{\alpha x} \frac{k_t\gamma_\alpha - \gamma k_{\alpha y}}{k_t(\varepsilon k_z + i\gamma)} E_{iz} \right], \tag{3.8}$$

$$E_{\alpha y} = \frac{2k_z(1-\varepsilon)}{\varepsilon\Gamma_\alpha + \gamma_\alpha} \xi_\alpha \left[\frac{-k_{\alpha x}k_{\alpha y}}{k_z + i\gamma} E_{ix} + i \frac{\gamma\Gamma_\alpha\gamma_\alpha - k_t\gamma_\alpha k_{\alpha y} - \gamma k_{\alpha x}^2}{k_t(\varepsilon k_z + i\gamma)} E_{iz} \right], \tag{3.9}$$

$$E_{\alpha z} = \frac{2k_z(1-\varepsilon)}{\varepsilon\Gamma_\alpha + \gamma_\alpha} \xi_\alpha \left[\frac{-ik_{\alpha x}\Gamma_\alpha}{k_z + i\gamma} E_{ix} + \frac{k_t k_\alpha^2 - \gamma\Gamma_\alpha k_{\alpha y}}{k_t(\varepsilon k_z + i\gamma)} E_{iz} \right], \tag{3.10}$$

where $\varepsilon \equiv \varepsilon(\omega)$, $\xi_s = \xi_q(t)$, $\xi_{as} = \xi_q^*(t)$.

The formulas (3.7)–(3.10) hold for media with arbitrary values of $\varepsilon(\omega)$. Analogous expressions also exist for fields outside the medium.[172]

The amplitudes of the diffracted waves (3.4)–(3.10) have a resonant dependence on $\mathbf{k}_\alpha$, owing to the presence of the quantity $\varepsilon(\omega)\Gamma_\alpha + \gamma_\alpha$ in the denominators of (3.8)–(3.10). We shall study, for example, the case of metals and melts of those semiconductors for which in the optical region of the spectrum $\varepsilon'(\omega) < 0$, and in addition

$$|\varepsilon'(\omega)| \gg \varepsilon''(\omega), \quad |\varepsilon'(\omega)| \gg 1. \tag{3.11}$$

In this case we have for the resonance factor, which appears in (3.8)–(3.10):

$$l_\alpha = \frac{k_0(\varepsilon-1)}{\varepsilon(\omega_\alpha)\Gamma_\alpha+\gamma_\alpha} \approx \frac{k_0}{|\varepsilon'|^{1/2}(\Delta k_\alpha - i\Gamma_p)}; \tag{3.12}$$

where

$$\Delta k_\alpha = k_\alpha - \left(\frac{|\varepsilon'|}{|\varepsilon'|-1}\right)^{1/2} k_0, \quad \Gamma_p = \frac{k_0\varepsilon''}{2|\varepsilon'|^2} \ll k_0. \tag{3.13}$$

The width of the electromagnetic resonance is determined by the decay constant of the SEW Γ_p.

From the relations (3.6), (3.8)–(3.10) and (3.12), (3.13) it is evident that the amplitudes of the diffracted waves grow resonantly (by a factor of $k_0/\Gamma_p|\varepsilon'|^{1/2} \gg 1$) when the moduli of their wave vectors $\mathbf{k}_\alpha$ are equal to those of the free SEW (i.e., $\Delta k_\alpha = 0$), while the diffracted waves correspond to induced SEW (their amplitudes, according to (3.4)–(3.6), decay exponentially away from the surface).

The resonance dependence of the amplitudes of the diffracted waves on $\mathbf{k}_\alpha$ occurs not only in the case of metals and melts of semiconductors ($\varepsilon' < 0$) but also for dielectrics ($\varepsilon' > 0$). This is illustrated in Fig. 21, which shows the qualitative dependences of the resonance factor l_α (α = s,as) on $\mathbf{k}_s$ in the case when $|\varepsilon| \gg 1$ ($\varepsilon^{1/2} \equiv n + im$). This resonance behavior of l_α is important for the interpretation of the experimental results on the generation of ordered structures.

It follows from the expressions (3.8)–(3.10) that the amplitudes of the diffracted waves grow linearly with $\xi_\mathbf{q}$. In particular, for metals near the resonance we have from the formula (3.8) $E_{\alpha x} \approx (2k_0\xi_\alpha)(|\varepsilon'|/\varepsilon'')E_{ix}$. It is evident from this expression that already for grating amplitudes of ~ 100 Å significant conversion of the pumping wave into the diffracted wave should be expected. Thus, for example, in the case of copper ($\varepsilon = -37 + i\cdot 3.4$ with $\lambda = 1.06\ \mu$m) for a grating with an amplitude of $2\xi_\alpha = 100$ Å we have $E_{\alpha x} \approx 0.6E_{ix}$. As shown in Refs. 137 and 205, taking into account terms which are nonlinear in $\xi_\mathbf{q}$ limits the growth of the fields $\mathbf{E}_\alpha$ and $\mathbf{E}'_\alpha$ with $\xi_\mathbf{q}$.

Most theoretical works on surface periodic structures are limited to the calculation and analysis of the expression for the spatial harmonic of the power $Q_\mathbf{q}$, absorbed in the medium due to interference[139,136,199,207] (electrodynamic model). The expression $Q_\mathbf{q}$ at $z = 0$ has the form ($\mathbf{D}$ is the displacement vector)

$$Q_\mathbf{q} \equiv \left(\mathbf{E}\frac{\partial \mathbf{D}}{\partial t}\right)_{z=0} \sim (f_s + f_{as})\, e^{-iqx} + \text{c.c.},$$

where f_s and f_{as} are determined by the formulas (3.24), (3.26), and (3.27). It is evident from these formulas that $Q_\mathbf{q}$ is proportional to electrodynamic resonance factors (see (3.12), (3.50), (3.51), and Fig. 21). In the electrodynamic model the extrema of $Q_\mathbf{q}$ as a function of the variables $\mathbf{q}$, φ_s, and φ_{as} determine the periods and the orientations of the dominant gratings. This approach enables predicting which structures are possible, but does not enable determining whether they are actually realized.

As will be shown in Sec. 3.4, the growth increments of CW also depend on resonance factor (3.50), (3.51) (cf. (3.54), (3.52)), and different situations, when one or another extremum of the resonance factors gives rise to the formation of the dominant grating, can be realized, depending on the pumping intensity. Thus the final conclusion regarding the realization of some specific grating and the optimal conditions for such a realization can be drawn only based on the theory of surface instabilities.

3.3. Feedback mechanisms in the premelting state. Generation of coupled surface electromagnetic and acoustic waves

This effect, arising due to nonuniform thermal expansion, is studied in detail in Ref. 165. It is of interest primarily for interpreting experiments with reversible gratings.[150] The solution of the equation of heat conduction and the equation for the displacement vector of the medium with the corresponding boundary conditions leads to a dispersion equation

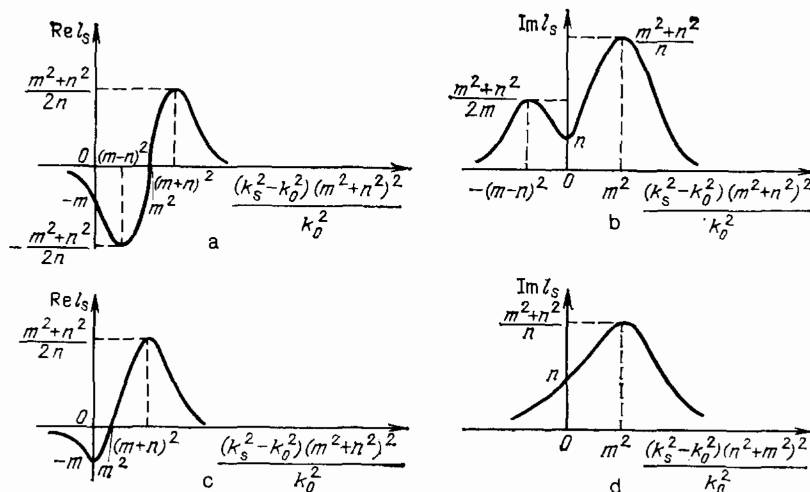

FIG. 21. a) Qualitative dependence of the real part of the electromagnetic factor Re l_s on k_s in the case of a metal [$\sqrt{\varepsilon} = n + im$, $m > n$, $|\varepsilon| \gg 1$ (according to the formula (3.51)]; b) qualitative dependence of Re l_s on k_s in the case of a dielectric ($m < n$, $|\varepsilon| \gg 1$); c) qualitative dependence of the imaginary part of the electromagnetic factor Im l_s on k_s in the case of a metal [$m > n$, $|\varepsilon| \gg 1$ (according to the formula (3.51))]; d) qualitative dependence of Im l_s on k_s in the case of a dielectric ($m < n$, $|\varepsilon| \gg 1$).

for $\Omega = \Omega_q - i\gamma_q$ ($\xi(\mathbf{r},t) = \xi_0 \exp(\gamma_q t + i\Omega_q t - i\mathbf{qr})$ + c.c., ξ_0 is the seed amplitude of the SAW). It follows from this equation that the critical pumping intensity for exciting Rayleigh SAW ($\Omega_q \sim c_t q$) is determined by the expression

$$|\mathbf{E}_i|^2_{cr} \approx \frac{\gamma_\eta 2\pi c_l^2 \rho c V}{K\alpha\omega} \quad (\gamma_q > 0 \text{ for } |\mathbf{E}_i|^2 > |\mathbf{E}_i|^2_{cr}),$$

where γ_η is the decay constant of SAW, $c_{l,t}$ are the longitudinal and transverse sound velocities, ρ is the density of the medium, c_V is the heat capacity per unit volume, K is the hydrostatic compression modulus, and α is the coefficient of thermal expansion. For copper, for example, using the data in Ref. 167, we have $I_{cr} \approx 2 \cdot 10^7$ W/cm^2 with $\lambda = 10.6\,\mu$m.

Aside from the usual (Rayleigh) SAW, the dispersion equation[165] also describes the excitation of a new class of SAW, for which Ω_q is determined by the intensity of laser pump and the characteristics of the excitation of SEW. These SAW were later studied in Ref. 216. Under normal incidence, for example, laser pumping excites a static SAW ($\Omega_q = 0$) with

$$\gamma_q = \frac{2}{3}\left[\frac{2\omega K\alpha\,|\mathbf{E}_i|^2}{\pi c_V \rho\,(c_l^2 - c_t^2)} - 2\chi K_0^2\right],$$

where χ is the coefficient of thermal diffusivity. The critical intensity for the case of copper ($\lambda = 1.06\,\mu$m) is equal to $I_{cr} \approx 2 \cdot 10^8$ W/cm^2. For $I_i > I_{cr}$ a static sinusoidal grating, whose period is equal to the wavelength of the exciting radiation λ and the vector $\mathbf{q}$ is parallel to the vector $\mathbf{E}_i$, appears on the surface.

A detailed study of the characteristics of laser-induced SAW as a function of the pumping parameters is carried out in Ref. 165. Figure 22 shows the results obtained there for the dependences of the increments of SAW on their direction of propagation. For oblique ($\theta = 0$) incidence of an s-polarized and quite intense pumping wave, in the case when $2\cos^2\theta > 1$, the absolute maximum of γ_q is achieved for $\cos\varphi_s = \cos\varphi_{as} = \sin\theta$ (see Fig. 22a). The corresponding frequency and direction of the SAW vector are determined by the expressions

$$\mathbf{q} \perp \mathbf{k}_t \text{ (i.e. } \mathbf{q} \parallel \mathbf{E}_i),\; q = k_0\cos\theta,\; \Omega_q = \beta c_t q. \qquad (3.14)$$

This absolute maximum of SAW is determined by the fact that for $\cos\varphi_s = \cos\varphi_{as} = \sin\theta$ (i.e., with $\mathbf{q}\perp\mathbf{k}_t$), as can be seen from Fig. 20a, both SEW waves—the Stokes wave (α = s) and the anti-Stokes wave (α = as)—are in resonance, while for other orientations only one wave, either α = s or α = as, is in resonance (see Fig. 20b).

For p polarization (as can be seen from Fig. 22b) the maximum of γ_q is achieved for two directions of $\mathbf{q}$($\cos\varphi_s = \pm 1$); in this case, two SAW with the parameters $\mathbf{q}\uparrow\downarrow\mathbf{k}_t$, $q = k_0(1 - \sin\theta)$; $\mathbf{q}\uparrow\uparrow\mathbf{k}_t$, $q = k_0(1 + \sin\theta)$ are generated.

3.4. Generation of capillary waves and evaporation waves accompanying the interaction of laser radiation with liquid metals, semiconductors, and dielectrics

In the presence of a spatially uniform surface melt (the pumping energy density $W > W_{melt}$) two instabilities can play the basic role: the capillary wave (CW) instability[146,168,169] and the interference spatially nonuniform evaporation instability (IEI).[170–173] These processes are usually studied separately. Under certain conditions, however, the hydrodynamic and evaporation effects can affect one another.[169,174] In this section we shall study both instabilities using a unified approach.

Feedback accompanying the generation of CW and IEI is formed by three mechanisms, depending on the degree of heating of the surface: 1) because of the dependence of the coefficient of surface tension σ on T, thermocapillary forces which build up CW with frequency Ω_q and wave vector $\mathbf{q}$, arise; 2) the recoil pressure in the process of spatially nonuniform evaporation of matter from the surface makes an additional contribution to building up of CW; 3) finally, the process of direct mass outflow accompanying spatially nonuniform evaporation also increases the amplitude of the modulation of the relief.

In this section a general dispersion equation taking into account the contributions of both the evaporative mechanism and generation of CW, whose solution $\Omega = \Omega_q - i\gamma_q$ gives the increment γ_q and the frequency Ω_q as a function of $\mathbf{q}$, ω, θ, and the intensity and polarization of the pumping wave for media with arbitrary dielectric permittivity $\varepsilon = \varepsilon' + i\varepsilon'' \equiv (n + im)^2$ is obtained. The dispersion equation obtained enables determining the regions where each of the three indicated mechanism of formation of gratings dominates and describing from a unified point of view the generation of both the usual ($\mathbf{q}\|\mathbf{E}_{it}$, $q \sim k_0$, see Fig. 18) and anomalous ($\mathbf{q}\perp\mathbf{E}_{it}$) gratings, as well as small-scale ($q \gg k_0$) structures ($\mathbf{q}\perp\mathbf{E}_{it}$), observed in Refs. 146 and 175 ($\mathbf{E}_{it}$ is the projection of $\mathbf{E}_i$ on the plane $z = 0$).

It is important to emphasize the CW responsible for the formation of gratings obey the dispersion law $\Omega = \Omega(\mathbf{q})$,

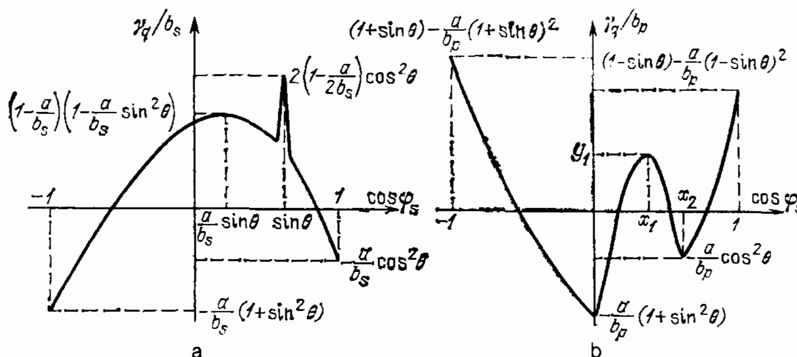

FIG. 22. a) The time-dependent growth increment γ_q of SAW as a function of $\cos\varphi_s$ (see Ref. 165) in the case of oblique incidence ($\theta \neq 0$) of an s-polarized pump wave; b) dependence of the time-dependent increment of SAW γ_q on $\cos\varphi_s$ in the case of oblique incidence ($\theta \neq 0$) of a p-polarized pump wave.

$x_1 = \sin\theta\cdot[1 + (2a/b_p)]/2$, $x_2 = \sin\theta$,

$y_1 = \sin^2\theta\cdot[1 + (4a^2/b_p^2)]/4 - (a/b_p)$,

$b_s \approx \frac{K\alpha}{4c_l^2}\,\frac{\omega\,|\mathbf{E}_i|^2}{\pi c_V}\cos^2\theta$,

$b_p = \frac{b_s}{\cos^2\theta + |\varepsilon'|^{-1}}$, $a \approx \nu k_0^2/2$

which depends substantially on the parameters of the laser radiation. For this reason the waves studied here form an essentially qualitatively new class of CW, which can be called laser-induced CW. The dispersion law obtained here for these waves describes the generation of CW doublets. The existence of laser-induced evaporation waves whose dispersion characteristics depend on the parameters of laser pumping and the value of $\varepsilon(\omega)$ also follows from the general dispersion equation (see Sec. 3.5).

3.4.1. Spatially nonuniform heating, evaporation and motion of liquid accompanying the interaction of radiation with matter

We shall assume that the melt occupies the half-space $z>\xi(x,t)$,

$$\xi(x,t)=\xi_1(x,t)+\xi_2(x,t)$$
$$=[\xi_1(t)+\xi_2(t)]e^{-iqx}+\text{c.c.}$$
$$=\xi_q(t)e^{-iqx}+\text{c.c.},\qquad(3.15)$$

where $\xi_1(x,t)$ is an arbitrary Fourier component of the relief formed when matter is removed from the surface during the evaporation process, and $\xi_2(x,t)$ is the relief arising owing to the excitation of CW (we note that in (3.15), in contrast to (3.2), $\xi_q(t)$ contains the full dependence on t).

We shall take into account the fact that because of the evaporation of matter from the surface the interface (3.15) moves as a whole with a velocity v_0 along the z axis. We introduce a moving coordinate system x, y, z, related to the stationary coordinate system by the relations $x=x'$, $y=y'$, $z=z'-v_0t$. In the moving coordinate system the interface will be described by the formula (3.15), while the distribution of the fields (3.5) will remain virtually unchanged owing to the shortness of the time over which stationary amplitudes $\mathbf{E}_t$, $\mathbf{E}_\alpha$ are established in calculating them it may be assumed that $\xi_q(t)=\text{const}$, $v_0=0$).

The saturation vapor pressure over the surface is given by the formula[176,177]

$$p_{\text{sat}}=p_c\exp\left[\frac{U}{R}\left(\frac{1}{T_c}-\frac{1}{T(x,z,t)}\right)-\frac{\sigma}{RT(x,z,t)}q^2\xi(x,t)\right],\qquad(3.16)$$

and the temperature dependence of the rate of evaporation of matter is determined by the expression

$$v_0+\frac{\partial\xi_1(x,t)}{\partial t}=C_0\exp\left[-\frac{U}{RT(x,z,t)}-\frac{\sigma q^2}{RT(x,z,t)}\xi(x,t)\right],\qquad(3.17)$$

where p_c is the saturated vapor pressure at the temperature of the surface equal to T_c, U is the activation energy per unit volume, $R=\bar{n}k_B$, $\bar{n}$ is the number of molecules of the material per unit volume, and k_B is Boltzmann's constant. The constant C_0 is determined from the experimental dependence of p_{sat} on T, if the following relation is used[176]

$$p_{\text{sat}}=v_0(2\pi\rho RT)^{1/2},\qquad(3.18)$$

where ρ is the density of the material. If it is assumed that in the evaporation process the molecules returning to the surface stick to the surface, then the recoil pressure is approximately equal to

$$p\approx\frac{p_{\text{sat}}}{2}.\qquad(3.19)$$

We shall assume that the melt is an incompressible liquid. In the moving coordinate system the motion of the liquid is described by the equation[158]

$$\Delta\varphi=0,\quad\frac{\partial\mathbf{A}}{\partial t}-v_0\frac{\partial\mathbf{A}}{\partial z}=\nu\Delta\mathbf{A},\quad\operatorname{div}\mathbf{A}=0,$$
$$\mathbf{v}=\operatorname{grad}\varphi+\operatorname{rot}\mathbf{A},\qquad(3.20)$$

where ν is the kinematic coefficient of viscosity, φ and $\mathbf{A}$ are the scalar and vector potentials of the velocity $\mathbf{v}$. We represent the temperature of the surface in the form

$$T(x,z,t)=T_0(z)+T_1(x,z,t),\qquad(3.21)$$

where $T_0(z)$ is the temperature characterized by the uniform heating along the surface $z=0$, and $T_1(x,z,t)\sim\xi(x,t)$ is the spatially nonuniform heating of the liquid. The boundary conditions at $z=0$ can be written down, with accuracy up to terms proportional to ξ^2 using (3.16)–(3.19), in the following form:

$$\frac{\partial\varphi}{\partial t}-v_0\frac{\partial\varphi}{\partial z}-g_0\xi(x,t)+\sigma_0\frac{\partial^2\xi(x,t)}{\partial x^2}+2\nu\frac{\partial v_z}{\partial z}+p_{0T}\left(T_1+\frac{\partial T_0}{\partial z}\xi(x,t)\right)-\frac{p_0\sigma q^2}{RT_{0s}}\xi(x,t)=0,$$

$$\nu\left(\frac{\partial v_x}{\partial z}+\frac{\partial v_z}{\partial x}\right)+\sigma_{0T}\left(\frac{\partial T_1}{\partial x}+\frac{\partial T_0}{\partial z}\frac{\partial\xi(x,t)}{\partial x}\right)=0,\qquad(3.22)$$

where $p_0=p_{\text{in}}/2\rho$, $\sigma_0=\sigma/\rho$, $\sigma_{\text{OT}}=\text{d}\sigma/\rho\text{d}T$, $p_{\text{OT}}=\text{d}p_{\text{in}}/2\rho\text{d}T$, $T_{\text{OS}}=T_0(z=0)$ $g_0=g_c/\rho$, g_c and g is the acceleration of gravity. The velocity component v_z is related to $\xi_2(x,t)$ by the relation

$$v_z(x,z=0,t)=\frac{\partial\xi_2(t)}{\partial t}.\qquad(3.23)$$

With the use of (3.7)–(3.10) the heating of the liquid in the presence of evaporation from a surface with the relief (3.15) is described in the moving coordinate system by the equation

$$\frac{\partial T}{\partial t}-v_0\frac{\partial T}{\partial z}+\mathbf{v}\nabla T=\chi\Delta T+f_0e^{-\gamma_0z}+[(f_se^{-(\gamma_s+\gamma^*)z}+f_{as}e^{-(\gamma_{as}^*+\gamma)z})\xi_q(t)e^{-iqx}+\text{c.c.}],\qquad(3.24)$$

$$T(x,z,t=0)=T_{\text{in}},\quad T(x,z=\infty,t)=T_{\text{in}},$$
$$\left.\frac{\partial T(x,z,t)}{\partial\mathbf{n}}\right|_{z=\xi(x,t)}=\frac{g_v}{\varkappa}\left(v_0+\frac{\partial\xi_1(x,t)}{\partial t}\right),\qquad(3.25)$$

where $\varkappa=c_p\chi$, c_p is the heat capacity per unit volume, $\gamma_0=\gamma+\gamma^*$, and g_v is the latent heat of vaporization per unit volume, T_{in} is the initial temperature, and $\mathbf{n}$ is the unit vector normal to the surface $z=\xi(x,t)$. The quantities f_0, f_s, and f_{as}, characterizing the intensity of the heat sources, in the case of s-polarized incident radiation and with arbitrary $\varepsilon(\omega)$ are given by

$$f_0=\frac{2\omega\varepsilon''k_z^2|\mathbf{E}_1|^2}{\pi c_p|k_z+i\gamma|^2},\qquad(3.26)$$
$$f_s=f_0(\varepsilon-1)\left(\frac{\gamma_s\Gamma_s\sin^2\varphi_s}{\varepsilon\Gamma_s+\gamma_s}-\frac{k_0^2\cos^2\varphi_s}{\Gamma_s+\gamma_s}\right);$$

and in the case of a p-polarized pumping wave we have

$$f_0=\frac{2\omega\varepsilon''}{\pi c_p}\frac{k_z^2}{|\varepsilon k_z+i\gamma|^2}\frac{|\gamma|^2+k_t^2}{k_0^2}|\mathbf{E}_i|^2,$$

$$f_s=\frac{2\omega\varepsilon''}{\pi c_p}\frac{k_z^2}{|\varepsilon k_z+i\gamma|^2}|\mathbf{E}_i|^2(1-\varepsilon)$$

$$\times\frac{|\gamma|^2(k_s^2\sin^2\varphi_s-\gamma_s\Gamma_s)+k_sk_t[k_tk_s+(\gamma_s\gamma^*-\gamma\Gamma_s)\cos\varphi_s]}{k_0^2(\varepsilon\Gamma_s+\gamma_s)}, \quad (3.27)$$

where $\cos\varphi_\alpha=(\mathbf{k}_t\mathbf{k}_\alpha)/k_tk_\alpha$, $\alpha=$ s, as. The quantities f_{as} for s- and p-polarized pumping waves are obtained from (3.26) and (3.27) by the substitution $\varepsilon\to\varepsilon^*$, $k_s\to k_{as}$, $\varphi_s\to\varphi_{as}$, $\gamma_s\to\gamma'_{as}$, $\Gamma_s\to\Gamma^*_{as}$, $\gamma\to\gamma^*$.

We shall solve the problem (3.24)–(3.27) in two stages. In the stationary state, in the zeroth-order approximation in $\xi(x,t)$ we obtain[2)] from (3.24)

$$-v_0\frac{dT_0(z)}{dz}=\chi\Delta T_0(z)+f_0e^{-\gamma_0z},$$

$$T_{0s}(z=0)=T_{0\pi},\quad T_0(z=\infty)=T_{in},\quad (3.28)$$

$$\left.\frac{dT_0(z)}{dz}\right|_{z=0}=\frac{gv_0}{\varkappa},$$

where T_{0s} is the as yet unknown surface temperature. The stationary solution of the problem (3.28) can be written in the form

$$T_0(z)=Ae^{-\gamma_0z}+Be^{-v_0z/\chi}+T_{in},$$

$$A=-\frac{f_0}{\gamma_0(\gamma_0\chi-v_0)},\quad B=\frac{f_0\chi}{v_0(\chi\gamma_0-v_0)}-\frac{g}{c_p},\quad (3.29)$$

$$v_0=\frac{f_0c_p}{\gamma_0[g+c_p(T_{0s}-T_{in})]}\quad (A+B=T_{0s}-T_{in}).\quad (3.30)$$

In the zeroth-order approximation in $\xi(x,t)$ we obtain from the formula (3.17)

$$v_0=C_0e^{-U/RT_{0s}}.\quad (3.31)$$

The expressions (3.30) and (3.31) determine the stationary values of v_0 and T_{0s} as a function of the intensity and polarization of the laser radiation.

We now proceed to the calculation of the spatially nonuniform (along the surface $z=0$) temperature distribution $T_1(x,z,t)$. In the approximation linear in $\xi(x,t)$ from (3.24) and (3.25) and using (3.28), we obtain the problem

$$\frac{\partial T_1}{\partial t}-v_0\frac{\partial T_1}{\partial z}=\chi\Delta T_1-v_z\frac{\partial T_0}{\partial z}$$

$$+[(f_se^{-(\gamma_s+\gamma^*)z}+f_{as}e^{-(\gamma^*_{as}+\gamma)z})\xi_q(t)e^{-iqx}+\text{c.c.}],$$

$$T_1(x,z,t=0)=0,\quad T_1(x,z=\infty,t)=0,\quad (3.32)$$

$$\left.\frac{\partial T_1(x,z,t)}{\partial z}\right|_{z=0}+\left.\frac{\partial^2T_0(z)}{\partial z^2}\right|_{z=0}\xi(x,t)=\frac{g}{\varkappa}\frac{\partial\xi_1(x,t)}{\partial t}.$$

To solve this problem it is necessary to calculate v_z. We shall seek the established solution of the problem (3.20) in the form

$$\varphi=\varphi_0\exp(-iqx-qz+i\Omega t)+\text{c.c.},\quad\Omega=\Omega_q-i\gamma_q,\quad (3.33)$$

$$A_y=a_0\exp(-iqx-\delta z+i\Omega t)+\text{c.c.},\quad A_x=A_z=0,$$

$$\xi_1(t)=\xi_{10}\exp(i\Omega t),\quad\xi_2(t)=\xi_{20}\exp(i\Omega t),\quad\xi_0=\xi_{10}+\xi_{20},\quad (3.34)$$

where φ_0, a_0, ξ_0 determine the motion of the liquid and the relief of the surface due to the presence of fluctuations and δ is a constant. Substituting (3.33) into (3.20) we obtain

$$i\Omega+v_0\delta=\nu(\delta^2-q^2),\ \text{i.e.},\ \delta=\frac{v_0}{2\nu}+\left(q^2+\frac{i\Omega}{\nu}+\frac{v_0^2}{4\nu^2}\right)^{1/2},\quad (3.35)$$

$$v_x=(-iq\varphi_0e^{-qz}+\delta a_0e^{-\delta z})e^{-iqx+i\Omega t}+\text{c.c.},\quad v_y=0,$$

$$v_z=(-q\varphi_0e^{-qz}-iqa_0e^{-\delta z})e^{-iqx+i\Omega t}+\text{c.c.}\quad (3.36)$$

From the formula (3.23), and using (3.15) and (3.34), we find the relation

$$\xi_{20}=-\frac{q\varphi_0+iqa_0}{i\Omega}.\quad (3.37)$$

We substitute (3.34), (3.36), (3.37) into (3.32), and we shall seek the established distribution $T_1(x,z,t)$ in the form

$$T_1(x,z,t)=T_{10}(z)\exp(-iqx+i\Omega t).$$

The quantity $T_{10}(z)$ is easily found from (3.32), but has a quite cumbersome form. To derive the dispersion equation, however, it is sufficient to determine $T_1(x,z=0,t)$. Introducing the notation

$$\left.\begin{aligned}A_1&=\frac{f_s}{\gamma_T[\chi(\gamma_T+\gamma_s+\gamma^*)-v_0]}+\frac{f_{as}}{\gamma_T[\chi(\gamma_T+\gamma^*_{as}+\gamma)-v_0]}\\&\quad-\frac{f_0}{\chi\gamma_T}-\frac{gi\Omega}{\gamma_T\varkappa}+\frac{gv_0}{\varkappa}\left(1-\frac{v_0}{\chi\gamma_T}\right),\\A_2&=\frac{f_0}{\chi\gamma_T[\chi(\gamma_T+\gamma_0+q)-v_0](\gamma_T+q)}+\frac{\chi(\gamma_T+q)-v_0}{\chi(\gamma_T+q)}\frac{g}{\gamma_T\varkappa},\\A_3&=\frac{f_0}{\chi\gamma_T[\chi(\gamma_T+\gamma_0+\delta)-v_0](\gamma_T+\delta)}+\frac{\chi(\gamma_T+\delta)-v_0}{\chi(\gamma_T+\delta)}\frac{g}{\gamma_T\varkappa},\end{aligned}\right\}\quad (3.38)$$

$$\gamma_T=\frac{v_0}{2\chi}+\left(q^2+\frac{i\Omega}{\chi}+\frac{v_0^2}{4\chi^2}\right)^{1/2},\quad(T_{10}(z)\sim e^{-\gamma_Tz}),$$

we shall write $T_1(x,z=0,t)$ in the form

$$T_1(x,z=0,t)$$

$$=\left[\left(A_1-\frac{gv_0}{\varkappa}\right)\xi_0-qA_2\varphi_0-iqA_3a_0\right]e^{-iqx+i\Omega t}+\text{c.c}.\quad (3.39)$$

Thus the temperature distribution is a linear function of the seed fluctuation amplitudes ξ_0, φ_0, a_0.

3.4.2. Dispersion equation for waves of modulation of the relief. Competition between three feedback mechanisms in the formation of surface structures as a function of the conditions of laser heating of the liquid

To obtain the temperature distribution on the surface $z=\xi(x,t)$, we shall expand (3.21) in a Taylor series up to terms proportional to ξ^2. Applying the last boundary condition (3.28) we obtain

$$T(x,z=\xi(x,t),t)=T_{0s}+\frac{gv_0}{\varkappa}\xi(x,T)+T_1(x,z=0,t).$$

Using this expression, we linearize the relation (3.17) with respect to $\xi(x,t)$. Keeping in mind (3.31), we obtain

$$\frac{\partial\xi_1(x,t)}{\partial t}=\left(\frac{gv_0^2U}{\varkappa RT_{0s}^2}-\frac{\sigma v_0}{RT_{0s}}q^2\right)\xi(x,t)$$

$$+\frac{v_0U}{RT_{0s}^2}T_1(x,z=0,t).\quad (3.40)$$

We now substitute (3.15), (3.34), (3.37), and (3.39) into Eq. (3.40) and the boundary conditions (3.22). As a result we arrive at a system of three linear homogeneous equations for the seed amplitudes ξ_0, φ_0, a_0:

$$\left.\begin{aligned}
&(i\Omega+\gamma_s-\gamma_s A_1)\,\xi_0+(v_T q A_2+q)\,\varphi_0+i\,(v_T q A_3+q)\,a_0=0,\\
&\left(\frac{\omega_0^2}{q}-p_{0T}A_1\right)\xi_0+(p_{0T}qA_2-i\Omega-2\nu q^2-v_0 q)\,\varphi_0\\
&\qquad +i\,(p_{0T}qA_3-2\nu q\delta)\,a_0=0,\\
&-\sigma_{0T}qA_1\xi_0+(\sigma_{0T}q^2A_2+2\nu q^2)\,\varphi_0+i\,[\sigma_{0T}q^2A_3\\
&\qquad +\nu\,(\delta^2+q^2)]\,a_0=0,
\end{aligned}\right\} \tag{3.41}$$

where

$$v_T=\frac{v_0 U}{RT_{0s}^2},\qquad p_{0T}=\frac{p_{\rm in}U}{2\rho RT_{0s}^2},$$

$$\gamma_{\rm in}=\frac{v_T\sigma T_{0s}q^2}{U},\qquad \omega_0^2=g_0 q+\sigma_0 q^3+\frac{p_{0T}\sigma T_{0s}q^3}{U}$$

(ω_0 is the frequency of free CW). The condition for a nontrivial solution of the system (3.41) yields the dispersion equation.

Analysis of the experimental data shows that in all cases of practical interest $\gamma_s \ll |\Omega|, 4\nu q^2$. Because of this the dispersion equation, following from (3.41), has the form

$$\begin{aligned}
&(i\Omega)^3+(i\Omega)^2\,[4\nu q^2+v_0(q+\delta)]\\
&\quad +i\Omega\,[4\nu^2q^3(q-\delta)+\omega_0^2+2\nu q^2 v_0(q+\delta)\\
&+v_0^2 q\delta]+\omega_0^2 v_0\delta=\{-\sigma_{0T}q^2\,[i\Omega+2\nu q(q-\delta)+v_0 q]\\
&\quad +p_{0T}q\,[i\Omega+v_0\delta]\\
&\quad +v_T\,[(i\Omega)^2+i\Omega\,(4\nu q^2+v_0(\delta+q))+4\nu^2q^3(q-\delta)\\
&+2\nu q^2 v_0(\delta+q)+v_0^2\delta q]\}\,A_1+\{-\sigma_{0T}q^2\,[i\Omega 2\nu q\delta+\omega_0^2]\\
&+p_{0T}q\,[(i\Omega)^2+i\Omega\,(2\nu q^2+\delta v_0)]-v_T\omega_0^2\,[i\Omega+\delta v_0+2\nu q^2]\}\,A_2\\
&\quad +\{-\sigma_{0T}q^2\,[(i\Omega)^2+i\Omega\,(2\nu q^2+v_0 q)+\omega_0^2]\\
&\qquad -p_{0T}qi\Omega 2\nu q^2+v_T 2\nu q^2\omega_0^2\}\,A_3
\end{aligned} \tag{3.42}$$

For pump wave parameters for which $\gamma_{\mathbf q} > 0$, the amplitudes of the corresponding Fourier components of the surface relief grow exponentially as a function of time. The rate of this growth is determined by the thermocapillary forces ($\sim\sigma_{0T}$), evaporation pressure forces ($\sim p_{0T}$), and the direct outflow of mass accompanying evaporation ($\sim v_T$). The contributions of these processes to Ω, according to (3.42), are in the approximate ratio $|\sigma_{0T}|q^2 : p_{0T}q : v_T|\Omega|$.

For quite low pumping intensities, when the surface temperature T_{0s} is such that the inequality

$$|\sigma_{0T}|\,q > \frac{p_{\rm in}U}{2\rho RT_{0s}^2} \tag{3.43}$$

holds, the thermocapillary mechanism of excitation of the modulations of the relief dominates. When the condition (3.33) breaks down, which occurs when the pumping intensity is raised, the effect of the pressure of evaporation on the motion of the liquid must be taken into account. As the intensity is further raised, when $|\Omega|$ grows to such an extent that (here we took into account the relation (3.18))

$$|\Omega| > \left(\frac{\pi RT_{0s}}{2\rho}\right)^{1/2} q, \tag{3.44}$$

the mass outflow accompanying evaporation is the determining factor.

The complex frequency $\Omega(\mathbf q)$, according to Eq. (3.42), depends substantially on the parameters of the incident radiation through the quantities A_1, A_2, A_3. The first two terms in the expression (3.38) for A_1 arise owing to the presence of interference thermal sources (f_s, f_{as}) in (3.32). Their magnitude depends on the orientation of $\mathbf q$ relative to the plane of incidence of the laser radiation. The third term in A_1, corresponding in the boundary conditions (3.32) to the term proportional to d^2T_0/dz^2, characterizes the thermal contribution to Ω which is independent of the orientation of $\mathbf q$. The quantities A_2 and A_3, taking into account the "magnification" in the liquid, are independent of the orientation of $\mathbf q$ and correspond in (3.32) to the term $v_z\,dT_0/dz$.

3.4.3. Generation of CW and the characteristics of the dominant surface structures for s polarization of the pumping wave

When the surface temperature is not much greater than the melting temperature, so that the condition (3.43) holds, we can set $v_0 = p_{0T} = v_T = 0$, in (3.35), (3.38), and (3.42), i.e., evaporation effects can be neglected. In this case, after some transformations, from (3.42) we shall obtain the dispersion equation describing the instability of the CW amplitudes with arbitrary polarization of the pump:

$$\begin{aligned}
&(i\Omega)^2+4i\Omega\nu q^2+4\nu^2q^3(q-\delta)+\omega_0^2\\
&=\frac{a_{\mathbf q}(\delta-q)}{\delta+q}-\left[\frac{2q\delta}{\delta^2-q^2}+\frac{\omega_0^2}{(i\Omega)^2}\right]b_{\mathbf q}\\
&\qquad +\left[\frac{\delta^2+q^2}{\delta^2-q^2}+\frac{\omega_0^2}{(i\Omega)^2}\right]c_{\mathbf q},
\end{aligned} \tag{3.45}$$

where

$$\begin{aligned}
a_{\mathbf q}&=|\sigma_{0T}|\left[\frac{f_s q^2}{\chi\gamma_T(\gamma_T+\gamma_s+\gamma^*)}+\frac{f_{as}q^2}{\chi\gamma_T(\gamma_T+\gamma_{as}^*+\gamma)}-\frac{f_0 q^2}{\chi\gamma_T}\right],\\
b_{\mathbf q}&=|\sigma_{0T}|\,\frac{f_0q^2(\gamma_T-q)}{\chi\gamma_T(\gamma_T+\gamma_0+q)},\\
c_{\mathbf q}&=|\sigma_{0T}|\,\frac{f_0q^2(\delta-\gamma_T)}{\chi\gamma_T(\gamma_T+\gamma_0+\delta)}\,\frac{\nu}{\chi-\nu}.
\end{aligned} \tag{3.46}$$

Here we took into account the fact that $\sigma_{0T} < 0$ by setting $(-\sigma_{0T}) = |\sigma_{0T}|$.

If f_0 and f_s are given by the formulas (3.26), then Eq. (3.45) describes the rate of growth (decay) of the Fourier amplitudes of the CW with s polarization of the pump and arbitrary $\varepsilon(\omega)$.

For simplicity we shall further assume that the conditions

$$\nu \ll \chi,\quad |\varepsilon| \gg 1,\quad \gamma_0 \gg |\gamma_T|,\quad |\Omega| \gtrless \omega_0,\quad |\Omega| \gg \nu q^2 \tag{3.47}$$

hold. This situation is often realized in experiments (for example, in Refs. 145, 139, and 153). It is easy to see that under the conditions (3.47) Eq. (3.45) is substantially simplified and assumes the form

$$(i\Omega)^2 = a_{\mathbf q} - \omega_0^2. \tag{3.48}$$

We substitute (3.26) into (3.46) and use the relation

$(k_\alpha^2 - \gamma_\alpha\Gamma_\alpha)(\Gamma_\alpha + \gamma_\alpha) = k_0^2(\xi\Gamma_\alpha + \gamma_\alpha), \quad \alpha = \mathrm{s}, \quad \mathrm{as}.$ Then the expression for $a_\mathbf{q}$ can be written in the form

$$a_\mathbf{q} = \frac{|\sigma_{0\mathrm{T}}| f_0 q^2}{\chi\gamma_\mathrm{T}}\Big[\frac{\varepsilon-1}{\gamma_\mathrm{T}+\gamma_\mathrm{s}+\gamma^*}\Big(\frac{k_\mathrm{s}^2\sin^2\varphi_\mathrm{s}}{\varepsilon\Gamma_\mathrm{s}+\gamma_\mathrm{s}} - \frac{k_0^2}{\Gamma_\mathrm{s}+\gamma_\mathrm{s}}\Big) + \frac{\varepsilon^*-1}{\gamma_\mathrm{T}+\gamma_\mathrm{as}^*+\gamma}\Big(\frac{k_\mathrm{a}^2\sin^2\varphi_\mathrm{as}}{\varepsilon^*\Gamma_\mathrm{as}^*+\gamma_\mathrm{as}^*} - \frac{k_0^2}{\Gamma_\mathrm{as}^*+\gamma_\mathrm{as}^*}\Big) - 1\Big]. \quad (3.49)$$

The number one in the brackets in (3.49) corresponds to the purely thermal, independent of the orientation of $\mathbf{q}$, contribution to Ω. We shall now show that $a_\mathbf{q}$ undergoes resonant growth, when $k_\mathrm{s} \approx k_0$ or $k_\mathrm{as} \approx k_0$. Keeping in mind the conditions (3.47), we can set in the expression (3.49) near resonance

$$\Gamma_\mathrm{s} + \gamma_\mathrm{s} \approx \gamma_\mathrm{s} \approx (m - in)k_0, \quad \Gamma_\mathrm{as}^* + \gamma_\mathrm{as}^* \approx \gamma_\mathrm{as}^* \approx (m+in)k_0,$$
$$\gamma_\mathrm{T} + \gamma_\mathrm{s} + \gamma^* \approx \gamma_\mathrm{T} + \gamma_\mathrm{as}^* + \gamma \approx 2k_0 m.$$

In this case the sum of the terms proportional to $k_0^2/(\Gamma_\alpha + \gamma_\alpha)$ exactly compensate the unit term in the brackets in (3.49). As a result near resonance we have

$$a_\mathbf{q} = \frac{|\sigma_{0\mathrm{T}}| f_0 q^2}{\chi\gamma_\mathrm{T}\cdot 2m}(l_\mathrm{s}\sin^2\varphi_\mathrm{s} + l_\mathrm{as}^*\sin^2\varphi_\mathrm{as}), \quad l_\alpha = \frac{\varepsilon k_0}{\varepsilon\Gamma_\alpha + \gamma_\alpha} \quad (\alpha = \mathrm{s}, \mathrm{as}). \quad (3.50)$$

We introduce the notation

$$x_\mathrm{s} = \Big(\frac{k_\mathrm{s}^2 - k_0^2}{k_0^2}\Big)^{1/2} - \beta_m, \quad y_\mathrm{s} = \Big(\frac{k_0^2 - k_\mathrm{s}^2}{k_0^2}\Big)^{1/2} + \beta_n,$$
$$\beta_m = \frac{m}{m^2+n^2}, \quad \beta_n = \frac{n}{m^2+n^2}.$$

In this notation the real and imaginary parts of l_s near resonance ($k_\mathrm{s} \approx k_0$) can be written in the form

$$\operatorname{Re} l_\mathrm{s} = \frac{x_\mathrm{s}}{x_\mathrm{s}^2+\beta_n^2}, \quad \operatorname{Im} l_\mathrm{s} = \frac{\beta_n}{x_\mathrm{s}^2+\beta_n^2}, \quad \text{if} \quad k_\mathrm{s} \geqslant k_0,$$
$$\operatorname{Re} l_\mathrm{s} = -\frac{\beta_m}{y_\mathrm{s}^2+\beta_m^2}, \quad \operatorname{Im} l_\mathrm{s} = \frac{y_\mathrm{s}}{y_\mathrm{s}^2+\beta_m^2}, \quad \text{if} \quad k_\mathrm{s} \leqslant k_0. \quad (3.51)$$

The qualitative dependence of $\operatorname{Re} l_\mathrm{s}$ and $\operatorname{Im} l_\mathrm{s}$ on k_s for metals ($m > n$) and dielectrics ($m < n$) are presented in Fig. 21. We shall further assume that $q^2 + (\gamma_\mathbf{q}/\chi) > \Omega_\mathbf{q}/\chi$, so that ($\gamma_\mathrm{T} \approx \gamma_{0\mathrm{T}} = [q^2 + (\gamma_\mathbf{q}/\chi)]^{1/2}$ may be regarded as a real quantity. Then, substituting (3.51) into (3.50), we obtain in the region $k_\alpha \geqslant k_0$

$$a = \frac{|\sigma_{0\mathrm{T}}| f_0 q^2}{\chi\gamma_{0\mathrm{T}}2m}\Big(\frac{x_\mathrm{s}\sin^2\varphi_\mathrm{s}}{x_\mathrm{s}^2+\beta_n^2} + \frac{x_\mathrm{as}\sin^2\varphi_\mathrm{as}}{x_\mathrm{as}^2+\beta_n^2}\Big),$$
$$b = \frac{|\sigma_{0\mathrm{T}}| f_0 q^2}{\chi\gamma_{0\mathrm{T}}2m}\Big(\frac{\beta_n\sin^2\varphi_\mathrm{s}}{x_\mathrm{s}^2+\beta_n^2} - \frac{\beta_n\sin^2\varphi_\mathrm{as}}{x_\mathrm{as}^2+\beta_n^2}\Big), \quad (3.52)$$

where $a \equiv \operatorname{Re} a_\mathbf{q}$, $b \equiv \operatorname{Im} a_\mathbf{q}$. Analogous expressions can be obtained for a and b in the region $k_\alpha \lesssim k_0$, in which for metals the quantity b has a local maximum (see Figs. 21c and d). The expression for f_0 in (3.52) for $|\varepsilon| \gg 1$ can be written, according to (3.26), in the form

$$f_0 \approx \frac{4k_0 I_1}{cp}\frac{2mn}{m^2+n^2}\cos^2\theta, \quad I_1 = \frac{c\,|\mathbf{E}_i|^2}{2\pi}. \quad (3.53)$$

In the notation of (3.52) the solution of Eq. (3.48) has the form

$$\gamma_\mathbf{q}^2 = \frac{a-\omega_0^2}{2} + \frac{1}{2}[(a-\omega_0^2)^2 + b^2]^{1/2},$$
$$\Omega_\mathbf{q} = \frac{b}{|b|}\Big\{-\frac{a-\omega_0^2}{2} + \frac{1}{2}[(a-\omega_0^2)^2 + b^2]^{1/2}\Big\}^{1/2}. \quad (3.54)$$

It is evident from (3.54) and (3.52) that $\gamma_\mathbf{q}$ is maximum for those CW for which a and b^2 assume their maximum values. In the case when $|\varepsilon| \gg 1$ (see Fig. 21) $a = \max$ when $k_\alpha^2 = k_0^2 + (m+n)^2k_0^2/(m^2+n^2)^2 \approx k_0^2$, and $b^2 = \max$ for $k_\alpha^2 = k_0^2 + m^2k_0^2/(m^2+n^2) \approx k_0^2$.

This means that for the dominant CW the modulus $|\mathbf{k}_\alpha| \approx k_0$ is fixed, and the orientation of $\mathbf{k}_\alpha$ for the time being remains arbitrary (see Fig. 20). In accordance with the law of conservation of momentum (3.1a) the wave vectors of these CW are found from the relation

$$q^2 = k_\alpha^2 + k_\mathrm{t}^2 - 2k_\alpha k_\mathrm{t}\cos\varphi_\alpha. \quad (3.55)$$

In what follows those CW for which $k_\mathrm{s} = k_\mathrm{a}$, $\sin^2\varphi_\mathrm{s} = \sin^2\varphi_\mathrm{a}$ will be called degenerate. The degenerate case of the orientation of $\mathbf{q}$ (or $\mathbf{k}_\alpha$) is realized for a) $\theta = 0$ and arbitrary values of φ_s and b) $\theta \neq 0$ and $\delta_\mathrm{s} = \pi/2$ (see Fig. 20a). All other CW will be called nondegenerate. For degenerate CW two diffracted electromagnetic waves (Stokes and anti-Stokes) make simultaneously the same resonant contribution to a (3.52), and in this case $b = 0$. In the nondegenerate case only one of the two waves (Stokes and anti-Stokes) can make a resonant contribution to a and b^2.

We introduce the quantity

$$a_1 = \frac{4k_0\,|\sigma_{0\mathrm{T}}|\,I_1 q^2\cos^2\theta\sin^2\varphi_\mathrm{s}}{\chi cp\,[q^2 + (\gamma_\mathbf{q}/\chi)]^{1/2}}. \quad (3.56)$$

Then, on the basis of the remarks made above, we shall formulate the results as follows. The quantity $\gamma_\mathbf{q}$ for degenerate CW assumes its maximum value when $k_\mathrm{s}^2 = k_0^2 + (m+n)^2k_0^2/(m^2+n^2)^2$ and is equal to ($a = \max$, $b = 0$)

$$\gamma_\mathbf{q}^2 = 0, \quad \Omega_\mathbf{q}^2 = \omega_0^2 - a_1, \quad \text{if} \quad a_1 \leqslant \omega_0^2,$$
$$\gamma_\mathbf{q}^2 = a_1 - \omega_0^2, \quad \Omega_\mathbf{q} = 0, \quad \text{if} \quad a_1 > \omega_0^2, \quad (3.57)$$

where in the expression (3.56) for a_1, according to (3.55), we must set $q \approx k_0\cos\theta$, $\sin^2\varphi_\mathrm{s} \approx \cos^2\theta$. The maximum values of $\gamma_\mathbf{q}$ for nondegenerate CW with $a_1 \leqslant 24\omega_0^2/7$ are attained when $k_\mathrm{s}^2 = k_0^2 + mk_0^2/(m^2+n^2)^2$ and are equal to ($a = 0$, $b = \max$)

$$\gamma_\mathbf{q}^2 = \frac{1}{2}[-\omega_0^2 + (\omega_0^4 + a_1^2)^{1/2}], \quad \Omega_\mathbf{q} = \frac{a_1}{2\gamma_\mathbf{q}}, \quad (3.58)$$

and for $a_1 > 24\omega_0^2/7$ the maximum values of $\gamma_\mathbf{q}$ are given by the formula ($k_\mathrm{s}^2 = k_0^2 + k_0^2(m+n)^2/(m^2+n^2)^2$, $a = \max$, $b \neq 0$)

$$\gamma_\mathbf{q}^2 = \frac{1}{2}\Big\{\frac{a_1}{2} - \omega_0^2 + \Big[\Big(\frac{a_1}{2} - \omega_0^2\Big)^2 + \frac{a_1^2}{4}\Big]^{1/2}\Big\}, \quad \Omega_\mathbf{q} = \frac{a_1}{4\gamma_\mathbf{q}}. \quad (3.59)$$

In the expressions (3.58) and (3.59) a_1 is determined by the formula (3.56). The formulas (3.57)–(3.59) give the frequencies of the dominant CW and the growth increments of the amplitudes as a function of the orientation of $\mathbf{q}$ and of the pumping intensity. Figure 23 shows the dependence of $\gamma_\mathbf{q}$ on $\cos\varphi_\mathrm{s}$ for three values of θ according to the formulas (3.57)–(3.59). The absolute maximum of $\gamma_\mathbf{q}$ corresponds to CW with the parameters

$$\mathbf{q} \,\|\, \mathbf{E}_1, \quad q = q_1 \equiv k_0(n^{*2} - \sin\theta)^{1/2}, \quad n^{*2} = 1 + \frac{(m+n)^2}{(m^2+n^2)^2}. \quad (3.60)$$

It is evident from Fig. 23 that for $\theta \gtrsim$ 35-40° $\gamma_\mathbf{q}$ assumes its absolute maximum value when $\cos\varphi_\mathrm{s} \approx 0$, i.e., for the nondegenerate wave with the parameters (see Fig. 20)

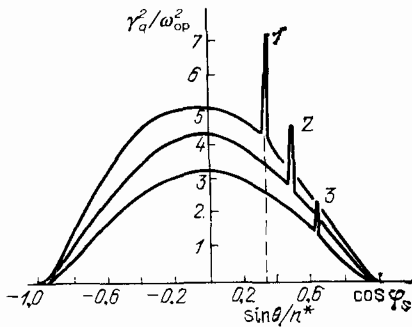

FIG. 23. Theoretical dependence of the increment γ_q of the dominant CW in a germanium melt on the orientation of **q** and the angle of incidence of the s-polarized pump wave according to the formulas (3.55)–(3.59). $T_{melt} = 1200$ K, $\rho = 5.51$ q/cm³, $\nu = 1.35 \cdot 10^{-2}$ cm²/s. $\chi = 0.1$ cm²/s, $c_p = 2.45 \cdot 10^7$ erg/cm³ · deg[181]; $\sigma = 600$ dynes/cm, $\sigma_0 T = 0.07$ cm³/s² · deg[182]; $\varepsilon = -32 + i\ 72$[153] Pumping parameters $\lambda = 1$ μm. $I_1 = 2 \cdot 10^7$ W/cm², $\omega_{op} = 1.64 \cdot 10^3$ c⁻¹. $1 - \theta = 20°$; $2 - \theta = 30°$, $3 - \theta = 40$.

$$q \approx k_0 (1 + \sin^2\theta)^{1/2}, \quad \cos\delta_s = -\frac{\sin\theta}{(1+\sin^2\theta)^{1/2}}. \qquad (3.61)$$

In this case the vector **q** of the wave (3.61) is neither parallel nor perpendicular to $\mathbf{E}_i$. We emphasize that Fig. 23 is more qualitative than quantitative in nature, since in calculating γ_q we set $q^2 + (\gamma_q/\chi) \approx q$ in (3.56).

We note that for both metals and dielectrics the increments of the dominant CW (and this is evident from (3.55)–(3.59)) are virtually independent of n and m. This occurs because of the fact that the dependence of the quantities a and b on m and n, appearing in (3.52) through f_0, is compensated by the dependence of the resonant factor (3.51) on m and n.

3.4.4. Generation of CW and the characteristics of the dominant surface structures for p polarization of the pumping wave

In this case the quantities f_0 and f_s in Eqs. (3.45) and (3.46) are given by the formulas (3.27). We shall study here metals ($m > n$) and dielectrics ($m < n$) for which $|\varepsilon| \gg 1$. As in the case of s polarization of the pump wave the quantity f_α (3.27) exhibits a resonance near $k_\alpha \approx k_0$. Near the resonance the expression (3.27) for f_s can be written in the form

$$f_s = f_0(\varepsilon - 1)\frac{k_0^3 f(\theta, \varphi_s)}{\varepsilon\Gamma_s + \gamma_s} - \frac{k_0^3}{\Gamma_s + \gamma_s}, \qquad (3.62)$$

where $f(\theta,\varphi_s) = n^*\cos^2\varphi_s - \sin\theta\cos\varphi_s$, $n^* = k_s/k_0 \approx 1$, while the quantity f_0, unlike the corresponding expression (3.53), right up to angles of incidence θ close to the glancing angle, is independent of θ and is equal to

$$f_0 = \frac{4k_0 I_1}{c_p}\frac{2mn}{m^2+n^2}. \qquad (3.63)$$

The expression for f_{as} is obtained from (3.62) with the help of the substitution indicated after the formula (3.27).

We shall assume that the conditions (3.47) hold. In this case the dispersion equation (3.45) reduces to the form (3.48), where

$$a_\mathbf{q} = \frac{|\sigma_{0T}|\, f_0 q^2}{\chi\gamma_T}\left[\frac{\varepsilon-1}{\gamma_T+\gamma_s+\gamma^*}\left(\frac{k_0^3 f(\theta,\varphi_s)}{\varepsilon\Gamma_s+\gamma_s} - \frac{k_0^3}{\Gamma_s+\gamma_s}\right) + \frac{\varepsilon^*-1}{\gamma_T+\gamma_{as}^*+\gamma}\left(\frac{k_0^3 f(\theta,\varphi_{as})}{\varepsilon^*\Gamma_{as}^*+\gamma_{as}^*} - \frac{k_0^3}{\Gamma_{as}^*+\gamma_{as}^*}\right) - 1\right]. \qquad (3.64)$$

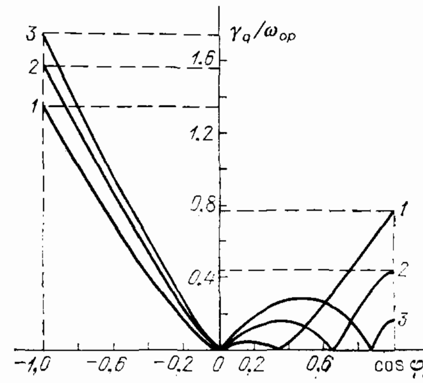

FIG. 24. Dependence of the growth increment of CW γ_q on the orientation of **q** with p polarization of the pump wave for the case of germanium. The parameters are the same as in Fig. 23 (according to the formulas (3.55), (3.57)–(3.59), (3.65)). 1) $\theta = 20°$; 2) $\theta = 40°$; 3) $\theta = 60°$.

Comparison of the formulas (3.49) and (3.64) shows that the expression (3.64) is obtained from (3.49) by the substitution f_0 (3.53)→f_0 (3.63) and $\sin^2\varphi_\alpha \to f(\theta,\varphi_\alpha)$. This means that the expressions for the increments of the dominant CW in the case of a p-polarized pumping wave will be given by the formulas (3.57)–(3.59), in which (3.56) must be replaced by

$$a_1 = \frac{4k_0\,|\sigma_{0T}|\, I_1 q^2}{\chi c_p\,[q^2+(\gamma_q/\chi)]^{1/2}} \times |n^*\cos^2\varphi_s - \sin\theta\cos\varphi_s|. \qquad (3.65)$$

We note that when $\theta \neq 0$, in the situation shown in Fig. 20a $f(\theta,\varphi_\alpha) = 0$.

Graphs of the dependence of the increments of the dominant CW on the orientation of their wave vectors **q** (i.e., on $\cos\varphi_s$), shown in Fig. 24, were constructed based on the formulas (3.55), (3.57)–(3.59), and (3.65). In addition, we set in (3.65) $q^2 + \gamma_q/\chi \approx q^2$. It is evident from these graphs that for small fixed angles θ the CW with $\cos\varphi_s = \pm 1$ have the largest values of γ_q. The parameters of these CW can be described by the formulas

$$\begin{aligned}\cos\varphi_s &= 1, \quad \mathbf{q} \parallel \mathbf{E}_{1t}, \quad q = k_0(n^* - \sin\theta) \equiv q_1,\\ \cos\varphi_s &= -1, \quad \mathbf{q} \parallel \mathbf{E}_{1t}, \quad q = k_0(n^* + \sin\theta) \equiv q_2,\end{aligned} \qquad (3.66)$$

where n^{*2} in accordance with (3.58) and (3.59) is equal to $n^{*2} = 1 + m^2/(m^2+n^2)^2$ for $a_1 > 24\omega_0^2/7$ and $n^{*2} = 1 + (m+n)^2/(m^2+n^2)^2$ for $a_1 > 24\omega_0^2/7$. As the angle θ is increased the increment of CW with q_2 increases, and the increment with q_1 decreases. The increments of structures with the parameters $0 < \cos\varphi_s < n^{*-1}\sin\theta$ increase with the angle θ.

3.4.5. Nature of doublet structures

Experiments[178,179,153] have established that together with the structures (3.60) and (3.66) structures with the same orientation but with somewhat smaller values of q are generated, i.e., a doublet of structures with close values of q is excited. We shall show (see Ref. 187) that this theory predicts generation of doublets of CW, whose wave vectors coincide with the experimental values of q for doublets of surface gratings.[153,3)] We shall do this for the case of s polarization of the pump wave and $\delta_s = \pi/2$ (see Fig. 20a)—

conditions corresponding to the experiment in Ref. 153.

We shall assume that the conditions (3.47) hold; in this case, Eq. (3.45) has the form (3.48), where $a_{\mathbf{q}}$ is given by the formula (3.49). We shall take into account the fact that for $\delta_s = \pi/2$, $k_s = k_{as}$, $\sin^2\varphi_s = \sin^2\varphi_{as}$. Then arguments analogous to those in Sec. 4.3 enable writing $a_{\mathbf{q}}$ near resonance ($k_s \gtrsim k_0$) in the form $a_{\mathbf{q}} \approx \left(\frac{|\sigma_{0T}| f_0 q^2}{\chi\gamma_T m}\right)\frac{x_s \sin^2\varphi_s}{(x_s^2+\beta_n^2)}$, $\sin^2\varphi_s \approx \cos^2\theta$. Let $q^2 \gg |\Omega|/\chi$; then $\gamma_T^{-1} \approx q^{-1} - (i\Omega/2\chi q^3)$ and from (3.48) we obtain $(i\Omega)^2 + 2A_{\mathbf{q}} i\Omega + \omega_0^2 - a_{\mathbf{q}}^{(0)} = 0$; $a_{\mathbf{q}}^{(0)} = |\sigma_{0T}| f_0 k_0 x_s \cos^3\theta/\chi m(x_s^2+\beta_n^2)$, $A_{\mathbf{q}} = |\sigma_{0T}| f 0 x_s \cos\theta/4\chi^2 k_0 m(x_s^2+\beta_n^2)$, where we have set $q \approx k_0\cos\theta$. The solution of this equation has the form

$$\gamma_{\mathbf{q}} + i\Omega_{\mathbf{q}} = -A_{\mathbf{q}} + (A_{\mathbf{q}}^2 + a_{\mathbf{q}}^{(0)} - \omega_0^2)^{1/2}. \qquad (3.67)$$

We note that (3.67) is a generalization of the formulas (3.57), in whose derivation it was assumed for simplicity that γ_T is real.

For high pumping intensities, such that the condition $\max\{A_{\mathbf{q}}^2 + a_{\mathbf{q}}^{(0)}\} > \omega_0^2$ holds, the increment $\gamma_{\mathbf{q}}$ has two positive peaks. The first peak in $\gamma_{\mathbf{q}}$, determined by the minimum of the quantity $\mathrm{Re}\, l_s$ (see Figs. 21a and b), corresponds to CW with the parameters

$$q = k_0(n^{*2} - \sin^2\theta)^{1/2}, \quad \mathbf{q} \parallel \mathbf{E}_t, \qquad (3.68)$$

where in the case of metals $n^{*2} = 1 + (m-n)^2/(m^2+n^2)^2$, while for dielectrics $n^{*2} = 1$. In this case $\gamma_{\mathbf{q}} = -A_{\mathbf{q}}$, $\Omega_{\mathbf{q}} = (\omega_0^2 - a_{\mathbf{q}}^{(0)} - A_{\mathbf{q}}^2)^{1/2}$. The second peak in $\gamma_{\mathbf{q}}$ is associated with the maximum of $\mathrm{Re}\, l_s$ (see Figs. 21a and b). The frequency of the corresponding CW is $\Omega_{\mathbf{q}} \approx 0$, and the vector $\mathbf{q}$ is determined by the formulas (3.60). The numerical solution for the full equation (3.45) for the case of germanium with $\delta_s = \pi/2$ is given in Figs. 25 and 26. It is evident that the peak values of the increments, obtained by the numerical calculation (see Fig. 25) and from the approximate formulas (3.47)–(3.49) (see Fig. 23), are somewhat different. For high pumping intensities, when the conditions (3.47) are better satisfied, these values converge to one another. It is evident from Fig. 25 that the magnitude of the peak and the width of the resonance for CW with large values of q is greater than the corresponding values of $\gamma_{\mathbf{q}}$ for CW with smaller values of $\mathbf{q}$. The positions of the peaks are

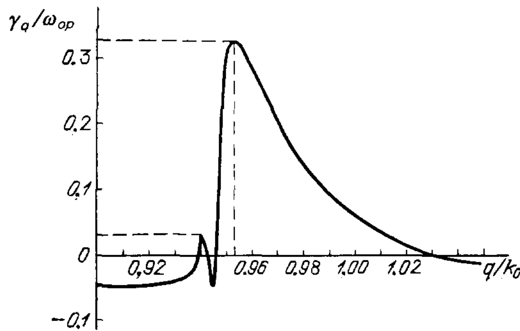

FIG. 25. Dependence of the increment of CW $\gamma_{\mathbf{q}}$ on the modulus of $\mathbf{q}$ for $\delta_s = \pi/2$ and an s-polarized pump in the case of germanium. The parameters of the material and of the pump are the same as in Fig. 23 (the numerical solution of Eq. (3.45)).

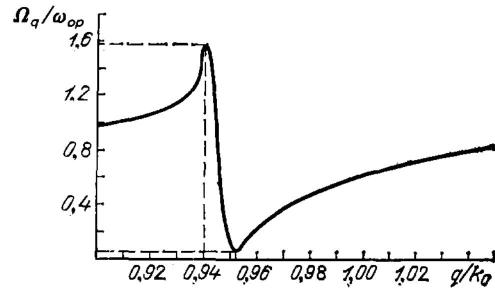

FIG. 26. The dependence of the frequency of CW $\Omega_{\mathbf{q}}$ on the modulus of $\mathbf{q}$. The parameters are the same as in Fig. 23 (numerical solution of Eq. (3.45)).

well described by the expressions (3.68) and (3.60). The experimental[153] and theoretical values of q (according to the formulas (3.60) and (3.68)) as a function of θ are compared in Fig. 27. It is evident that they are in good agreement with one another. The appearance of doublets of gratings can also be explained by other mechanisms, which take into account the presence of two extrema in the electromagnetic factor (see Fig. 21). Thus it is concluded in Refs. 153 and 202 based on the experiments performed that generation in the upper branch of Fig. 27 is determined by CW and generation in the lower branch is determined by the appearance of a nonuniform melt on the surface (see also Ref. 209). In Ref. 127 the formation of doublet structures is interpreted differently—the structures are interpreted as being the consequence of splitting of the dispersion curve of SEW.

3.4.6. Generation of small-scale structures under the action of laser radiation[187]

Thus far we have studied generation of CW under the condition that $q \sim k_0$. We shall show that Eq. (3.45) also describes excitation of CW with $q \gg k_0$ (small-scale structures, observed experimentally[146,175]).

We shall assume that the conditions

$$\nu \ll \chi, \quad \nu q^2 \ll |\Omega| \ll \chi q^2, \quad |\Omega|^2 \gtrsim \omega_0^2 \gg \nu q^2 \qquad (3.69)$$

hold. In this case the general equation (3.45) simplifies and has the form (3.48), where $a_{\mathbf{q}}$ in the case of s polarization (to whose analysis we shall confine our attention here) is given by the formula (3.49). In the region $q \gg k_0$ in (3.49) we

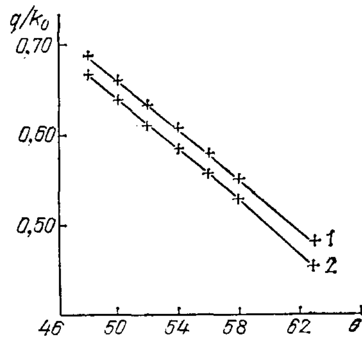

FIG. 27. Comparison of the theoretical (according to formulas (3.60) and (3.68)—solid lines) and experimental [153] (+) dependences of the doublet of values of $\mathbf{q}$ on θ in the case of germanium. The parameters are the same as in Fig. 23.

can set $\Gamma_s \approx \Gamma_{as} \approx k_\alpha \approx q$, $\gamma_s \approx \gamma_{as} \approx (q^2 - k_0^2\varepsilon)^{1/2}$, $\cos^2\varphi_s \approx \cos^2\varphi_{as}$. In addition, in accordance with (3.69) in the formula (3.49) we substitute $\gamma_T \simeq (1/q) - (i\Omega/2\chi q^3)$. Then after some transformations Eq. (3.48) acquires the form

$$(i\Omega)^2 + A_q i\Omega - (a_q^{(0)} - \omega_0^2) = 0, \quad (3.70)$$

$$a_q^{(0)} = \frac{|\sigma_{0T}| f_0 q}{\chi} \left\{ 2\,\mathrm{Re}\left[\frac{\varepsilon - 1}{q + \gamma_s + \gamma^*} \times \left(\frac{\gamma_s\Gamma_s \sin^2\varphi_s}{\varepsilon\Gamma_s + \gamma_s} - \frac{k_0^2\cos^2\varphi_s}{\Gamma_s + \gamma_s}\right)\right] - 1\right\},$$

$$b_q^{(0)} = \frac{|\sigma_{0T}| f_0 q}{\chi}\, 2\,\mathrm{Re}\left[\frac{q(\varepsilon - 1)}{(q + \gamma_s + \gamma^*)^2} \times \left(\frac{\gamma_s\Gamma_s\sin^2\varphi_s}{\varepsilon\Gamma_s + \gamma_s} - \frac{k_0^2\cos^2\varphi_s}{\Gamma_s + \gamma_s}\right)\right],$$

$$A_q = \frac{a_q^{(0)} + b_q^{(0)}}{2\chi q^2},$$

where f_0 is given by the formula (3.53). We shall now study separately the following cases:

$$k_0 \ll q \ll k_0 m, \quad m \gg 1, \quad (3.71)$$

$$q \gg k_0 |\varepsilon|^{1/2}, \quad |\varepsilon| \gg 1. \quad (3.72)$$

In the region determined by the inequalities (3.71), from (3.70) we obtain ($\omega_0^2 - a_q^{(0)} \gg Q_q^2/4$)

$$\Omega_q \approx (\omega_0^2 - a_q^{(0)})^{1/2}, \quad \gamma_q \approx \frac{|\sigma_{0T}| f_0}{4\chi^2 m k_0}\cos^2\varphi_s, \quad (3.73)$$

$$a_q^{(0)} \approx -\frac{|\sigma_{0T}| f_0 q^2}{\chi m k_0}\left(\frac{3}{2} - \sin^2\varphi_s\right).$$

In the region determined by the formulas (3.72), from Eq. (3.70) we have

$$\Omega_q \approx (\omega_0^2 - a_q^{(0)})^{1/2}, \quad \gamma_q \approx \frac{|\sigma_{0T}| f_0}{4\chi^2 q}\left(\cos^2\varphi_s - \frac{1}{2}\sin^2\varphi_s\right), \quad (3.74)$$

$$a_q^{(0)} = -\frac{|\sigma_{0T}| f_0 q}{\chi}\cos^2\varphi_s.$$

Analysis of the formulas (3.73) and (3.74) shows that for arbitrary angles of incidence θ in the region $q \gg k_0$ the CW for which $\cos^2\varphi_s = 1$ should have the highest values of γ_q. These CW, unlike the previously studied structures, correspond to waves with orientation $\mathbf{q} \perp \mathbf{E}_i$. Comparison of (3.73) and (3.74) shows that the transition from (3.73) to (3.74) occurs at $q \simeq k_0 m$. In this case, in the region $k_0 \ll q \ll k_0 m$ the quantity γ_q is independent of q, and in the region $q > k_0 m$ it decreases as q increases. Therefore, the continuum of dominating structures should have the parameters

$$\mathbf{q} \perp \mathbf{E}_i, \quad k_0 \ll q \lesssim k_0 m. \quad (3.75)$$

In the case of a germanium melt with $\lambda = 1.06\ \mu$m, $\varepsilon = -32 + i \cdot 72$.[153] Using this expression for ε, in accordance with Drude's model we find that for $\lambda = 10.6\ \mu$m $\varepsilon = -38.9 + i870$, i.e., $n = 20.4$ and $m = 21.3$. Therefore at $\lambda = 10.6\ \mu$m the periods of the frozen dominant "fine" structures must lie, according to (3.75), in the region $\lambda/m \simeq 0.5\ \mu\mathrm{m} \lesssim d \ll \lambda = 10.6\ \mu$m. This is in good agreement with experiment,[146] where independently of θ a continuum of structures with $0.8\ \mu\mathrm{m} \lesssim d \lesssim 3\ \mu$m and the orientation (3.75) was generated.

We shall calculate γ_q from the formula (3.73) with the characteristic experimental intensity $I_1 = 10^8$ W/cm^2 ($\lambda = 10.6\ \mu$m, $\tau_p = 2 \cdot 10^{-7}$ s[146]). According to (3.53) and (3.73), we have at $\theta = 0$:

$$\gamma_q = \frac{|\sigma_{0T}| I_1}{\chi^2 c_p} \cdot \frac{2n}{m^2 + n^2}.$$

For estimates we shall use the data which are presented in the caption to Fig. 23, and the value of ε calculated based on Drude's model. For these parameters we obtain $\gamma_q = 1.35 \cdot 10^7\ \mathrm{s}^{-1}$, i.e., $\gamma_q \tau_p = 2.7$. This means that the mechanism of the instability of CW gives rise to substantial growth of the amplitudes of small CW over the time τ_p. For p polarization the results are analogous.

3.5. Dependence of the interference instability of laser evaporation on the dielectric permittivity of the medium

For sufficiently high pumping intensities (when the condition (3.44) holds) evaporation waves begin to play the main role in the formation of surface structures. In this case the wave of modulation of the relief is given as before by the formula (3.15), where now $\xi_1(t) \gg \xi_2(t)$. The dispersion relation for the evaporation wave is derived most simply from the system (3.41), neglecting in it the hydrodynamic terms ($\varphi_0 = a_0 = 0$). Then from the first equation of (3.41) we have (using the condition $v_T A_1 \gg \gamma_s$)

$$i\Omega = v_T A_1. \quad (3.76)$$

This dispersion relation can also be obtained from the general dispersion equation (3.42), when $|\Omega| \gg \nu q^2, v_0 q, \omega_0$.

The dependence of the growth increments γ_q in the presence of IEI on $\varepsilon(\omega)$, following from (3.76), is studied in detail in Ref. 172. We shall elucidate the basic characteristics of this dependence here for the example of s polarization of the pumping wave.

Substituting v_T and A_1 from (3.41) and (3.38) into Eq. (3.76) and using the relation $(k_\alpha^2 - \gamma_\alpha\Gamma_\alpha)(\Gamma_\alpha + \gamma_\alpha) = k_0^2(\varepsilon\Gamma_\alpha + \gamma_\alpha)$, we obtain an expression for the increment γ_q which is valid for arbitrary values of $\varepsilon(\omega)$ and angles of incidence θ. In so doing we shall neglect the thermal instability associated with the uniform surface heating[177] and we shall study only IEI (for a more detailed discussion see Ref. 172). Under the condition that $q^2 \sim k_0^2 \gg v_0^2/\chi, |\Omega|/\chi$ the expression for the increment has the form

$$\gamma_q = \frac{2\omega\varepsilon''}{\pi g}\frac{k_z^2|E_{iz}|^2}{|k_z + i\gamma|^2}\left[\frac{\varepsilon - 1}{\gamma_s + \gamma^* + q}\left(\frac{\gamma_s\Gamma_s\sin^2\varphi_s}{\varepsilon\Gamma_s + \gamma_s} - \frac{k_0^2\cos^2\varphi_s}{\Gamma_s + \gamma_s}\right) + \frac{\varepsilon^* - 1}{\gamma_{as}^* + \gamma + q}\left(\frac{\gamma_{as}^*\Gamma_{as}^*\sin^2\varphi_{as}}{\varepsilon^*\Gamma_{as}^* + \gamma_{as}^*} - \frac{k_0^2\cos^2\varphi_{as}}{\Gamma_{as}^* + \gamma_{as}^*}\right)\right]. \quad (3.77)$$

The expression (3.77) contains two types of terms, proportional to $\sin^2\varphi_s$ and $\cos^2\varphi_s$, reflecting the characteristics of the diffraction of the incident wave by the modulation of the relief.[4)] If we study for simplicity the case of normal incidence ($\theta = 0$), then in (3.77)

$$\Gamma_s = \Gamma_{as},\ \gamma_s = \gamma_{as},\ k_s = k_{as} = q,\ \cos^2\varphi_s = \cos^2\varphi_{as}.$$

Then the expression (3.77) can be represented in the following general form:

$$\gamma_q = b(\varepsilon, \mathbf{q})\sin^2\varphi_s + a(\varepsilon, \mathbf{q})\cos^2\varphi_s. \quad (3.78)$$

It can be shown that if $\varepsilon' < -1$, $|\varepsilon'| \gg \varepsilon''$, then the first term describing the excitation of SEW plays the main role in

TABLE V. The dependence of the periods and orientations of gratings on $\varepsilon = \varepsilon' + i\varepsilon'' = (n + im)^2$[2,172] $(|\varepsilon'| \gg \varepsilon'')$.

ε	$\varepsilon' < -1$	$-1 < \varepsilon' < 0$	$0 < \varepsilon' < 1$	$\varepsilon' > 1$
Type of lattice	Normal	Anomalous	Anomalous	Normal
Orientation and period with s polarization	$\mathbf{q} \parallel \mathbf{E}_{1x}$, $\frac{\lambda}{(n^{*2} - \sin^2\theta)^{1/2}}$	$\mathbf{q} \perp \mathbf{E}_{1x}$, $0 < q < k_0$	$\mathbf{q} \perp \mathbf{E}_{1x}$, $\frac{\lambda}{\lvert(\varepsilon')^{1/2} \pm \sin\theta\rvert}$	$\mathbf{q} \parallel \mathbf{E}_{1x}$, $\frac{\lambda}{(n^{*2} - \sin^2\theta)^{1/2}}$
Orientation and period with p polarization	$\mathbf{q} \parallel \mathbf{E}_{1y}$, $\frac{\lambda}{n^* \pm \sin\theta}$	$\mathbf{q} \perp \mathbf{E}_{1y}$, $0 < q < k_0$	$\mathbf{q} \perp \mathbf{E}_{1y}$, $\frac{\lambda}{(\varepsilon' - \sin^2\theta)^{1/2}}$	$\mathbf{q} \parallel \mathbf{E}_{1y}$, $\frac{\lambda}{n^* \pm \sin\theta}$

$n^{*2} = 1 + (n+m)^2/(m^2+n^2)^2$ for $|\varepsilon| \gg 1$. $n^{*2} = |\varepsilon'|/(|\varepsilon'| - 1) \simeq 1$ for $\varepsilon' \ll -1$ (sew).

(3.78) (at resonance $b/a \sim |\varepsilon'|/\varepsilon'' \gg 1$). For this reason, the normal gratings with $\sin^2\varphi_s = 1$ (i.e., $\mathbf{q} \perp \mathbf{k}_t$) dominate in this case. The angular dependences of the increments of IEI are analogous to those of SAW or CW, obtained for the same values of ε.[172]

In the case when $-1 < \varepsilon' < 1$, $|\varepsilon'| \gg \varepsilon''$, conversely, $a(\varepsilon, \mathbf{q}) > b(\varepsilon, \mathbf{q})$, i.e., the increment $\gamma_\mathbf{q}$ reaches a maximum with $\cos^2\varphi_s = 1$. In this case the "anomalous" gratings with $\mathbf{q} \parallel \mathbf{k}_t$ will grow most rapidly.

Finally, when $\varepsilon' > 1$, $\varepsilon' \gg \varepsilon''$, it turns out that $b(\varepsilon, \mathbf{q}) > a(\varepsilon, \mathbf{q})$ and in this case the "normal" gratings with $\mathbf{q} \perp \mathbf{k}$ are generated.

Table V summarizes the results for the periods and orientations of the dominant gratings occurring with IEI as a function of ε and θ, obtained in Ref. 172.

We note that the general expressions for the increments of SAW and CW are entirely analogous to the expressions for $\gamma_\mathbf{q}$ for IEI. This means that the general characteristics of the dependence of $\gamma_\mathbf{q}$ on $\varepsilon(\omega)$, presented in Table V, could also be valid for these instabilities (in the case $|\varepsilon| \gg 1$ as shown in Refs. 168, 165, and 171, this is indeed so). This analogy is made possible, as already pointed out, by the universality of the first two stages of instabilities—diffraction, interference, and creation of a temperature field on the surface.

3.6. Experiments on the excitation of surface gratings and the theory of laser-induced instabilities

As we saw in Secs. 3.3–3.5, the characteristics of all laser-induced instabilities studied are determined by the value of the dielectric permittivity $\varepsilon(\omega)$. For this reason the case of metals in which $\varepsilon(\omega)$ is least subjected to changes during the laser pulse admits the most unambiguous interpretation.

In all experiments carried out on metals[144–146] it was found that for not very large angles $0 < \theta \lesssim 35°$ gratings whose front is perpendicular to the projection of the field $\mathbf{E}_i$ on the $z = 0$ plane ($\mathbf{q} \parallel \mathbf{E}_{it}$) are generated. For s polarization one grating with the period $d \approx \lambda/\cos\theta$ is generated, while for p polarization two gratings with the periods $d_\pm \approx \lambda/(1 \mp \sin\theta)$ are generated (see Fig. 19).

From the viewpoint of the theory of laser-induced instabilities (SAW—Sec. 3.3, CW—Sec. 3.4, or IEI—Sec. 3.5) the dominant gratings correspond to surface waves with maximum growth increments $\gamma_\mathbf{q}$. For $\varepsilon' < -1$ the predictions of the theory of all three instabilities are in agreement with the above-indicated experimental results (compare Figs. 22–24).

Gratings with the same orientation for s or p polarization of the laser wave are also the main gratings in the case of semiconductors.

If, on the other hand, circularly polarized pulses interact with the semiconductor, then in accordance with the theory of the CW or IEI instability for a quite long exposure time all gratings with $\gamma_\mathbf{q} > 0$ should grow on the surface; in addition, in the approximation linear in $\xi_\mathbf{q}$ their amplitudes must be all the higher the larger is the value of $\gamma_\mathbf{q}$. The experiment in Ref. 180 confirms this conclusion (compare Fig. 28 with Figs. 23 and 24). The sharp peaks in $\gamma_\mathbf{q}$ for $\cos\varphi_s \approx \sin\theta$ in Fig. 23 correspond to sharp diffraction peaks for $\mathbf{q} \perp \mathbf{k}_t$ in Fig. 28, and the wide peaks for $\mathbf{q} \uparrow\uparrow \mathbf{k}_t$ and $\mathbf{q} \uparrow\downarrow \mathbf{k}_t$ in Fig. 28 correspond to values of $\gamma_\mathbf{q}$ with $\cos\varphi_s = \pm 1$ in Fig. 24. Finally, the local peaks for $\cos\varphi_s = 0$ in Fig. 23 or the local peak in Fig. 24 correspond to the additional small peaks in Fig. 28.

The theoretical study of the heating of a surface by a laser pulse (see below) shows that under conditions typical for experiments on ILA and generation of surface gratings melting of the surface is achieved in both metals and semi-

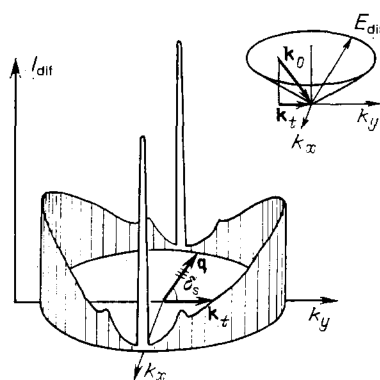

FIG. 28. Angular spectrum of diffraction of the probe wave, probing the complicated periodic structure frozen on the Ge surface. The structure was created by pulsed circularly polarized radiation with $\lambda = 1.06$ μm (the photograph of this surface is shown in Fig. 17c; from Ref. 180). The positions of the peaks in the angular spectrum are in good agreement with the theory (Figs. 23 and 24).

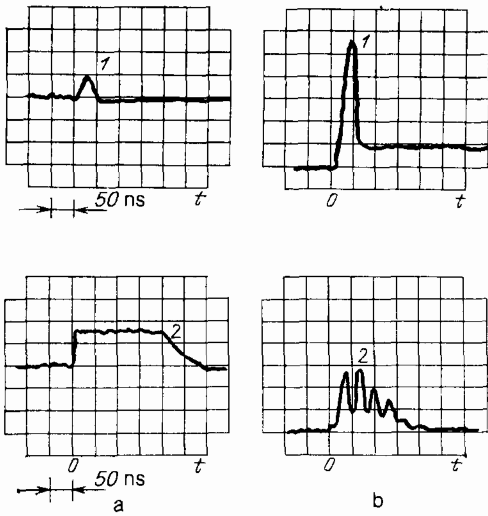

FIG. 29. Time dependence of the specular reflection (a) and diffraction (b) of the probing radiation from the Ge surface subjected to the action of a laser pulse with $\tau_p = 20$ ns and intensity I_i. The pulse begins at $t = 0$. 1: $I_i \approx 5 \cdot 10^6$ W/cm^2; the surface is nonuniformly melted; the intensity of specular reflection is low; 2: $I_i \approx 2.5 \cdot 10^7$ W/cm^2, uniform melting of the surface: the specular reflection reaches 75%, the oscillations are determined by the excited CW.

conductors. In Refs. 153 and 202 the presence of a uniform melt was confirmed by a) the appearance of a phase of high optical reflection and b) the appearance of oscillations in the intensity of the diffraction of the probing radiation, owing to the presence of CW on the surface (Fig. 29). Then the fact that the characteristic intensities for which the surface gratings are formed in metals are approximately an order of magnitude higher than in semiconductors is explained by the higher melting threshold of metals.

It should be noted that thus far no experiment which would unequivocally elucidate the feedback mechanism accompanying generation of surface gratings has been performed. Thus in the experiments of Refs. 152, 153, and 202 the duration of the pumping pulse is of the same order of magnitude as the frequency ω_0 of free CW. These experiments therefore essentially record the fact that the perturbation of the relief of the surface arising during the laser pulse spreads out after the pulse terminates in the form of damped free CW. In this connection we shall present below theoretical estimates indicating the high efficiency of the mechanism of generation of CW with pumping intensities characteristically used in experiments.

We shall estimate the threshold intensity of radiation required for melting. From the solution of the nonstationary equation (3.28) with $v_0 = 0$ in the zeroth-order approximation in ξ_q ($v \sim \xi_q$) we obtain an expression for the temperature (valid over the times $\gamma_0^2 \chi t \gg 1$, $t \gg \dfrac{z^2}{4\chi}$):

$$T_0(z,\ t) - T_{in} \approx \frac{2f_0}{\gamma_0}\left(\frac{t}{\pi\chi}\right)^{1/2}.$$

From here, using for f_0 the expression (3.26) for s polarization and (3.27) for p polarization we obtain the threshold melting intensity $|\mathbf{E}_{melt,\alpha}|^2 (\alpha = \mathrm{s,p})$ in the case of metals ($\varepsilon' \ll -1$, $|\varepsilon'| \gg \varepsilon''$)

$$|E|^2_{melt}\,\mathrm{p} = \frac{\pi\Delta T\,(\pi\varkappa c_p)^{1/2}}{2c\tau_p^{1/2}}\,\frac{|\varepsilon'|^{3/2}}{\varepsilon''},\quad |E|^2_{melt}\,\mathrm{s} = \frac{|E|^2_{melt}\,\mathrm{p}}{\cos^2\theta},\tag{3.79}$$

where $\Delta T = T_{melt} - T_{in}$.

Analogously, for dielectrics ($\varepsilon' \gg \varepsilon''$, $|\varepsilon| \gg 1$) we have

$$|E|^2_{melt}\,\mathrm{p} = \frac{\pi\Delta T\,(\pi\varkappa c_p)^{1/2}}{4c\tau_p^{1/2}}\,(\varepsilon')^{1/2},\quad |E|^2_{melt}\,\mathrm{s} = \frac{|E|^2_{melt}\,\mathrm{p}}{\cos^2\theta}.\tag{3.80}$$

We shall make some numerical estimates which demonstrate the possibility of efficient generation of CW for the case of Ge under the conditions of the experiments of Refs. 153 and 202 (where $\lambda = 1.06\,\mu$m, $\tau_p = 20$ ns, $I_i = 2.5 \cdot 10^7$ W/cm^2). The melting threshold according to the formula (3.80) is $I_{melt} = 6.4 \cdot 10^6$ W/cm^2 (for Ge in the solid phase $\rho = 5.46$ Г/cm^3, c_p (400 K) $= 1.87 \times 10^7$ erg/cm$^3 \cdot$ deg, $\varkappa$(273 K) $= (0.6 \cdot 10^7$ erg/cm $\cdot$ s $\cdot$ deg. $T_{melt} = 1210$ K,[182] $\varepsilon = 16 + i \cdot 0.8$[153]). The threshold for excitation of a static grating on the surface of the melt ($\theta = 0$, $q = k_0 = 2\pi/\lambda$, $\Omega_q = 0$) in accordance with (3.57) is equal to $I_{gen} = 6.1 \cdot 10^6$ W/cm^2 (the data for liquid Ge required for the estimates are presented in the caption to Fig. 23). Since $I_{gen} < I_{melt}$, generation of static gratings is possible immediately after melting of the surface. For an intensity of $I_{th} = 9.3 \cdot 10^6$ W/cm^2, according to the formula (3.80) melting is achieved after 9.8 nsec, and during the remaining $\Delta\tau = 10.5$ ns, in accordance with the formulas (3.56) and (3.57), the static grating with $\mathbf{q} \| \mathbf{E}_i$ and $q \simeq k_0$ with an increment $\gamma_q = 10^8$ s^{-1} will grow, so that $\gamma_q \Delta\tau = 1$. Thus for all $I_1 > I_{th}$ (in particular for the intensities used in Refs. 153 and 202) over the time τ_p appreciable growth will occur in the amplitude of the static grating. After the laser pulse terminates, this perturbation of the surface gives rise to the appearance of two free CW ($\Omega_q = \omega_0$), traveling toward one another and decaying over a time $\gamma_q = 2\nu q^2 \sim 10^7$ s^{-1}, which was recorded in Refs. 153 and 202.

An analogous estimate can be obtained in the case of Al. in the experiment of Ref. 145 $\lambda = 1.06\ \mu$m, $\tau_p = 7$ ns, $I_i = 4 \cdot 10^8$ W/cm^2. The data required for the calculations are taken from Refs. 181, 182, and 208. For this pumping intensity, according to (3.79), (3.56), and (3.57), the Al surface melts after 4 ns. Then, during the remaining $\Delta\tau = 3$ ns, a grating with $q \approx k_0$, $\mathbf{q} \| \mathbf{E}_i$ and an increment $\gamma_q = 10^9$ s^{-1} grows. As a result $\gamma_q \Delta\tau = 3$, which demonstrates the possibility of significant growth in the amplitude of the grating owing to the excitation of CW.

The theory of laser-induced CW instability (see Sec. 3.4) also explains the experimentally observed change in the orientation of the vector $\mathbf{q}$ of the dominant gratings as the angle θ is increased in the region $\theta \gtrsim 35°$, for example at $\theta = 60°$ the angle δ_s (see Fig. 20b), according to the data in Ref. 139, is equal to $\delta_s = 46°$. As is evident from Fig. 23, γ_q reaches its absolute maximum value for $0 \leqslant \theta \leqslant 30°$ when $\cos\varphi_s = n^{*-1}\sin\theta \approx \sin\theta$ (i.e., $\mathbf{q} \perp \mathbf{E}_{it}$), and when θ increases from 30° to 40° the absolute maximum already appears at $\cos\varphi_s = 0$. At $\theta = 60°$ the theoretical value of δ_s, according to (3.61) is equal to $\delta_s = 49°$, which is close to the above-indicated experimental value. As already mentioned

above, even more subtle effects, such as the generation of doublet structures (two gratings with almost the same orientation) (see Sec. 3.4.5) and fine structures (see Sec. 3.4.6) can also be quantitatively explained on the basis of the theory of the CW instability.

It may thus be concluded that the CW instability is primarily responsible for generation of irreversible gratings on the surface of metals and semiconductors. (IEI and the recoil pressure mechanism could make an additional contribution (see Sec. 3.4 and Ref. 169).) At the same time, generation of SAW under conditions up to melting of the surface could also be responsible for the formation of reversible gratings, existing only for the duration of the pulse. Thus in the experiments of Ref. 150, at intensities of $I_i = 5 \cdot 10^7 - 2 \cdot 10^8$ W/cm^2, $\lambda = 1.06$ μm, $\tau_p = 200$ ns reversible changes were recorded on the surface of Cu with the help of the diffraction of the probing radiation, while for $I_i > 2 \cdot 10^8$ W/cm^2 the changes became irreversible. According to the estimate in Sec. 3.3, the critical intensity for excitation of SAW under these conditions is equal to $I_{cr} = 2 \cdot 10^7$ W/cm^2. The theoretical estimate of the melting threshold of copper according to the formula (3.79) is equal under these conditions to $I_{melt} \approx 2.8 \cdot 10^8$ W/cm^2 (in the solid phase $\rho = 8.93$ g/cm^3, $\varkappa(573\ \text{K}) = 3.73 \cdot 10^7$ erg/cm$^2 \cdot$ s $\cdot$ deg, $c_p(600\ \text{K}) = 3.71 \cdot 10^7$ erg/cm$^2 \cdot$ s $\cdot$ deg, $T_{melt} = 1357$ K[182], $\varepsilon = -37 + i \cdot 3.4(\lambda = 1\ \mu\text{m})$[208]). Both values are in good agreement with experiment.[150]

We shall now examine the characteristics of generation of gratings in dielectrics (crystalline and fused quartz[149]) under the action of CO_2 laser radiation. For $\lambda = 10.6$ μm ($\nu = 1/\lambda = 943.4$ cm^{-1}) or ($\nu = 973.7$ cm^{-1}) gratings with the usual orientation ($\mathbf{q} \| \mathbf{E}_{it}$) appear on their surfaces: one with s polarization and two with p polarization (see Fig. 19). When exciting radiation with ($\nu = 1072$ cm^{-1}) was used, however, the situation changed radically. For all $\theta \geqslant 0$ gratings with the "anomalous" orientation $\mathbf{q} \perp \mathbf{E}_{it}$ appeared. In this case, two gratings appeared for s polarization and one grating for p polarization. As can be seen from Fig. 8 of Ref. 149, at $\theta = 0$ the periods of normal gratings satisfy $d < \lambda$, while the periods of the "anomalous" gratings satisfy $d > \lambda$, which corresponds to the results of the IEI theory (see Table V). According to the analysis of IEI[172] (see Sec. 3.5) anomalous gratings should appear when $|\varepsilon'| < 1$, $|\varepsilon'| \gg \varepsilon''$ (this is also valid for the cases of SAW or CW instability when $|\varepsilon'| < 1$, $|\varepsilon'| \gg \varepsilon'$, which were not explicitly studied here). The value of ε' in the polariton region of quartz glass is estimated in Ref. 149. In the region of the melting temperature of quartz $T = 1100$ °C, $\varepsilon'(1040\ \text{cm}^{-1}) = 0$,a $\varepsilon'(1120\ \text{cm}^{-1}) = -1$. It is evident from this estimate that for $\lambda = 9.33$ μm $|\varepsilon'| < 1$. From the viewpoint of the IEI (or SAW and CW) theory (see Table V) anomalous gratings should be generated at the wavelength $\lambda = 9.33$ μm, which corresponds to experiment. The link between the types of surface structures and the value of $\varepsilon(\omega)$ was also pointed out in Refs. 166 and 143.

All examples discussed above concern the case when the laser wave is incident from the vacuum into the medium with a dielectric permittivity ε. In the more general case when the wave is incident from a medium with a dielectric permittivity ε_1 onto a medium with the dielectric permittivity ε the resonance denominator in the formulas (3.8)–(3.10) is replaced by the symmetrical expression $D_p = \varepsilon(k_\alpha^2 - \varepsilon_1 k_0^2)^{1/2} + \varepsilon_1(k_\alpha^2 - \varepsilon k_0^2)^{1/2}$. Under the condition that $|\varepsilon| \gg |\varepsilon_1|$, $|\varepsilon| \gg 1$, we have $D_p \sim (k_\alpha^2 - \varepsilon_1 k_0^2)^{1/2} - \varepsilon_1 k_0/(-\varepsilon)^{1/2}$, i.e., a sharp resonance appears at $k_\alpha \approx (\varepsilon_1)^{1/2} k_0$. In this case it should be expected that the period of the fluting will be equal to $\lambda/\varepsilon_1^{1/2}$. We note that precisely this period of fluting was observed on the surface of wide-gap dielectrics in the experiments of Ref. 203, where the laser radiation was focused on the output face of a plane-parallel plate. The required inequality $|\varepsilon| \gg |\varepsilon_1|$ can be ensured by melting or formation of a plasma on the output face.

Thus we can draw the general conclusion that the predictions of the theory of laser-induced instabilities (SAW, CW, and IEI) is on the whole in good agreement with experiment and that the nature of the gratings inscribed on the surface is determined by the value of the dielectric permittivity of the medium $\varepsilon(\omega)$.

CONCLUSIONS

1. We shall summarize our discussion. Modern laser technology, which has mastered in the last two to three years the femtosecond range of generated optical pulse durations, has for all practical purposes completely solved the problem of excitation and recording of nonequilibrium states in condensed media and has reached the natural limit of the rate of optical response of such media, determined by the duration of one cycle of the optical field.

In application to crystalline semiconductors and metals this technique now enables injecting extremely rapidly (over a time of 10^{-14} s) significant energy into the electronic subsystem of the surface layers and then following in detail the numerous stages of the transformation of this energy into the usual thermal excitation of the crystal lattice and subsequent cascade of phase transformations on the surface. The scale of experimentally accessible relaxation processes in solids now extends from the most rapid electron-electron dephasing and energy relaxation processes (with characteristic durations of $\lesssim 10^{-14}$ s) through the stage of electron-phonon relaxation with the emission of LO phonons (10^{-14}–10^{-13} s) and LA phonons (10^{-13}–10^{-9} s) right up to interband recombination processes in a semiconductor and numerous phase transformations and heat and mass transfer processes with characteristic times in the nanosecond range and longer.

2. The experiments on laser annealing of semiconductors with the use of nanosecond and picosecond pulses, which have recently given rise to great interest and discussion, have now been completely explained quantitatively on the basis of the foregoing scale of relaxation processes with the use of the "thermal" model. According to this model, when a very short and intense laser pulse with energy greater than the gap width, interacts with the surface of a semiconductor, the light energy absorbed by the electron-hole subsystem of the crystal is transferred over a time of $\lesssim 1$ ps from

the superexcited free carriers above the bottom of the conduction band to the crystal lattice and gives rise to rapid melting. The front of the melt moves with a velocity of the order of the sound velocity into the bulk of the sample, and after the laser pulse and energy injection terminate, it stops at a definite depth and then returns back to the surface over nanosecond time intervals, accompanied by the process of epitaxial restoration of the crystal lattice. Amongst the problems of ILA which remain unsolved, we must once again call attention to the question of the degree of equilibrium (or nonequilibrium) of the phonon subsystem of the crystal up to the moment at which melting begins,[5)] as well as the possibility of the existence of new types of phase transitions in the presence of a superdense hot plasma of free carriers at the first stage of ILA (at times <1 ps). The reason for the intense formation of point and other defects in laser-annealed sections is still not completely understood. Moreover, the laser-induced formation of point defects in the surface layers begins, according to the experiments of Refs. 183–185, long before melting and cannot be explained on the basis of a purely thermal model. Defect formation induced by the dense electron-hole plasma at the first stage of ILA apparently plays a definite role here.[185,186,214]

Defect formation in semiconductors can also be caused by the nonlinear optical instability of the deformations, recently studied in Ref. 190; under certain conditions this mechanism can also be responsible for the ultrafast (nonthermal) melting of the surface of the semiconductor. According to Ref. 190, for quite high intensities of the optical pulse, as a result of transitions in the electronic subsystem the lattice atoms can be subjected (through the acoustic strain potential) to strong static displacement from the positions of equilibrium, so that the energy of the laser excitation is transformed into the potential energy of the acoustic subsystem—unlike the usual picture of electron-phonon relaxation, described above, according to which the energy of the electron excitation is transferred to the lattice in a kinetic form, thereby heating up the lattice. Intensified generation of dislocations begins as a result of the appearance of static deformations and then the lattice becomes unstable—"cold" ultrafast (over a time of $\sim 10^{-13}$ s) melting of the crystal occurs.

3. In connection with the unsolved problems of the physics of ILA listed above, new directions for diagnostics of ultrafast phase transformations on the surface of semiconductors and metals appear at the forefront. Aside from the nonlinear optical techniques described in detail in Sec. 2, which depend on the generation of optical harmonics and the sum or difference frequencies in reflection, we should also call attention to pico- and femtosecond active spectroscopy of Raman scattering by optical phonons, plasmons, and acoustic oscillations of the laser-excited crystal. The "hybrid" technique of laser picosecond electron diffraction, developed in the last two years, could become an extremely interesting and informative method for studying in real time structural transformations in the surface layers of laser-excited crystals.[191,192] In this method, picosecond light pulses are used to obtain (by the external photoeffect from the surface of the cathode of the electron gun) powerful short electron bunches which are time-synchronized with the laser pulses and which after acceleration in a pulsed high-voltage electric field can be directed onto the section of the laser-excited surface under study in order to record the "instantaneous" diffraction pattern and its evolution in time with picosecond time resolution. The first data on the picosecond dynamics of laser-induced phase transformations in crystalline aluminum have already been obtained using this technique.[191]

Graphic pictures of the changes in the external appearance of sections of a silicon surface irradiated by powerful femtosecond annealing pulses, recorded successively with an interval of ~ 100 fs using the technique of stroboscopic photography, were recently obtained by Downer *et al.*[193] This technique can evidently also be classified as ultrafast cinematography with the minimum time interval between frames determined by the duration of the illuminating pulse—in this case 100 fs.

Interesting data on the dynamics of the first phase of ILA in silicon were obtained by Malvezzi *et al.* by recording the photo-emission of charged particles (on a picosecond time scale).[194]

The variety of new highly informative laser methods of diagnostics of fast phototransformations on the surfaces of solids promises to reduce substantially in the near future the number of questions regarding the nature and details of the course of such processes which today remain unanswered.

4. In this review we emphasized repeatedly the fact that in speaking about powerful laser excitation of surface layers of semiconductors and metals it should not be forgotten that the energy required for this must be injected into the crystal through its surface. Under the action of the laser radiation, as described in detail in Sec. 3, periodic structures, which can substantially reduced the coefficient of reflection, form on the surface. According to the data in Refs. 210, 211, and 213 the absorptivity of the surface increases severalfold at the same time. These effects as well as the complicated self-excited processes which appear at the same time must be taken into account in the analysis of all real experiments associated with laser excitation of the surface of solids, including experiments on ILA, laser cutting, welding, and hardening of metals, interaction of laser radiation with biological objects and tissues, etc. At the same time, the theory developed in Sec. 3 of this review, linear in the amplitude of the light-induced grating, represents only the first step in the complete quantitative description of all these interesting and practically important processes occurring on the surfaces of solids.

[1)]The dipole surface contribution does not vanish in a centrosymmetrical medium because the inversion symmetry is evidently broken in the direction perpendicular to the surface.

[2)]We note that replacing the stationary problem (3.28) by the nonstationary problem has no effect on the form of the dispersion equations (3.42) and (3.45).

[3)]In Ref. 179 the formation of doublet structures is interpreted as being the consequence of the splitting of the dispersion curve of SEW on a rough surface.

[4)]The formula (3.77) holds if $g > \theta \equiv \frac{\varkappa R T_{os}}{v_0 U}$ where γ_T is given by the formula (3.38). If $g < \theta$, then the substitution $g \to \theta$ must be made in (3.77).

[5)]We note that very recently there appeared the possibility of direct recording and spectroscopy of short-wavelength acoustic phonons, arising in the process of interaction of short (including pico- and subpicosecond) laser pulses with the surface of a semiconductor.[195-198]

[1]J. Ready, Deĭstvie moshchnogo lasernogo izlucheniya (Action of Powerful Laser Radiation), Mir, M., 1974; Promyshlennoe primenenie laserov (Industrial Application of Lasers), Mir, M., 1981.

[2]S. I. Anisimov, Ya. A. Imas, G. S. Romanov, and Yu. V. Khodyko, Deĭstvie izlucheniya bol'shoĭ moshchnosti na metally (Interaction of High-Power Radiation with Metals), Nauka, M., 1970.

[3]W. Duley, *Laser Processing of Materials*, Plenum Press, New York, 1983.

[4]N. G. Basov and G. V. Sklizkov, Nagrev i szhatie termoyadernykh misheneĭ lazerom (Laser Heating and Compression of Thermonuclear Targets), VINITI, M., 1982.

[5]I. B. Khaĭbullin, E. I. Shtyrkov, M. M. Zaripov *et al.*, Rad. Eff. **36**, 225 (1978).

[6]L. V. Dvurechenskiĭ, G. A. Kachurin, N. V. Nidaev, and L. S. Smirnov, Impul'snyĭ otzhig poluprovodnikovykh materialov (Impulsive Annealing of Semiconductor Materials), Nauka, Novosibirsk, 1982.

[7]S. D. Ferris, H. J. Leamy, and J. M. Poate [Eds.], Laser-Solid Interactions and Laser Processing, Amer. Inst. Phys., New York, 1979.

[8]C. W. White and P. S. Peercy [Eds.], Laser and Electron Beam Processing of Electronic Materials, Academic Press, New York (1980).

[9]C. L. Anderson, G. K. Cellar, and G. A. Rozgonyi [Eds.], Laser and Electron Beam Processing of Electronic Materials, ECS Inc., Princeton (1980).

[10]J. F. Gibbon, L. D. Hess, and T. W. Sigmon [Eds.], Laser and Electron Beam Solid Interactions and Materials Processing, North-Holland, New York, 1981.

[11]E. Kaldis [Ed.], Current Topics in Materials Science, North-Holland, Amsterdam, 1982, Vol. 8.

[12]B. R. Appleton and G. K. Cellar [Eds.], Laser and Electron Beam Interaction with Solids, North-Holland, Amsterdam, 1982.

[13]C. V. Shank, Science **219**, 1027 (1983). R. L. Fork, B. I. Greene, and C. V. Shank, Appl. Phys. Lett. **38**, 671 (1981). R. L. Fork, C. V. Shank, and R. Yen, *ibid.* **41**, 273 (1982).

[14]K. B. Eisenthal and R. Hochstrasser [Eds.], Picosecond Phenomena. III, Springer-Verlag, New York, 1982 (Springer Series in Chemical Physics, Vol. 23).

[15]J. G. Fujimoto, A. M. Weiner, and E. P. Ippen, Appl. Phys. Lett. **44**, 832 (1984).

[16]C. V. Shank, R. Yen, and C. Hirlimann, Phys. Rev. Lett. **50**, 454 (1983), 51, 900.

[17]F. V. Bunkin, N. A. Kirichenko, and B. S. Luk'yanchuk, Usp. Fiz. Nauk **138**, 45 (1982) [Sov. Phys. Usp. **25**, 662 (1982)]; Izv. Akad. Nauk SSSR, Ser. Fiz. **48**, 1485 (1984) [Bull. Acad. Sci. USSR. Phys. Ser.

[18]S. A. Akhmanov, M. F. Galyautdinov, N. I. Koroteev *et al.*, Kvant. Elektron. **10**, 1077 (1983) [Sov. J. Quantum Electron. **13**, 687; Opt. Commun. **43**, 202 (1983).

[19]H. W. K. Tom, T. F. Heinz, and Y. R. Shen, Phys. Rev. Lett. **51**, 1983 (1983).

[20]a) Abstracts of Reports at the 5th All-Union Conference on Nonresonant Interaction of Optical Radiation with Matter, Leningrad (1981); b) Abstracts of Reports at the 6th All-Union Conference on Nonresonant Interaction of Optical Radiation with Matter, Leningrad (1984).

[21]S. A. Akhmanov and N. I. Koroteev, Metody nelineĭnoĭ optiki v spektroskopii rasseyaniya sveta (Methods of Nonlinear Optics in the Light Scattering Spectroscopy), Nauka, M. (1981).

[22]A. R. Beattie and P. T. Landsberg, Proc. R. Soc. London **249**, 16 (1959).

[23]A. Haug, Solid State Electron. **21**, 1281 (1978).

[24]E. J. Yoffa, Phys. Rev. B **21**, 2415 (1980).

[25]A. V. Keldysh, Usp. Fiz. Nauk **100**, 514 (1970) [Sov. Phys. Usp. **13**, 291 (1970)].

[26]W. P. Dumke, Phys. Lett. A **78**, 477 (1980).

[27]R. Biswas and V. Ambegaokar, Phys. Rev. B **26**, 1980 (1982).

[28]C. L. Tang and D. J. Erskine, Phys. Rev. Lett. **51**, 840 (1983).

[29]E. Conwell and M. Vassell, IEEE Trans. **ED-13**, 22 (1966).

[30]J. Shah, J. Phys. (Paris) **42**, Suppl. No. 10, C7-445 (1981).

[31]T. Rice, J. Hansel, T. Phillips, and G. Thomas, Élektronno-dyrochnaya zhidkost' v poluprovodnikakh (Electron-Hole Liquid in Semiconductors), Mir, M. (1980).

[32]I. Van Vechten, J. Phys. (Paris) **44**, Supp. Nr. 10, C5-11 (1983).

[33]E. J. Yoffa, *ibid.* **41**, Suppl. Nr. 5, C4-7 (1981).

[34]Phonon Scattering in Solids, Plenum Press, New York (1976).

[35]D. von der Linde, J. Kuhl, and H. Klingenberg, Phys. Rev. Lett. **44**, 1505 (1980).

[36]R. G. Ulbrich, V. Narayanamurti, and M. A. Chin, *ibid.* **45**, 1432.

[37]M. Greenstein, M. A. Tamor, and J. P. Wolfe, Solid State Commun. **45**, 355 (1983).

[38]G. A. Northrop and J. P. Wolfe, Bull. Amer. Phys. Soc. **28**, 252 (1983).

[39]H. Kurz, L. A. Lompre, and J. M. Liu, J. Phys. (Paris) **44**, Suppl. Nr. 10, C5-23 (1983).

[40]R. F. Wood and G. E. Giles, Phys. Rev. B **23**, 2923 (1981). R. F. Wood, J. R. Kirkpatrick, and G. E. Giles, *ibid.* **23**, 5555.

[41]A. Lietoila and J. F. Gibbons in: Ref. 10, p. 23.

[42]R. Orbach, IEEE Trans. **SU-14**, 140 (1967).

[43]Kh. Rissel and I. Ruge, Ionnaya implantatsiya (Ion Implantation), Nauka, M. (1983).

[44]W. Wittmer and G. A. Rozgonyi in: Ref. 11, Ch. 1.

[45]M. Bertolotti and G. Vitali, *ibid.*, Ch. 2.

[46]A. Compaan, G. Contreras, M. Cardona, and R. Axmann, J. Phys. (Paris) **44**, Supp. Nr. 10, C5-197 (1983).

[47]J. Wagner, A. Compaan, and R. Axmann, *ibid.*, C5-61.

[48]A. Slaoui, E. Fogarassy, J. C. Muller, and P. Siffert, *ibid.*, C5-65.

[49]Zh. I. Alferov, V. N. Abakumov, Yu. V. Koval'chuk, G. V. Ostrovskaya, E. L. Portnoi, V. B. Smirnitskiĭ, and I. A. Sokolov, Fiz. Tekh. Poloprovodn. **17**, 235 (1983) [Sov. Phys. Semicond. **17**, 152 (1983)].

[50]E. I. Shtyrkov, I. B. Khaibullin, N. F. Galyautdinov, and M. M. Zaripov, Opt. Spektrosk. **38**, 103 (1975).

[51]A. V. Andreev and S. A. Akhmanov, Preprint No. 26/1981, Moscow (1981). A. V. Andreev, S. A. Akhmanov, and E. K. Kov'ev, Izv. Akad. Nauk SSSR, Ser. Fiz. **47**, 1898 (1983).

[52]J. Ziman, *Principles of the Theory of Solids*, Cambridge University Press, 1964 [Russ. Transl. Mir, M., 1974].

[53]Q. Stritzker, A. Pospieszczyk, and J. A. Tagle, Phys. Rev. Lett. **47**, 356 (1981).

[54]B. C. Larson, C. W. White, T. S. Noggle, and D. M. Mills, Phys. Rev. Lett. **48**, 337 (1982).

[55]B. C. Larson, C. W. White, T. S. Noggle, J. F. Barhorst, and D. M. Mills in: Ref. 12, p. 13.

[56]R. T. Williams, M. N. Kablet, J. P. Long, J. C. Rife, and R. T. Royt, *ibid.*, p. 97.

[57]M. O. Thomson, G. J. Calvin, J. W. Mayer, B. B. Hammond, N. Paulter, and P. S. Peercy, *ibid.*, p. 209.

[58]C. W. White, *ibid.*, p. 109.

[59]I. A. van Vechten and A. A. Compaan, Solid State Commun. **39**, 867 (1981).

[60]J. Bok, J. Phys. (Paris) **44**, Suppl. Nr. 10, C5-3 (1973).

[61]A. Compaan, H. W. Lo, M. C. Lee, and A. Aydinli, Phys. Rev. B **26**, 1079 (1982).

[62]D. von der Linde, G. Wartmann, and A. Ozols in: Laser-Solid Interactions and Transient Thermal Processing of Materials, edited by J. Narajan, W. L. Brown, and L. A. Lemons, Academic Press, New York, 1983.

[63]D. von der Linde and G. Wartmann, Appl. Phys. Lett. **41**, 700 (1982).

[64]R. F. Wood, M. Rasolt, and G. E. Jellison in: Ref. 12, p. 61.

[65]A. Compaan, M. C. Lee, H. W. Lo, G. J. Trott, and A. Aydinly, J. Appl. Phys. **54**, 5950 (1983).

[66]D. von der Linde, G. Wartmann, and A. Compaan, Appl. Phys. Lett. **43**, 613 (1983).

[67]I. A. Van Vechten in: Ref. 12, p. 49.

[68]M. I. Kaganov, I. M. Lifshitz, and L. V. Tanatarov, Zh. Eksp. Teor. Fiz. **31**, 232 (1956) [Sov. Phys. JETP **4**, 173 (1957)]; S. I. Anisimov, B. L. Kapeliovich, and T. L. Perel'man, Zh. Eksp. Teor. Fiz. **66**, 776 (1974) [Sov. Phys. JETP **39**, 375 (1974)].

[69]G. L. Eesley, Phys. Rev. Lett. **51**, 2140 (1983).

[70]V. V. Kapaev, Yu. V. Kopaev, and S. N. Molotkov, Mikroelektronika **12**, 499 (1983).

[71]I. M. Suslov, Pis'ma Zh. Eksp. Teor. Fiz. **39**, 449 (1984) [JETP Lett. **39**, 544 (1984)].

[72]J. G. Fujimoto, J. M. Liu, E. P. Ippen, and N. Bloembergen in: Ref. 75, p. 140.

[73]J. G. Fujimoto, S. G. Shevel, and E. P. Ippen, Solid State Commun. **49**, 605 (1984).

[74]A. S. Piskarskas *et al.*, Parametricheskie generatory sveta i pikosekundnaya spektroskopiya (Parametric Light Generators and Picosecond Spectroscopy), edited by A. S. Piskarskas, Mokslas, Vilnyus (1983).

[75]D. H. Auston and K. B. Eisnthal [Eds.], Ultrafast Phenomena. IV,

Springer-Verlag, New York, 1984 (Springer Series in Chemical Physics, Vol. 38).
[76]S. Shapiro [Ed.], Sverkhkorotkie svetovye impul'sy (Ultrashort Light Pulses), Mir, M. (1981).
[77]C. V. Shank, E. Ippen, and S. Shapiro [Eds.], Picosecond Phenomena, Springer-Verlag, New York (1978) (Springer Series in Chemical Physics, Vol. 4).
[78]Sverkhbystrye protsessy v spektroskopii (Ultrafast Processes in Spectroscopy), Valgus, Tallin (1979).
[79]C. V. Shank, R. Hochstrasser, and W. Kaiser [Eds.], Picosecond Phenomena, II, Springer-Verlag, New York (1980) (Springer Series in Chemical Physics, Vol. 14).
[80]"Picosecond light phenomena" in: Abstracts of Reports at the 10th, 11th, and 12th All-Union Conferences on Coherent and Nonlinear Optics, Kiev (1980); Erevan (1982); Moscow (1985).
[81]D. H. Auston, C. M. Surko, T. N. C. Venkatesan, R. E. Slusher, and J. A. Solovchenko, Appl. Phys. Lett. **33**, 437 (1978).
[82]D. H. Auston, J. A. Solovchenko, A. L. Simons, C. M. Surko, and T. N. C. Venkatesan, *ibid.* **34**, 777 (1979).
[83]D. von der Linde and N. Fabricius, *ibid.* **41**, 991 (1982).
[84]J. M. Lui, H. Kuz, and N. Bloembergen, *ibid.* **41**, 643 (1982).
[85]M. Combescot, Phys. Rev. Lett. **51**, 519 (1983).
[86]M. Lui, R. Yen, H. Kurz, and N. Bloembergen, Appl. Phys. Lett. **39**, 755 (1981).
[87]N. Bloembergen, H. Kurz, J. M. Lui and R. Yen in: Ref. 12, p. 37.
[88]R. Yen, J. M. Lui, H. Kurz, and N. Bloembergen, Appl. Phys. A **27**, 153 (1982).
[89]L. A. Lompre, J. M. Kui, H. Kurz, and N. Bloembergen, Appl. Phys. Lett. **44**, 3 (1984).
[90]H. M. van Driel, L. A. Lompre, and N. Bloembergen, *ibid.*, 285.
[91]A. Aydinli, H. W. Lo, and A. Compaan, Phys. Rev. Lett. **46**, 1640 (1981).
[92]A. Compaan, A. Aydinli, M. C. Lee, and H. W. Lo in: Ref. 12, p. 43.
[93]S. C. Moss and Q. Marquardt, *ibid.*, p. 79.
[94]D. H. Lowndess, Phys. Rev. Lett. **48**, 267 (1982).
[95]H. W. Lo and A. Compaan, Phys. Rev. Lett. **44**, 1604 (1980). A. Compaan, W. H. Lo, A. Aydinli, and M. C. Lee in: Ref. 10, p. 15.
[96]M. C. Lee, H. W. Lo, A. Aydinli, and A. Compaan, Appl. Phys. Lett. **38**, 499 (1981).
[97]R. F. Wood, D. H. Lowndess, and G. E. Giles in: Ref. 12, p. 67.
[98]M. Schmidt and K. Dransfeld, Appl. Phys. A **28**, 211 (1982).
[99]V. I. Emel'yanov and I. F. Uvarova, Akust. Zh. **31**, 481 (1985) [Sov. Phys. Acoust. **31**, 284 (1985)].
[100]E. L. Portnoi, Yu. V., Koval'chuk, G. V. Ostrovskaya, A. S. Piskarskas, V. I. Skopina, V. I. Smil'gyavichyus, and V. V. Smirnitskiĭ, Pis'ma Zh. Tekh. Fiz. **8**, 462 (1982) [Sov. Tech. Phys. Lett. **8**, 201 (1982)].
[101]V. N. Abakumov, Zh. I. Alferov, Yu. V. Koval'chuk, and E. L. Portnoi, *ibid.* **8**, 966 (1982) [Sov. Tech. Phys. Lett. **8**, 417 (1982)].
[102]Zh. I. Alferov, Yu. V. Koval'chuk, O. V. Smol'skii, and I. A. Sokolov, *ibid.* **9**, 897 (1983) [Sov. Tech. Phys. Lett. **9**, 387 (1983)].
[103]Zh. I. Alferov, Yu. V. Koval'chuk, Yu. V. Pogorel'skii, O. V. Smol'skiĭ, and I. A. Sokolov, *ibid.*, 1373 [Sov. Tech. Phys. Lett. **9**, 591 (1983)].
[104]V. P. Aksenov and B. G. Zhurkin, Dokl. Akad. Nauk SSSR **265**, 1365 (1982) [Sov. Phys. Dokl. **27**, 630 (1982)].
[105]N. Bloembergen and P. Pershan, Phys. Rev. **128**, 606 (1962).
[106]F. de Martini and Y. R. Shen, Phys. Rev. Lett. **36**, 216 (1976).
[107]F. de Martini, M. Colocci, S. E. Kohn, and Y. R. Shen, *ibid.* **38**, 1223 (1977).
[108]Y. R. Shen, C. K. Chen, and A. R. B. Castro in: Proceedings of the VIII International Conference on Raman Spectroscopy, Ottawa, Canada, 1980, edited by W. F. Murphy, North-Holland, New York, 1980, p. 659.
[109]C. K. Chen, T. F. Heinz, D. Ricard, and Y. R. Shen, Phys. Rev. Lett. **46**, 1010 (1981).
[110]T. F. Heinz, C. K. Chen, D. Ricard, and Y. R. Shen, Chem. Phys. Lett. **83**, 180 (1981).
[111]O. A. Aktsipetrov and E. A. Mishina, Pis'ma Zh. Eksp. Teor. Fiz. **38**, 442 (1983) [JETP Lett. **38**, 535 (1983)].
[112]J. P. Heritage and J. G. Bergman in: Light Scattering in Solids, edited by J. L. Birman, H. Z. Cummins, and K. K. Rebane, Plenum Press, New York (1979), p. 167.
[113]S. A. Akhmanov, M. F. Galyautdinov, N. I. Koroteev, G. A. Paityan, I. B. Khaĭbullin, E. I. Shtyrkov, and I. L. Shumaĭ, Pis'ma Zh. Tekh. Fiz. **10**, 1900 (1984) [*sic*]. S. A. Akhmanov, M. F. Galiautdinov, N. I. Koroteev, G. A. Paitian, I. B. Khaibullin, E. I. Shtyrkov, and I. L. Shumay, J. Opt. Soc. Amer. B **2**, 283 (1985).
[114]S. A. Akhmanov, M. F. Galyautdinov, N. I. Koroteev, G. A. Raĭtyan, I. L. Shumaĭ *et al.*, Izv. Akad. Nauk SSSR, Ser. Fiz. **49**, 506 (1985).
[115]H. Cheng and P. B. Miller, Phys. Rev. A **134**, 683 (1964).
[116]N. Bloembergen, R. K. Chang, S. S. Jha, and C. H. Lee, *ibid.* **174**, 813 (1968).
[117]S. A. Akhmanov and R. V. Khokhlov, Problemy nelineĭnoĭ optiki (Problems in Nonlinear Optics), VINITI, M., 1964.
[118]N. Bloembergen, *Nonlinear Optics*, Benjamin, New York, 1965 [Russ. Transl. Mir, M., 1966].
[119]S. Sing in: Spravochnik po lazeram (Laser Handbook), edited by A. M. Prokhorov, Sov. radio, Moscow (1978), Vol. 2, p. 237.
[120]L. B. Meisner and S. M. Saltiel, *ibid.*, p. 271.
[121]J. F. Nye, Physical Properties of Crystals, Clarendon Press, Oxford, 1957 [Russ. Transl. Mir, M., 1967].
[122]J. Ducuing and C. Flytzanis in: Optical Properties of Solids, edited by F. Abeles, North-Holland, Amsterdam, 1972, p. 863.
[123]J. Ducuing and N. Bloembergen, Phys. Rev. Lett. **10**, 474 (1963).
[124]C. H. Lee, R. K. Chang, and N. Bloembergen, *ibid.* **18**, 167 (1967).
[125]O. A. Aktsipetrov and E. D. Mishina, Dokl. Akad. Nauk SSSR **274**, 62 (1984) [Sov. Phys. Dokl. **29**, 37 (1984)].
[126]C. V. Shank, R. Yen, and C. Hirlimann, Phys. Rev. Lett. **51**, 900 (1983).
[127]A. M. Malvezzi, J. M. Lui, and N. Bloembergen, Appl. Phys. Lett. **45**, 1019 (1984).
[128]J. C. Diels, Laser Focus **19**, 26 (1893).
[129]D. Guidotti, T. A. Driscoll, and H. J. Gerritsen, Solid State Commun. **46**, 337 (1983).
[130]T. A. Driscoll and D. Guidotti, Phys. Rev. B **28**, 1171 (1983).
[131]D. E. Aspnes and A. A. Studna, *ibid.* **27**, 985.
[132]A. B. Belonozhko, V. I. Emel'yanov, G. A. Paityan, and A. A. Sumbatov, Vestn. Mosk. un-ta, Ser. Fizika, Astronomiya **26**, No. 4, 67 (1984).
[133]M. Born and E. Wolf, *Principles of Optics*, Pergamon Press, Oxford, 1970 [Russ. Transl. Nauka M., 1973].
[134]J. Litwin, D. J. Moss, J. E. Sipe, and H. M. van Driel, "Comparison of nanosecond and picosecond harmonic generation from centrosymmetric semiconductors," Post-Deadline Paper WII29-1, presented at the 13th International Quantum Electronics Conference, Anaheim, USA (1984).
[135]M. J. Birnbaum, Appl. Phys. **36**, 3688 (1965).
[136]A. M. Bonch-Bruevich, M. K, Kochengina, M. N. Libenson, S. D. Pudkov, and V. V. Trubaev, Izv. Akad. Nauk SSSR, Ser. Fiz. **46**, 1186 (1982).
[137]A. M. Prokhorov, V. A. Sychugov, A. V. Tishchenko, and A. A. Khakimov, Pis'ma Zh. Tekh. Fiz. **8**, 961, 1409 (1982) [Sov. Tech. Phys. Lett. **8**, 415, 605 (1982)].
[138]G. G. Gromov and V. B. Ufimtsev, Dokl. Akad. Nauk SSSR **272**, 1405 (1983), Pis'ma Zh. Tekh. Fiz. **9**, 580 (1983) [Sov. Tech. Phys. Lett. **9**, 249 (1983)].
[139]J. F. Young, J. S. Preston, H. M. van Oriel, and J. E. Sipe, Phys. Rev. B **27**, 1141, 1155 (1983).
[140]M. Oron and G. Sorensen, Appl. Phys. Lett. **35**, 782 (1979).
[141]P. M. Fauchet and A. E. Siegman, *ibid.* **40**, 824 (1982); in Ref. 75, p. 129; Appl. Phys. A **32**, 135 (1983).
[142]P. V. Bazakutsa, A. M. Prokhorov, V. A. Sychugov, and A. V. Tishchenko, Pis'ma Zh. Tekh. Fiz. **9**, 705 (1983) [Sov. Tech. Phys. Lett. **9**, 303 (1983)].
[143]V. V. Bazhenov, A. M. Bonch-Bruevich, M. N. Libenson, V. S. Makin, S. D. Pudkov, and V. V. Trubaev, Pis'ma Zh. Tekh. Fiz. **9**, 932 (1983) [Sov. Tech. Phys. Lett. **9**, 402 (1983)].
[144]N. R. Isenor, Appl. Phys. Lett. **31**, 148 (1977).
[145]A. K. Jain, V. N. Kulkarni, D. K. Sood, and J. C. Uppal, J. Appl. Phys. **52**, 4882 (1981).
[146]V. N. Anisimov, V. Yu. Baranov, L. A. Bol'shov, A. M. Dykhne, D. D. Malyuta, V. D. Pis'mennyi, A. Yu. Sbrant, and M. A. Stepanva, Poverkhnost', No. 7, 138 (1983).
[147]P. A. Temple and M. J. Soleau, IEEE J. **QE-17**, 2067 (1981).
[148]V. I. Konov, A. M. Prokhorov, V. A. Sychugov, A. V. Tishchenko, and V. N. Tokarev, Zh. Tekh. Fiz. **53**, 2283 (1983) [Sov. Phys. Tech. Phys. **28**, 1404 (1983)].
[149]F. Keilmann and Y. H. Bai, Appl. Phys. A **29**, 9 (1982).
[150]J. C. Koo and R. E. Slusher, Appl. Phys. Lett. **28**, 614 (1976).
[151]S. R. J. Brueck and D. J. Ehrlich, Phys. Rev. Lett. **48**, 1678 (1982).
[152]F. Keilmann, *ibid.* **51**, 2097 (1983).
[153]J. F. Young, J. E. Sipe, and H. M. van Driel, Optics Lett. **8**, 431 (1983).
[154]T. F. Heinz, M. M. T. Loy, and W. A. Thompson, Phys. Rev. Lett. **54**, 63 (1985).
[155]I. A. Viktorov, Zvukovye poverkhnostnye volny v tverdykh telakh (Surface Acoustic Waves in Solids), Nauka, M. (1981).

[156]R. Sandercock, Solid State Commun. **26**, 547 (1978).
[157]N. L. Rowell and G. I. Stegeman, Phys. Rev. B **18**, 2598 (1978).
[158]L. D. Landau and E. M. Lifshitz, Mekhanika sploshnykh sred (Mechanics of Continuous Media), Fizmatgiz, M., 1953 [Engl. Transl. Fluid Mechanics; Theory of Elasticity, Pergamon Press, Oxford, 1959].
[159]S. S. Jha, J. R. Kirtley, and J. C. Tsang, Phys. Rev. B **22**, 3973 (1980).
[160]V. I. Emel'yanov, E. M. Zemskov, and V. N. Seminogov, Poverkhnost' **2**, 38 (1984).
[161]V. I. Emel'yanov and N. I. Koroteev, Usp. Fiz. Nauk **135**, 345 (1981) [Sov. Phys. Usp. **24**, 864 (1981)].
[162]B. Ya. Zel'dovich and I. I. Sobel'man, Usp. Fiz. Nauk **101**, 3 (1970) [Sov. Phys. Usp. **13**, 307 (1970)].
[163]A. V. Kats and V. V. Maslov, Zh. Eksp. Teor. Fiz. **62**, 496 (1972) [Sov. Phys. JETP **35**, 258 (1972)].
[164]F. V. Bunkin, A. A. Samokhin, and N. V. Fedorov, Zh. Eksp. Teor. Fiz. **56**, 1057 (1969) [Sov. Phys. JETP **29**, 568 (1969)].
[165]V. I. Emel'yanov and V. N. Seminogov, Zh. Eksp. Teor. Fiz. **86**, 1026 (1984) [Sov. Phys. JETP **59**, 598 (1984)].
[166]V. L. Maslennikov, A. M. Prokhorov, V. A. Sychugov, and A. V. Tishchenko, Pis'ma Zh. Tekh. Fiz. **9**, 679 (1983) [Sov. Tech. Phys. Lett. **9**, 292 (1983)].
[167]Fiziko-khimicheskie svoĭstva élementov (Physico-Chemical Properties of the Elements), Naukova dumka, Kiev (1965).
[168]V. I. Emel'yanov and V. N. Seminogov, Kvant. Elektron. **11**, 871 (1984) [Sov. J. Quantum Electron. **11**, 591 (1984)].
[169]G. A. Golubenko, A. A. Samokhin, and V. A. Sychugov, *ibid.*, 1850 [Sov. J. Quantum Electron. **11**, 1239 (1984)].
[170]M. I. Tribel'skii and S. M. Gol'dberg, Pis'ma Zh. Tekh. Fiz. **8**, 1227 (1982) [Sov. Tech. Phys. Lett. **8**, 526 (1982)].
[171]V. I. Emel'yanov, E. M. Zemskov, and V. N. Seminogov, Kvant. Elektron. **10**, 2389 (1983) [Sov. J. Quantum Electron. **10**, 1556 (1983)].
[172]V. I. Emel'yanov, E. M. Zemskov, and V. N. Seminogov, *ibid.* **11**, 2283 (1984) [Sov. J. Quantum Electron. **11**, 1484 (1984)].
[173]A. M. Bonch-Bruevich, M. N. Libenson, and V. S. Makin, Pis'ma Zh. Tekh. Fiz. **10**, 3 (1984) [Sov. Tech. Phys. Lett. **10**, 1 (1984)].
[174]A. A. Samokhin, Kvant. Elektron. **10**, 2022 (1983) [Sov. J. Quantum Electron. **10**, 1347 (1983)]; Preprint No. 34, FIAN SSSR, Moscow (1984).
[175]J. F. Fiqueira and S. J. Thomas in: Surface Studies with Lasers, edited by F. R. Ausenegg, A. Leitner, and M. E. Lippitsch, Springer-Verlag, New York (1982), p. 212 (Chemical Physics, Vol. 33).
[176]L. D. Landau and E. M. Lifshitz, Statisticheskaya fizika, Nauka, M., 1976, Pt. 1, p. 281. [Engl. Transl. Statistical Physics, Pergamon Press, Oxford, 1980].
[177]S. I. Anisimov, M. I. Tribel'skiĭ, and Ya. G. Epel'baum, Zh. Tekh. Fiz. **78**, 1597 (1980) [*sic*].
[178]A. M. Prokhorov, V. A. Sychugov, A. V. Tishchenko, and A. A. Khakimov, Pis'ma Zh. Tekh. Fiz. **9**, 65 (1983) [Sov. Tech. Phys. Lett. **9**, 28 (1983)].
[179]V. V. Bazhenov, A. M. Bonch-Bruevich, M. N. Libenson, V. S. Makin, S. D. Pudkov, and V. V. Trubaev, *ibid.*, 1268 [Sov. Tech. Phys. Lett. **9**, 544 (1983)].
[180]V. P. Aksenov and B. G. Zhurkin, Preprint No. 56, 194, FIAN, Moscow (1982).
[181]A. R. Regel' and V. M. Glazov, Fizicheskie svoĭstva élektronnykh rasplavov (Physical Properties of Electronic Melts), Nauka, M., 1980.
[182]I. K. Kikoin [Ed.], Tablitsy fizicheskikh velichin, Spravochnik (Tables of Physical Quantities Handbook), Atomizdat, M., 1976.
[183]P. K. Kashkarov, V. F. Kiselev, and A. V. Petrov, Poverkhnost', No. 12, 47 (1982).
[184]Y. J. Chabal, J. E. Rowe, and S. B. Christman, J. Vacuum Sci. Technol. **20**, 763 (1982).
[185]S. N. Karjagin, P. K. Kashkarov, V. F. Kiselev, and A. V. Petrov, Surf. Sci. (Letters) **146**, L582 (1984).
[186]M. Wautelet, M. Failley-Lovato, and L. Laude, J. Phys. C **13**, 5504 (1980).
[187]V. I. Emel'yanov and V. N. Seminogov, Poverkhnost', No. 11, 142 (1985).
[188]F. Keilmann in: Ref. 175, p. 207.
[189]C. Jacoboni, C. Canali, G. Ottaviani, and A. Alberigi, Solid State Electron. **20**, 77 (1977).
[190]V. I. Emel'yanov, "Nonlinear-optical deformation of the acoustic subsystem and ultrafast melting of semiconductor surfaces by powerful short laser pulses," Preprint No. 5, Moscow (1985).
[191]G. Mourou and S. Williamson, Appl. Phys. Lett. **41**, 44 (1982).
[192]S. A. Akhmanov, V. N. Bagratashvili, V. V. Golubkov, A. V. Zgurskiĭ, A. A. Ishcheno, S. A. Krikunov, and V. G. Tunkin, Pis'ma Zh. Tekh. Fiz. **11**, 162 (1985) (Presented at the 3rd International Conference on Ultrafast Processes) [*sic*].
[193]M. Downer, R. L. Fork, and C. V. Shank in: Ref. 75, p. 114.
[194]A. M. Malvezzi, H. Kurz, and N. Bloembergen, *ibid.*, p. 118.
[195]W. Eisenmenger [Ed.], Phonon Scattering in Condensed Matter, Springer-Verlag, New York (1984).
[196]S. A. Wolf, J. C. Cubbertson, U. Strom, and P. B. Klein, Phy. Rev. B **29**, 7054 (1984).
[197]S. M. Avanesyan, S. A. Akhmanov, M. M. Bonch-Osmolovskii, V. E. Gusev, N. I. Zheludev, and E. G. Petrosyan in: Ref. 20, p. 148.
[198]S. A. Avanesyan, V. E. Gusev, and N. I. Zheludev, Appl. Phys. A **29**, 5 (1985).
[199]Z. Gnosheng, P. M. Fauchet, and A. E. Siegman, Phys. Rev. B **26**, 5366 (1982).
[200]R. W. Wood, Philos. Mag. **4(6)**, 396 (1902); Phys. Rev. **48**, 928 (1935).
[201]Rayleigh, Philos. Mag. **14(6)**, 60 (1907).
[202]J. F. Young, J. E. Sipe, and H. M. van Driel, Phys. Rev. B **30**, 2002 (1984).
[203]M. J. Soileau, IEEE J. **QE-20**, 464 (1984).
[204]A. M. Bonch-Bruevich, M. N. Libenson, and V. S. Makin in: Ref. 20b, p. 4.
[205]R. Reinisch and M. Neviere, Opt. Engng. **20**, 629 (1981).
[206]A. V. Andreev, Usp. Fiz. Nauk **145**, 113 (1985) [Sov. Phys. Usp. **28**, 70 (1985)].
[207]P. V. Bazakutsa, V. A. Sychugov, and A. M. Prokhorov, Kvant. Elektron. (Moscow) **11**, 2127 (1984) [Sov. J. Quantum Electron. **11**, 1420 (1984)].
[208]M. A. Ordal, L. L. Long, R. J. Bell, S. E. Bell, R. W. Alexander, and C. A. Ward, Appl. Optics **22**, 1099 (1983).
[209]I. A. Avrutskiĭ, P. V. Bazakutsa, V. A. Sychugov, and A. V. Tishchenko, Pis'ma Zh. Tekh. Fiz. **10**, 1333 (1984) [Sov. Tech. Phys. Lett. **10**, 563 (1984)].
[210]I. Ursu, I. N. Mihailescu, Al. Popa, A. M. Prokhorov, V. I. Konov, V. P. Ageev, and V. N. Tokarev, Appl. Phys. Lett. **45**, 365 (1984).
[211]V. I. Konov and V. N. Tokarev, "Size effects accompanying laser irradiation of periodic surface structures," (In Russian) Preprint No. 70, Institute of Optical Physics of the USSR Academy of Sciences, Moscow (1985).
[212]G. Wartman, M. Kemmler, and D. von der Linde, Phys. Rev. B **30**, 4850 (1984).
[213]V. I. Emel'yanov and V. N. Seminogov in: Abstracts of Reports at the 12th All-Union Conference on Coherent and Nonlinear Optics, Moscow (1985), p. 399.
[214]"Laser radiation and surfaces," *ibid.*
[215]G. Gorodetzky, J. Kanicki, T. Kazyaka, and R. Melcher, Appl. Phys. Lett. **40**, 547 (1985).
[216]B. I. Makshantsev and N. F. Pilipetski, Appl. Phys. A **36**, 205 (1985).

Translated by M. E. Alferieff